Ultra Wide Band (UWB) Planar Antennas for Microwave Imaging Applications

By

Iftekhar Hossain

A thesis submitted to the Faculty of Graduate Studies of

The University of Manitoba

in partial fulfillment of the requirements of the degree of

MASTER OF SCIENCE

Department of Electrical and Computer Engineering

University of Manitoba

Winnipeg, Canada

THE UNIVERSITY OF MANITOBA

FACULTY OF GRADUATE STUDIES

*****

COPYRIGHT PERMISSION

Ultra Wide Band (UWB) Planar Antennas for Microwave Imaging Applications

BY

Iftekhar Hossain

A Thesis/Practicum submitted to the Faculty of Graduate Studies of The University of Manitoba in partial fulfillment of the requirement of the degree

MASTER OF SCIENCE

Abstract

UWB is an emerging technology finding a myriad of applications nowadays, mainly in communication and Microwave Imaging (MI). This is due to its capability of providing high data throughput and reasonably good image resolution, respectively. Antenna design for UWB applications especially for MI offers significant challenges, as a number of design constraints have to be satisfied. In this thesis, novel designs of two UWB antennas, a printed monopole and a slot antenna, have been proposed. The proposed antennas have impedance BandWidth (BW) of more than 100% which makes them suitable for UWB applications. Prototypes of both antennas were constructed and their frequency and time domain characteristics were investigated numerically and experimentally. Moreover, a performance study was performed for these antennas when immersed in three different coupling materials to asses the feasibility of using them in the experimental microwave imaging set up for breast cancer diagnosis.

Acknowledgements

First and foremost, I would like to have the opportunity to express my heartiest appreciation and profound gratitude to my supervisor Dr. Sima Noghanian for her continuous support and active guidance throughout this research work. I am really grateful to her for providing me the opportunity to work on this project. Her constant supervision, constructive criticisms and inspiration during this entire research work were really invaluable to shape my ideas into this dissertation.

I would also like to convey my special gratitude to Dr. Lotfollah Shafai and Dr. Stephen Pistorious for serving on my examination committee and for their valuable time to read my dissertation.

I am also thankful to all of my colleagues of *Microwave Imaging Group*, University of Manitoba for their cordial co-operation and suggestions that made my graduate studies really pleasant and enjoyable. Officials at machine shop and antenna lab at the University of Manitoba also deserve much appreciation for their technical help during the prototype fabrication and measurement procedures.

Last but not the least, my sincere gratefulness should be extended to University of Manitoba, Mathematics of Information Technology and Complex Systems (MITACS), Cancer Care Manitoba (CCMB) and Government of Manitoba for supporting this research financially.

Table of Contents

List of Tables

List of Figures

List of Copyrighted Materials for which Permission was Obtained

List of Acronyms and Symbols Used

AUT	Antenna Under Test
BW	Band Width
CATR	Compact Antenna Test Range
CPW	Co-Planar Waveguide
CMI	Confocal Microwave Imaging
DAPRA	Defense Advanced Research Projects Agency
EMI	Electromagnetic Interference
FBW	Fractional BandWidth
FCC	Federal Communication Commission
FDTD	Finite Difference Time Domain
FE	Finite Element
GPS	Global Positioning System
GA	Genetic Algorithm
GD	Gaussian Derivative
GHz	Giga Hertz
HPBW	Half Power Beam width
mGy	Milligray
MI	Microwave Imaging
MRI	Magnetic Resonance Imaging
PET	Position Emission Tomography

PLF	Polarization Loss Factor
PSO	Particle Swarm Optimization
RFID	Radio Frequency Identification
RL	Return Loss
RP	Rectangular Plate
SLL	Side Lobe Level
TEM	Transverse Electromagnetic
TSAR	Tissue Sensing Adaptive Radar
UWB	Ultra Wide Band
VNA	Vector Network Analyzer
VSWR	Voltage Standing Wave Ratio
WLAN	Wireless Local Area Network

ε_r= Relative Permittivity

σ= Conductivity

λ= Wavelength

Γ= Reflection co-efficient

Ω= Ohm

Chapter 1 : Introduction

1.1 Project Motivation and Objectives

With the evolution of technology, numerous applications of electromagnetics have necessitated the exploration and utilization of most of the electromagnetic spectrum [1] Ultra Wide Band (UWB) technology is the outcome of that quest for optimum utilizations of available frequency resources. UWB has brought revolutionary progress in the area of communication, RADAR (Radio Detection and Ranging) and Microwave Imaging (MI) with substantial alleviation of system performance.

This advent of high BandWidth (BW) systems initiated the demand for designing radiators compatible with all the constraints associated with it. The design of antennas with features like convenient geometry, being economical and lightweight, and most importantly desirable radiation performance over a large frequency span is imperative in UWB systems. These specifications have introduced both a myriad of opportunities and challenges to the UWB antenna designers.

In addition to communication systems, UWB has found applications in various RADAR and imaging systems because it offers good image resolution and high sensitivity. Specifically, in MI for breast cancer detection, UWB systems have promising potential because of the high dielectric characteristics contrast between normal breast tissue and

malignant tissue [2]. Although, X-Ray mammography is the most widely used method for breast cancer detection, it has some shortcomings including the failure to detect cancer in some cases, difficulty in detecting lesion in dense breast tissue and risk of harmful radiations [3]-[8]. Therefore, MI can be a promising supplement to mammography.

In the MI set up, selection of a proper antenna system is vital as the antenna behaves as a band pass filter and reshapes the spectra of microwave pulses. In this method, the antenna is positioned to illuminate the imaging object with a microwave pulse, and either scattered or reflected electric fields from the object are captured through the antenna. From the received scattered electric field, the dielectric configuration of the imaging object is constructed which is called tomography. In the radar-based imaging, locations of strongly scattering objects can be determined from the reflected field with sophisticated signal processing algorithms.

In order to transmit and receive very short electromagnetic pulses efficiently, an antenna has to maintain good matching characteristics over a very broad range. The spatial resolution of the image solely depends on the BW of the system. However, after a certain high frequency limit around 10.00 GHz, electromagnetic waves get attenuated rapidly in the breast tissue that signals can't penetrate any deeper in the object [9]. At the same time, lower limit of frequency of operation is determined by the size of the antenna used, as at very low frequencies antenna size may be of unfeasible to be implemented. Therefore, a good compromise between the image resolution and antenna size is needed. Although, many antennas exhibit good frequency domain impedance matching, they have

poor time domain pulse radiation. A good time domain performance is desirable in the imaging applications. This corresponds to a linear antenna phase response in frequency domain. High radiation efficiency and constant gain are imperative for UWB imaging antennas as the power level of the UWB systems is quite low. Excessive losses incurred by antenna can potentially compromise the performance of the antenna in the imaging system. Therefore, conductor, dielectric and other losses associated have to be minimized in order to maximize the overall radiation efficiency.

Compact volumetric antennas such as bow-ties [3], slot line bow-tie hybrid [4], ridged pyramidal horn [10], resistively loaded dipoles [11], and specially designed bow-tie [12] have been used in MI. Although, these antenna systems were able to provide images of the breast with different resolutions, they have some shortcomings. Resistively loaded dipoles [11] do not have broad BW and resistive loading compromise the overall efficiency of the antenna. Bow-ties [12] have the similar limitations. The compact crossed bow ties [3] have a complex configuration to be implemented and fabrication of very small ridged horn with launching plane and lumped resistors [10] is not convenient. Moreover, fabrication of array of these complex structures is difficult.

Printed antennas are simple, easy to fabricate and cost-effective. Moreover, planar printed antennas are easily integrable with other circuitry and an array of printed antennas can be easily fabricated. Although, small, printed UWB antennas are finding numerous communication applications, they are not considered for the imaging set-ups.

In this thesis, an attempt has been made to study the possibility of using small printed UWB planar antennas in MI. With this objective in mind, two different designs comprising a printed monopole and a printed slot antenna are proposed. The performance of these antennas in some coupling materials is investigated to imitate antenna behavior in an actual imaging set up environment. The main objective of this research is to design and implement UWB printed antennas with high impedance BW, good time domain response, stable radiation characteristics and convenient geometric features.

1.2 Thesis Overview and Outline

The subsequent chapters of this thesis are arranged in the following way:

Chapter 1 is dedicated to the introduction of the problem, a brief study of the current trends of UWB antennas in communication and imaging applications, the motivation behind UWB antenna design and the main objectives associated with this research.

Chapter 2 will provide a comprehensive background of some of the most elementary antenna parameters that are used for the design and performance evaluation of most antennas whether they are of narrowband or broadband types. Moreover, brief discussion of antenna measurement facilities and testing process has been provided in this chapter.

Chapter 3 includes the background of the specific antenna of interest. A few key references have been studied to achieve sufficient insight into different UWB antenna topologies mainly designed for communication, GPR and MI applications. As our main objective is the antenna design for MI, more specifically for breast imaging for cancer

diagnosis, a glossary of the different features of existing microwave breast imaging techniques has also been presented.

In Chapter 4, a new printed UWB monopole antenna is proposed. The design features of the antenna in free space are studied. The simulated and measurement results are presented. Antenna performance while immersed in three coupling materials is also studied to investigate the feasibility of using that antenna under realistic imaging conditions.

In chapter 5, a novel UWB printed slot antenna design has been proposed. Moreover, some of the frequency and time domain computed and measurement results have also been discussed. Antenna performance while immersed in three coupling materials has also been investigated.

Finally, in chapter 6, a summary of the contributions of this thesis and comparisons between the two designed antennas are presented. In conclusion, future work and recommendations for improvement in the designs are discussed.

Chapter 2 : Antenna Fundamentals

2.1 Introduction

In this chapter, various parameters that are used during the design and performance evaluation of an antenna are introduced. The measurement of antenna characteristics is an important component in the design and implementation of new antenna. A solid understanding of the antenna measurement systems and procedures also helps visualize some of the important antenna parameters.

2.2 Fundamental Antenna Parameters

Antenna performance is evaluated based on the satisfaction of some predefined parameter specifications. This parameter specification is application specific. In order to have an insight into an antenna, a good understanding of these parameters is necessary. The fundamental parameters used to fully characterize an antenna behavior include impedance BW, radiated field regions, radiation patterns, beamwidth, group delay and phase linearity, polarization, gain and efficiency.

2.2.1 Impedance Bandwidth (BW)

In general, the BW of antenna is the frequency span where the performance of the antenna satisfies some predefined desirable values. Usually, the BW of the antenna is

calculated by examining both its input impedance and variation of radiation characteristics with a change of frequency. For those antennas whose pattern variations are sensitive to a change in frequency, BW is usually determined using parameters like the radiation beamwidth, gain or Side Lobe Level (SLL). Electrically small antennas are usually more prone to impedance variation with frequency and their bandwidth is impedance limited. To improve the BW, the antenna has to fully utilize the spherical volume surrounding its structure [13]. The impedance BW describes the frequency span where the antenna is sufficiently matched to the input source or transmission line in such a way that 10% or less of the incident power is lost due to reflection at the port. Impedance BW of an antenna is basically characterized by the terms Return Loss (RL) and Voltage Standing Wave Ratio (VSWR). To have a detailed insight of antenna impedance BW, a through study of the antenna input impedance and S-parameters is essential.

2.2.1.1 Input Impedance

Input impedance which is one of the fundamental parameters of an antenna system is the impedance presented by an antenna at its input terminal. When the antenna is isolated from other objects, input impedance is the self impedance of the antenna. Self impedance is the combination of the real part, self resistance and the imaginary part, self reactance. Self resistance has two components: radiation resistance and loss resistance. The radiation resistance involves the energy radiated by an antenna whereas loss resistance represents conductor and dielectric losses incurred by the antenna structure. Self-

reactance is used to represent the electric and magnetic energy stored in the vicinity of the near-field region of the antenna.

If a coupling exists between the antenna and its surrounding objects, the input impedance of the antenna is greatly affected by the mutual impedance as well. This phenomenon is important in the design of an array of antennas, where separation between the elements is crucial and has substantial effect on the antenna performance.

In most of the antennas, input impedance is not frequency independent. Therefore, matching is band limited and usually efforts are adopted for increasing the impedance matching BW. The matching is usually done for 50Ω, 75Ω or 220Ω transmission line impedance by modifying the antenna geometry and feed structures.

2.2.1.2 S Parameters

Scattering parameters or S-parameters are widely used in the design and analysis of antenna and other microwave devices and systems. From the analysis of the S-parameters, other important antenna specifications such as BW, RL and isolation can be derived.

If in a transmission line with characteristic impedance of Z_0 and load impedance of $Z(l)$, $Z_0=Z(l)^*$; there will be no reflection at the port where load is connected. Thais means all the power supplied by the source will be absorbed by the load. If the terminated load value differs from $Z(l)^*$, a portion of the incident power will be reflected back based on

the difference between the load and characteristic impedance value. This mismatch is expressed by a parameter called Reflection Coefficient, Γ. This is defined as the ratio of reflected voltage (V_2) to incident voltage (V_1) by the following formula:

$$\Gamma = \frac{V_2 e^{-\gamma l}}{V_1 e^{\gamma l}} = \frac{Z(l) - Z_0}{Z(l) + Z_0} \tag{2.1}$$

where, γ is the propagation constant and l is the length of the transmission line. A perfect impedance match is obtained when Γ=0 and worst impedance match is given by Γ= +1 or Γ=-1 that corresponds to open or short circuited load respectively. The reflection coefficient can also be expressed in the time domain in a similar way to its frequency domain counterpart, by the ratio of reflected signal over the incident signal:

$$\Gamma_t = \frac{\int_{-\infty}^{+\infty} |V_2(t)| dt}{\int_{-\infty}^{+\infty} |V_1(t)| dt} \tag{2.2}$$

The relationship between the traveling waves can be illustrated for a two port microwave device using the Signal Flow Graph (SFG) of Fig. 2-1.

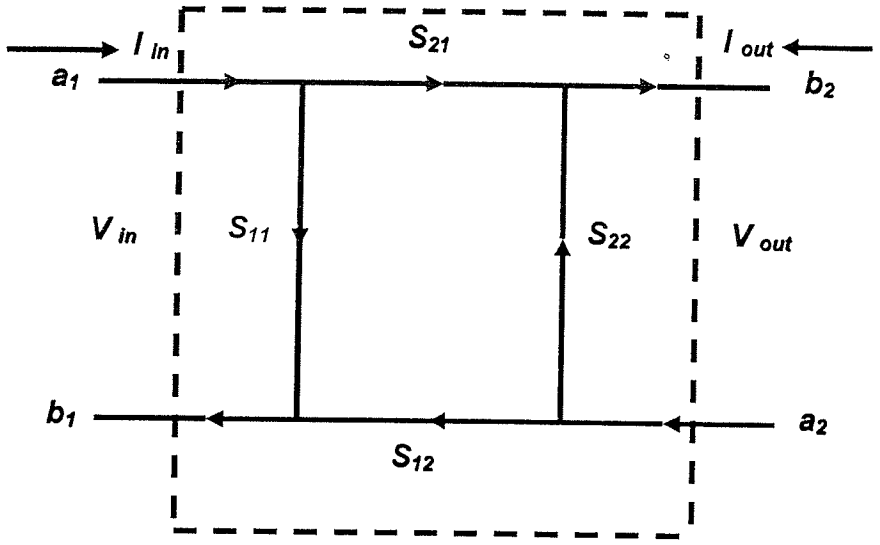

Fig. 2-1 A two-port device S parameters

Here, at each port the term 'a' denotes incoming traveling waves and the term 'b' denotes outgoing traveling wave, both normalized to Z_0.

From the SFG of Fig. 2-1, the relation between the incoming and outgoing traveling waves can be expressed as:

$$b_1 = S_{11}a_1 + S_{12}a_2 \text{ and } b_2 = S_{21}a_1 + S_{22}a_2 \tag{2.3}$$

where,

$$S_{11} = \left.\frac{b_1}{a_1}\right|_{a_2=0}, S_{12} = \left.\frac{b_1}{a_2}\right|_{a_1=0}, S_{21} = \left.\frac{b_2}{a_1}\right|_{a_2=0} \text{ and } S_{22} = \left.\frac{b_2}{a_2}\right|_{a_1=0} \tag{2.4}$$

where, S_{11} and S_{22} are the input and output reflection co-efficient, respectively, and S_{21} and S_{12} are forward and reverse transmission co-efficient, respectively. S_{11} and S_{22} indicate signal transmission between two ports of the system.

The antenna *RL* can be calculated by taking the logarithm of the magnitude of S_{11} and multiplying it by 20,

$$RL = 20\log|S_{11}| \tag{2.5}$$

A good impedance matching is usually indicated by the RL value of less than or equal to -10 dB. By plotting the RL as a function of frequency, the frequency span, where antenna RL is less than a specific value are determined to evaluate the impedance BW of the antenna.

The same criteria can be described by another widely used parameter called Voltage Standing Wave Ratio (*VSWR*). An imperfectly matched load causes a negative traveling wave propagating down the transmission line and thus creates standing waves in the transmission line. *VSWR* is the indication of the ratio of the amplitudes of maximum standing waves (V_{max}) to minimum standing waves (V_{min}) and is given by,

$$VSWR = \frac{V_{\max}}{V_{\min}} = \frac{1+|\Gamma|}{1-|\Gamma|} \tag{2.6}$$

Typically, *VSWR* value of 2 corresponds to the RL of -10 dB or less.

2.2.2 Antenna Field Regions

The field regions surrounding a radiating antenna can be subdivided into three regions (Fig. 2-2):

- Reactive near field region,
- Radiating near field (Fresnel) region,

- Far-field (Fraunhofer) region.

Though field configurations at the boundaries do not change abruptly, still some distinct differences among them exist. The reactive near field region is the immediate vicinity of the antenna where the reactive field components are predominant. For most antennas, the outer boundary of this region can be calculated by the following formula [1]:

$$r_1 \leq 0.62\sqrt{\frac{D^3}{\lambda}} \tag{2.7}$$

where, D is the largest dimension of the antenna and λ is the operating wavelength of the antenna. Radiating near field is the region between the reactive near field and far-field regions. In this region radiation fields predominate, but the angular field distribution is dependent upon the distance from the antenna. This is also called 'Fresnel' region. The inner (r_1) and outer boundaries (r_2) of this region (Fig. 2-2) can be formulated as [1],

$$r_1 \geq 0.62\sqrt{\frac{D^3}{\lambda}} \quad \text{and} \quad r_2 \langle 2\frac{D^2}{\lambda} \tag{2.8}$$

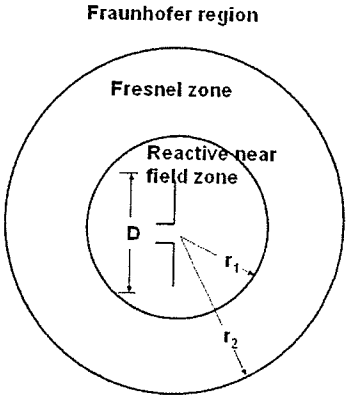

Fig. 2-2 Field regions of an antenna

In the far-field or Fraunhofer region, the angular field distribution is independent on the distance from the antenna. In this region, the field attains a specific form and field components are essentially transverse. The inner boundary of far-field region is given by, $r_2 = 2\frac{D^2}{\lambda}$ and the outer boundary is infinity. Fig. 2-3 shows a typical field pattern variation of an antenna as observation distance from it changes.

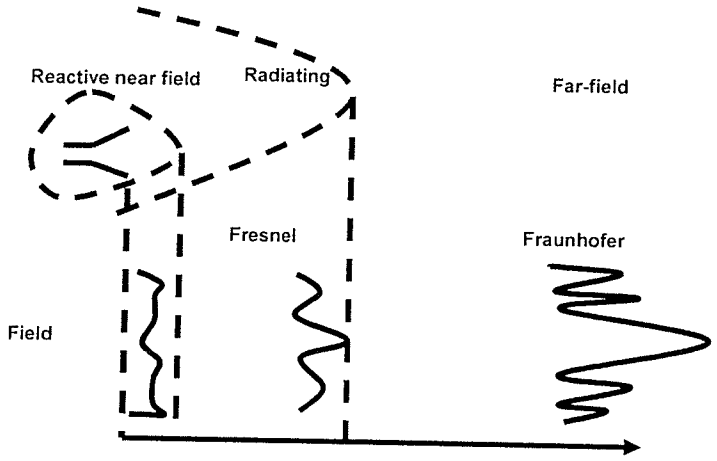

Fig. 2-3 Typical change of radiated field pattern from reactive near field to far-field

2.2.3 Radiation Pattern

Radiation pattern is also an important performance specification for certain applications. For example, cell phones antennas usually need to have near omnidirectional radiation patterns for optimal reception of the signal as users are continuously changing the location or alignment of the antenna. On the other hand, for satellite applications, highly directive radiation is desirable to direct most of the radiated energy towards a specific direction or receive radiated energy from a known source at a known location.

The radiation pattern is basically the graphical representation of the distributed electromagnetic energy radiated by an antenna system. Radiation pattern is usually described as a function of two spherical coordinate parameters, θ and φ, keeping the radial distance from the antenna constant. Two specific types of radiation patterns are most commonly used and these are the power pattern and the field pattern. The power pattern is the representation of the spatial distribution of power radiated by the antenna whereas the field pattern depicts the variation of electric or magnetic fields in space. These two patterns are the same if they are measured in decibels.

Depending on the radiation characteristics, an antenna can be classified as isotropic, directional or omnidirectional. An isotropic antenna is a hypothetical lossless antenna with uniform radiation over all the directions. Even though an isotropic antenna is not physically realizable, this kind of antenna is used as a reference antenna to evaluate the directive properties of other practical antennas. A directive antenna radiates more energy in a specific direction. This kind of antennas usually contains major or main lobes in the desired directions and some minor lobes in undesired directions. Electromagnetic horns or the reflectors are examples of this kind of antenna. An omnidirectional antenna is a specific type of antenna where radiation is uniform in one plane and directive in the planes perpendicular to that plane. A simple half wave length dipole is an example of omnidirectional antenna.

2.2.3.1 Half Power BeamWidth (HPBW)

The HPBW is the angular distance from the center of the main beam of the antenna to a point at which radiated field power is half of that power of the center. In a high gain antenna, very narrow beam width and low SLL can be achieved by adopting a careful design and structural modifications of the antenna.

2.2.4 Phase Center and Group Delay

The 'Phase center' of an antenna is a virtual point from which electromagnetic radiation spreads spherically outward, with phase of the radiated electromagnetic field being the same for all the points on the sphere (Fig. 2-4).

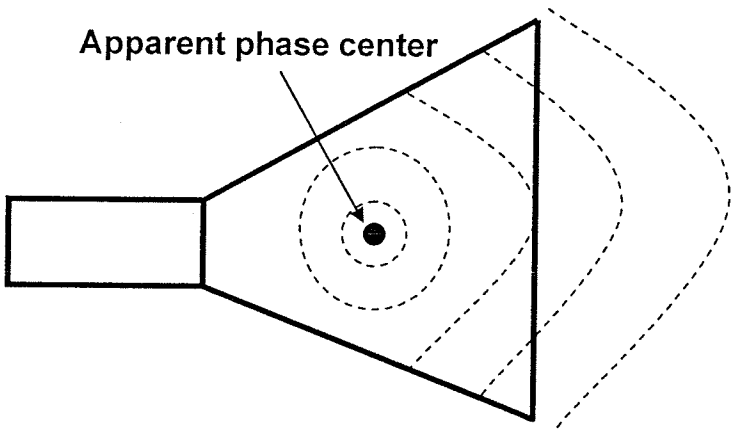

Fig. 2-4 Depiction of apparent phase center of a typical horn antenna

Group delay is the parameter that corresponds to how long it takes for a signal to traverse an antenna, or its transit time through the antenna. Group delay is a strong function of the length of the antenna, and typically a weak function of frequency. It is usually expressed

in units of time, pico-seconds for short distances or nanoseconds for longer distances [15].

Flat and constant group delay as a function of frequency is important in UWB antenna systems. The frequency content of a UWB pulse is complex and spans more than one GHz of bandwidth. Therefore, at the time of processing the pulse, its spectrum has to be treated the same over the intended BW, otherwise distortion will render pulse measurements inaccurate.

2.2.5 Polarization

The polarization of an antenna is the polarization of the radiated electric field of the antenna. The polarization of a radiated wave can be defined as: "that property of an electromagnetic wave describing the time varying direction and relative magnitude of the electric field vector; specifically, the figure traced as function of time by the extremity of the vector at a fixed location in space, and the sense in which it is traced, as observed along the direction of propagation" [1]. At a specific direction and location in space, the polarization of an antenna is evaluated by tracking the end point of the electric field vector as function of time.

The polarization of an antenna can be classified as linear, circular or elliptical. Linear and circular polarization can be considered as a form of elliptical polarization.

Linear polarization can be achieved if electric field vector possesses only one component or two linear orthogonal components that are in time phase or 180^0 (or multiples of 180^0) out of phase [1]. Linearly polarized antennas are widely used in the wireless and telecommunication applications. Dipoles and monopoles are example of linearly polarized antennas.

To attain circular polarization, the field must have two orthogonal linear components of same magnitudes and they should have phase difference of 90^0 or odd multiples of 90^0. If the rotation of the electric field vector trace is clockwise, it is called Right Hand Circular Polarization (RHCP) and for left hand rotation of the electric field vector trace, it is called Left Hand Circular Polarization (LHCP) [1]. Electrically large spiral antennas and some specially modified microstrip patch antennas are circularly polarized.

A wave is elliptically polarized, if it is not linearly or circularly polarized. Like the circular polarization, elliptical polarization can be clockwise or counterclockwise rotated based on the direction of rotation. In elliptical polarization, axial ratio and the tilt angle of the ellipse are two crucial factors to specify the phenomenon of the electromagnetic wave [13].

Power received by an antenna from an incident wave of specific polarization is maximized, if the polarization of the transmitting and receiving antenna matches to each other. The difference between the polarization between the transmitting and the receiving

antennas is termed as 'polarization mismatch'. This amount of loss is determined by a factor called 'Polarization Loss Factor' (*PLF*).

If electric field of the incoming signal E_i is given by, $E_i = \hat{\alpha} e_i$, where $\hat{\alpha}$, is the unit vector in the direction of incoming signal vector and if the field of the receiving antenna is termed as, $E_a = \hat{\beta} e_a$, where $\hat{\beta}$ is the unit vector in the direction of receive signal, *PLF* of the antenna in transmitting mode can be defined as,

$$PLF = \left|\hat{\alpha}.\hat{\beta}\right|^2 = \left|\cos\psi_p\right|^2 \tag{2.9}$$

where, ψ_p is the angle between the two unit vectors.

Another figure of merit of the polarization characteristics of an antenna is 'polarization efficiency' which is "the ratio of the power received by an antenna from a given plane wave of arbitrary polarization to the power that would be received by the same antenna from a plane wave of the same power flux density and direction of propagation, whose state of polarization has been adjusted for a maximum received power" [1]. This can be expressed as,

$$p_e = \frac{\left|l_e.E_{inc}\right|^2}{\left|l_e\right|^2\left|E_{inc}\right|^2} \tag{2.10}$$

where, l_e=vector effective length of antenna, and E_{inc}= expression of the incident electric field on antenna.

2.2.6 Directivity

As the name implies, the directivity of an antenna is a measure of how an antenna guides radiated power in a specific direction or receives power from certain specific direction. This is calculated by taking the ratio of radiation intensity in a given direction for a given polarization over its average over all directions. If the direction is not specified, the direction of maximum radiation has been assumed. An antenna which is not isotropic, directivity is given by taking the radiation intensity in the specific direction over that of isotropic source. In mathematical form directivity can be expressed as,

$$D_\theta = \frac{4\pi U_\theta}{P_{rad}} \text{ and } D_\varphi = \frac{4\pi U_\varphi}{P_{rad}} \tag{2.11}$$

where, U_θ= Radiation intensity for a specific direction contained in E_θ field component, U_φ= Radiation intensity for a specific direction contained in E_φ field component and P_{rad} =Total power radiated in all directions by the antenna.

2.2.7 Efficiency

There are a number of factors associated with the overall efficiency of an antenna. Total efficiency, (η_0) considers losses in the input terminals and losses within the antenna structure. The main losses associated with an antenna can be divided into,

1) Reflection loss (η_r) due to the mismatch between the antenna port and source, which is proportional to ($1-|\Gamma|^2$), where Γ is the reflection coefficient at input.

2) Conduction (η_c) and dielectric losses (η_d) in the antenna structure.

The overall efficiency can be written as,

$$\eta_0 = \eta_r \eta_c \eta_d = \eta_{cd}\left(1-|\Gamma|^2\right) \tag{2.12}$$

where, η_{cd} is the radiation efficiency.

Usually, antenna efficiency varies from 60%- 90% depending on the dielectric substrates and the type of conductors used. High efficiency is desirable to reduce power loss and enhance the radiated power in the antenna.

2.2.8 Gain

Gain is another widely used antenna performance evaluation parameter. Gain takes both efficiency and directivity of an antenna into account. Gain is simply calculated by the multiplication of directivity and efficiency of an antenna. In another form, gain expression can be written as

$$Gain_\theta = \frac{4\pi U_\theta(\theta,\varphi)}{P_{in}} \text{ and } Gain_\varphi = \frac{4\pi U_\varphi(\theta,\varphi)}{P_{in}} \tag{2.13}$$

where, $U_\theta(\theta,\varphi)$= Radiation intensity in a given direction contained in E_θ field component, $U_\varphi(\theta,\varphi)$= Radiation intensity in a given direction contained in E_φ field component, and P_{in}= Total accepted power at the input.

2.3 Antenna Parameter Measurement

Antenna performance parameter measurement is an essential step in antenna design and implementation process. Even though, antenna design and analysis have become extremely time and cost effective due to the availability of commercial Electromagnetic simulation softwares and high speed computers, measurement is still needed to evaluate antenna's performance in reality and to have a comparison between the prediction and actual performance. Moreover, due to complexity in feed systems and structures of antennas, some antennas are computationally rigorous and intensive to analyze. In that case, experimental investigation is the sole method for evaluating antenna performance.

There are several considerations that have to be taken into account for implementing antenna measurement process. It is usually more convenient to use Antenna Under Test (AUT) in receiving mode if the antenna is reciprocal in nature. Reciprocity in antenna means similar characteristics (gain, radiation pattern, etc.) are shown by the antenna in both transmitting and receiving mode. The ideal condition for measuring far-field radiation characteristics of an antenna is to illuminate the AUT with a plane wave of uniform amplitude and phase, i.e. antennas should be placed in the far-field. For phase error to be less than 22.50^0, the distance between the transmitting antenna and the AUT should be $\frac{2D^2}{\lambda}$ or greater [14]. Reflection from ground and neighboring objects and interference also contribute to degrading the antenna illumination for measurement process.

Depending upon the site of the test set up, antenna test range can be classified as outdoor and indoor ranges. They both have some advantages as well as drawbacks.

Generally, outdoor ranges are employed for measuring electrically large antenna system where indoor facilities can not accommodate the measurement set up. It allows for the performance of an antenna to be evaluated in an external environment which is applied for outdoor applications. The main limitations associated with the outdoor range are the unwanted reflections from the ground and surrounding objects, electromagnetic interference and uncontrolled environmental conditions. With indoor ranges using proper absorbing materials a controlled environment free of interference can be achieved.

The free space ranges (indoor and outdoor) of antenna measurement facility mainly include elevated ranges, slant ranges, anechoic chambers, compact ranges and near field ranges [1].

2.3.1 Anechoic Chamber

The anechoic chamber is widely used for indoor free space measurement range of antenna radiation pattern because of its all-weather capability, minimized interference and security. Pyramidal or wedge shaped RF absorbing materials are used to cover the internal walls of the chamber. The performance of the absorbing materials highly depends on the operating frequency. As the operating frequency decreases, the thickness of the absorbing material has to be increased [1].

Two basic types of anechoic chamber configurations, rectangular and tapered chambers, are widely used. The design of both types of chambers uses the principle of geometrical optics. Sufficient high quality RF absorber should be used to minimize the reflection. Tapered anechoic chambers are usually in the shape of a pyramidal horn and a uniform plane wave in the 'quiet zone' can be achieved by properly locating the source antenna near the apex of the chamber. In the 'quiet zone' direct and reflected rays add constructively to provide a smooth amplitude illumination taper to the test antenna. For very high frequency measurements, a very high gain antenna should be used, and this source antenna should be moved away from the apex and placed near the end of the tapering section. At the same time, a very high absorbing material should be used in the side walls to maintain the reflected waves under a certain minimum level [1].

2.3.2 Compact Ranges

In a Compact Antenna Test Range (CATR), a planar wave front in the 'quiet zone' is achieved by collimating incident wave from the feed by reflector antenna system (Fig. 2-5). Thus a planar wave front can be achieved within a very short distance compared to the minimum range of $\frac{2D^2}{\lambda}$. The frequency of operation of CATR is dependent on the size and the surface accuracy of the reflector. Though, CATR reduces the system range in a great extent, it is still subject to several shortcomings like aperture blockage, diffraction at the rim of the reflector, direct radiation from the feed to test antenna and depolarization coupling, and reflection at the walls [1].

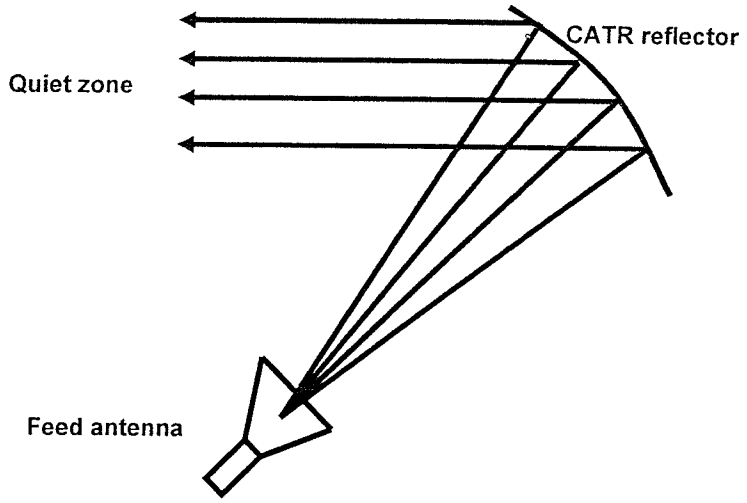

Fig. 2-5 Planer wave front generation in 'quiet zone' by CATR reflector

Aperture blockage and diffraction can be minimized using offset fed reflector. Moreover, quiet zone ripple of field wave produced by diffraction at the edges can be minimized by using reflector with serrated (Fig. 2-6) or rolled edges.

The radiation measurements of the antennas described in this thesis have been performed in the antenna lab at University of Manitoba facilitated with a CATR system comprising of a reflector with serrated edge. The whole chamber is shielded with RF absorber material with high absorption co-efficient.

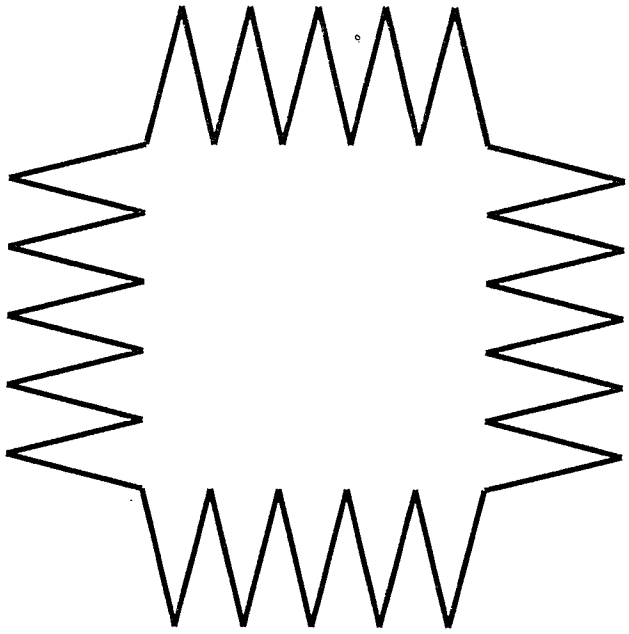

Fig. 2-6 Reflector with serrated edges

2.3.3 Return Loss and Group Delay Measurement

The impedance BW of antennas is determined by measuring the RL of the antenna. This measurement is performed using a Vector Network Analyzer (VNA). A VNA is used for measuring reflection and transmission characteristics and impedance behavior of a microwave network over a broad frequency range. The RL of an antenna can be directly plotted and displayed as a function of frequency and from that impedance BW can be evaluated.

The group delay variation of a microwave device can also be measured directly by a VNA. The VNA provides group delay variation of a device with reference to free space. RL and group delay measurement of the antennas described in this thesis have been performed using Anritsu ME7808 VNA in the antenna lab of University of Manitoba.

2.3.4 Radiation Pattern Measurement

The radiation pattern of a typical antenna is measured using a transmitting antenna and receiving antenna. If, like most practical antennas, the AUT is reciprocal, it is more convenient to use it in receiving mode. To measure the far-field pattern, the antenna has to be illuminated by a plane wave. This condition is achieved by using CATR system. In fact, even at the far-field of the transmitting antenna, there are some phase errors, as ideal planar wavefront can not be achieved with a finite separation distance. Fig. 2-7 shows a simplified block diagram of antenna radiation pattern measurement set up which comprises an anechoic chamber, transmit antenna, receive antenna, VNA, antenna position control device and personal computer to interpret the measured data. While measuring the radiation patterns in the antenna lab at University of Manitoba, the AUT was placed in the quiet zone and its position was controlled through a rotating device by an automatic computer interface program. After setting up the rotation angle and incremental steps, the interface program initiates each incremental rotation, and transmission coefficient between the two antennas are recorded in the computer program for every angular position. The measured values are normalized and processed properly to get the actual value of far-field radiation values.

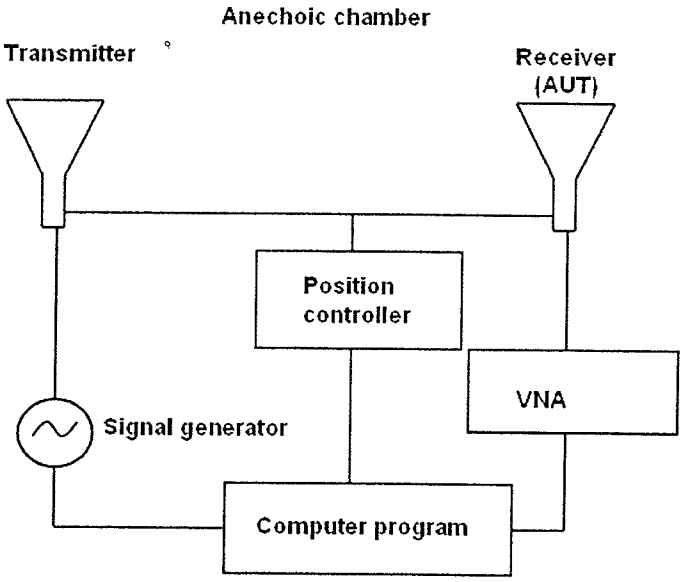

Fig. 2-7 Simplified block diagram of antenna radiation measurement set up

2.4 Chapter Summary

The topics covered in this chapter were mainly focused on two subjects. First, some of the frequency and time domain antenna parameters that are required in the design and implementation of an antenna have been described. In the second section, a glossary of the most widely used antenna measurement systems along with parameters measurement principles has been discussed.

In the next chapter, emphasis will be given to UWB antennas. As some of the references have provided an intuitive understanding of UWB antenna topologies for communication, radar and imaging applications, a very brief review of previous work will be given to provide an insight to the development of research in this area.

Chapter 3 : UWB Antennas and Microwave Imaging

3.1 Introduction

UWB antennas can be defined as non-resonant low Q radiators which can operate over the UWB range of frequencies. There are two criteria available for identifying when an antenna may be considered UWB antenna. One definition by Defense Advanced Research Project Agency (DARPA) requires a UWB antenna to have a fractional bandwidth grater than 0.25. An alternate and more recent definition by the Federal Communications Commission (FCC) places a limit of 0.20. The Fractional BandWidth (*FBW*) is given by:

$$FBW = \frac{BW}{f_c} = \frac{2(f_H - f_L)}{(f_H + f_L)} \tag{3.1}$$

where, f_H is the upper end of the antenna's operational band and f_L is the bottom, or low, end of the antenna's operational band. Additionally, the FCC provides an alternate definition whereby a UWB antenna is an antenna with a bandwidth grater than 500 MHz. According to the FCC, the upper and lower ends of the operational band are defined by the points where the radiated power is down 10 dB from its peak level. This FCC definition dose not, strictly speaking, define antenna bandwidth because radiated power also depends on the spectral response of the transmitted power [16]. UWB antennas are usually designed for use in conjunction with the approximately 3:1 bandwidth, 3.10 –

10.60 GHz systems as authorized by the FCC. These antennas potentially use much, if not all, of their bandwidth at the same time. Thus, they must be well behaved and consistent across the antenna's operational band. Their properties include pattern, gain, impedance matching, and a requirement for low or no dispersion [16].

FCC spectrum can be used for communications, imaging, surveillance, vehicular radar system and Radio Frequency Identification (RFID) applications with maximum allowable power of -41.30 dBm/MHz. Although, a number of UWB antennas have been proposed, they can not cover the whole allocated frequency span of 7.50 GHz. In this thesis emphasize will be given only to the antennas having BW at least for a span of 7.50 GHz.

3.2 Current and Previous Research

3.2.1 UWB Antennas for Communication

UWB technology is one of the most revolutionary approaches to modern communication systems due to its high data rate and excellent immunity to multipath interference [17]. After the allocation of 3.10-10.60 GHz as the UWB band for unlicensed commercial use for communication, radar and imaging applications by FCC, a great deal of interest has been created in the UWB system design both in industries and academia. The FCC allocated UWB spectral density is only -41.3 dBm/MHz which is a very low power level. This ensures a peaceful coexistence of the UWB systems with other existing technologies. Moreover, UWB systems should not cause any Electromagnetic Interference (EMI) with the neighboring communication channels like WLAN (Wireless

Local Area Network), Global Positioning Systems (GPS) and Bluetooth technologies [18]. For example, the frequency band of 5.150 GHz-5.825 GHz is occupied by IEEE 802.11a and HIPERLAN/ 2. Therefore, for some cases a band rejection is desired in this range to avoid interference with IEEE 802.11a and HIPERLAN/ 2.

It is quite challenging to satisfy all the requirements associated with UWB systems in comparison to narrowband systems and intensive research is still going on with this relatively new technology. Most UWB antennas proposed to date are planar printed or slot types. In the next few sections, the current state of the art of UWB communication antennas will be summarized. Comprehensive details of all the antennas for UWB communications is out of the scope of this thesis.

3.3 UWB Printed Antennas

UWB printed antennas are modified versions of narrowband planar antennas. These antennas are designed by adopting various bandwidth enhancing techniques of conventional printed antennas. These are the most popular among the UWB communication antennas as they are low profile, inexpensive and easily integrable with the other circuitry.

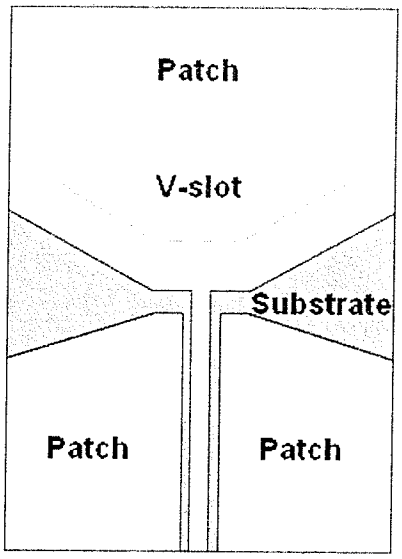

Fig. 3-1 CPW fed hexagonal patch antenna with 'V' slot

(SOURCE: [18] © 2004 IEE), permission granted on August 29, 2007

In April, 2004, Kim *et al.* [18] proposed a Co-Planar Waveguide (CPW) fed UWB antenna (Fig. 3-1) with size of 22.00 mm × 31.00 mm made on FR4 epoxy substrate with the impedance BW of 2.80- 10.60 GHz. The antenna has hexagonal radiating patch and a frequency notch of 10-12 dB at 5.25 GHz has been achieved by inserting a V-shaped slot. The slot has the half length of $\lambda/8$ at 5.25 GHz, which is the center frequency of WLAN frequency band. The notch frequency band of that antenna is changeable by adjusting the V-slot length. This antenna has the average boresight gain of 2.30 dBi and gain pattern is relatively stable in the whole UWB range. No time domain performance analysis of the antenna was presented.

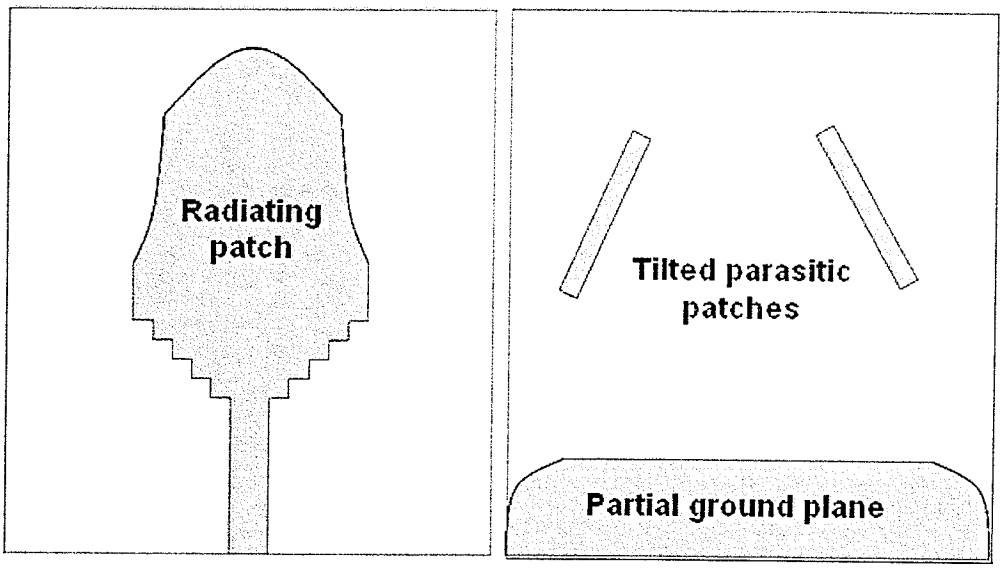

Fig. 3-2 Monopole with stair case and bell shaped patch (a) front view (b) back view

(SOURCE: [19] © 2005 IEE), permission granted on August 29, 2007

In July 2005, Kim *et al.* [19] proposed a microstrip fed UWB antenna of size 30.00 mm × 30.00 mm and with partial ground plane (Fig. 3-2). This antenna has the physical structure of staircase and bell shape that helps reduce the overall size of the antenna by lengthening the current path along the antenna length. A band rejection characteristic around center frequency of 5.00 GHz has been achieved by applying two tilted parasitic patches of length $\lambda/4$ at the back of the antenna side (Fig. 3-2). At the notch frequency current flows in the parasitic patches are in opposite directions to that of the main radiating patch and a null radiation is achieved. The gain of the antenna varies from 2.00 dBi to 6.00 dBi over the frequency band and radiation patterns are not very stable in the frequency band.

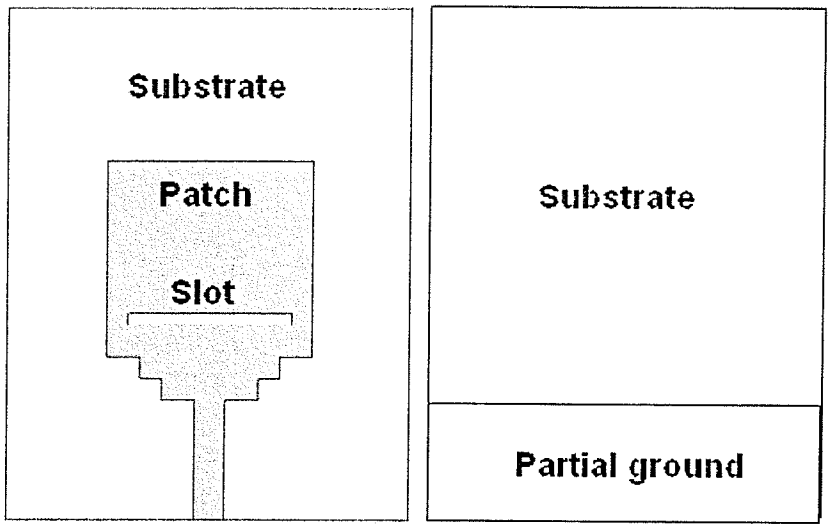

Fig. 3-3 Rectangular patch with two steps and one slot (a) front view (b) back view

(SOURCE: [20] © 2004 Wiley Periodicals, Inc)

A new UWB antenna with size of 35.00 mm × 30.00 mm was designed on an FR4 epoxy substrate by Choi *et al.* [20]. It has the impedance BW of 3.20-12.00 GHz. The antenna comprises some special features like rectangular patch with two steps, a partial ground plane and a single slot in the patch (Fig. 3-3). The antenna has the group delay variation less than 0.50 ns over the bandwidth of operation. However, the cross-polarization components of the antenna's radiation field are high and comparable to the co-polarization components. No features were proposed on that antenna design to have any band rejection capabilities.

A printed circular disc monopole antenna with partial ground plane (Fig. 3-4) with frequency bandwidth of 2.78-9.78 GHz has been proposed in [21]. UWB antennas very similar to that have been proposed in [25] that has elliptical radiating patch instead of

circular. Moreover, a size reduction method has been demonstrated by slight modification on the elliptical patch and introduction of top loading by modification of ground plane shape.

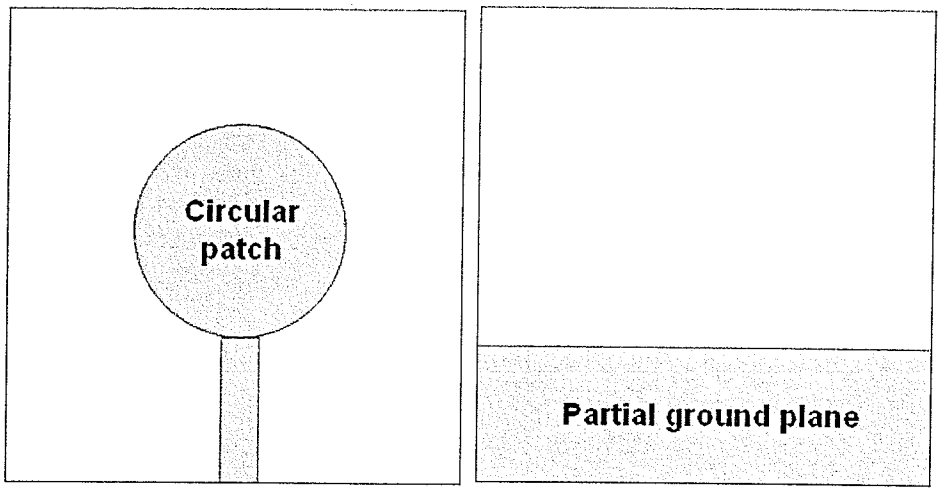

Fig. 3-4 Microstrip fed circular patch antenna (a) front view (b) back view

(SOURCE: [21] © 2004 IEE), permission granted on August 29, 2007

An interesting design named 'double sided printed bow tie antenna' has been published in [22], which is a modified form of conventional printed bow-tie antennas (Fig. 3-5). Thai antenna shows good matching (better than -10 dB) for the entire UWB band, while a conventional bow-tie can not be matched for such a BW. This antenna has a quasi-omnidirectional radiation pattern. Gain curve of this antenna is fairly flat over the frequency of operation and the antenna shows good phase response.

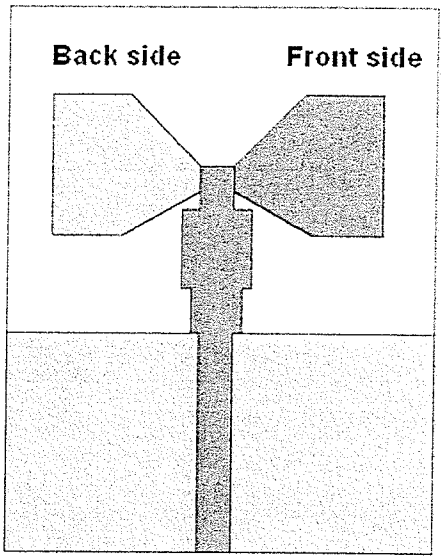

Fig. 3-5 Double sided printed bow-tie antenna

(SOURCE: [22] © 2004 IEEE), permission granted on September 4, 2007

Printed UWB planar monopoles with partial ground plane have been proposed in ([23]-[24]) for UWB communication applications which have good matching behaviors in the frequency of operation. But, no time domain studies were mentioned.

3.3.1.1 UWB Slot Antennas

UWB slot antennas are another vital group of antennas finding application in UWB communications. Actually, planar slot antennas have the capability to achieve impedance BW that covers the whole defined UWB range. Wide slot antennas have the same advantages as the printed antennas like small size, low cost, ease of fabrication and integrability to other RF circuitry [26]. In addition to these advantages, slot antennas can achieve very large impedance BW compared to the typical printed counterpart. Moreover, UWB slot antennas are less prone to the near-field coupling. This is a positive

feature that allows slot antennas to be used in near-field sensing applications as well. The drawback is that, as the slot size increases, radiation pattern usually starts to distort. An effective way to increase the BW of these antennas with reasonable slot size is to modify the feeding stubs [26].

There are numerous combinations of slot shapes like rectangular, square, circular, elliptical and some complex shapes. Feed shapes such as bow-tie, T, cross, fork-like, radial stub, double-T, pi, rectangular and circular have been proposed in the literature [26]-[38] It has to be mentioned that not all of these combinations give desired performance for UWB applications.

Qu *et al.* [26] proposed two wide slot antennas, one with CPW feed and one with microstrip feed. Both of the antennas show a very wide impedance BW and stable radiation patterns over a very wide frequency range. It was suggested that the radius of curvature of the arc of both slot and feed stub corners have a significant influence on the impedance BW and CPW fed slot antenna shows slightly better radiation performance.

Liu *et al.* [27] published a comprehensive study on the interaction between various feeds and slots. Based on [27], feed and slot of similar shape usually provide optimum coupling and feed area should be one third to half of the area of the slot (Fig. 3-6). In addition, feed-slot gap also plays a major role in the impedance matching of the UWB slot antennas. Moreover, slots of triangular shape usually give more stable radiation pattern compared to other slot shapes.

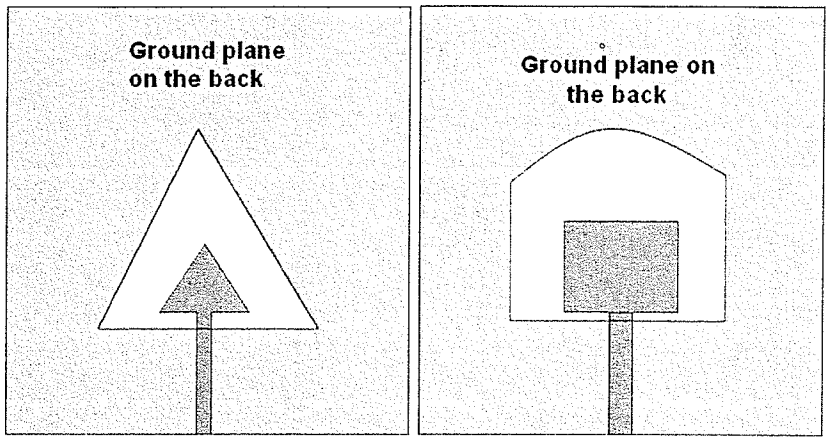

(a) (b)

Fig. 3-6 (a) Triangular slot antenna (b) rectangular slot antenna

(SOURCE: [27] © 2004 IEEE), permission granted on September 4, 2007

A compact circular slot antenna (Fig. 3-7) has been described in [28] which have the impedance BW of 143.20%. This antenna shows a stable radiation characteristic at higher frequency. On the other hand, size of the antenna is large compared to other wide slot antennas.

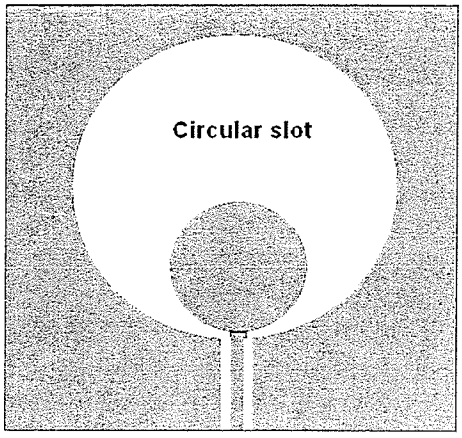

Fig. 3-7 Circular slot antenna

(SOURCE: [28] © 2006 IEEE), permission granted on September 4, 2007

Abbosh *et al.* [32] in 2006, proposed another circular slot antenna fabricated on RT6010LM substrate with a high dielectric constant value of ε_r =10.20. This antenna shows a very good omnidirectional property over the whole UWB range. It has also the band rejection capability from 4.00 GHz-6.00 GHz to avoid interference with the existing IEEE 802.11a and HIPERLAN/2 system. This band rejection at that desired frequency range are achieved by introducing a half circular slot with radius of $\lambda/4$ at 5.00 GHz in the circular tuning stub.

3.3.1.2 UWB Plate Monopole Antennas

Plate monopole antennas are another class of UWB antennas widely used in UWB applications which can exhibit a significantly broader BW. Most of these antennas suffer from degraded omnidirectional property at higher frequencies which is not desirable in communication applications.

Wong *et al.* [39] proposed a tri-plate monopole antenna constructed over a finite sized ground plane. Each plate is folded at two points. They are spaced 120^0 apart, and connected together at the antenna's central axis. The antenna also shows good gain characteristics over the operating BW.

Fabres *et al.* demonstrated UWB planar antenna design in [40] using plates which shapes like Double Square Plate (DSP), Rectangular Plate (RP), circular plate with slits along with an intensive study of current distribution along those structures.

Wong *et al.* [41] designed a planar square plate monopole with trident shaped feeding strips. This trident feeding helps to acquire more uniform vertical current distribution along the metal plate and thus improves the antenna polarization and matching characteristics. It was stated that trident feed can achieve impedance BW of three times more than that of the case of single feed.

Although, a great number of papers have been published based on the plate UWB antennas [42], planar antennas are more preferable in communication or Microwave Imaging (MI) applications due to their structural compactness and ease of fabrication.

3.3.2 UWB Antennas for Ground Penetrating Radar (GPR)

UWB technology is used in the pulse based technologies like radar as high resolution radar images can be attained with this technology. UWB antennas have found a great application in GPR to detect buried objects such as landmines. In addition, UWB antennas are being used in numerous radar systems for applications like locating steel reinforcement bars in the concrete construction, identifying electrical wiring behind walls, locate trapped persons under debris or snow, and locating hidden persons behind a wall [43].

As MI has some similarities with GPR, antennas used for GPR systems are also potential candidates for the use in MI.

The TEM horn is a widely used antenna for GPR applications. However, modifications are required to the conventional horn antennas for GPR applications as these antennas are subject to large geometrical size, poor matching to ground and most importantly, late time pulse ringing. To overcome these difficulties, dielectric loading of the horn antennas is usually adopted [44], [45].

A microstrip line fed UWB quasi-horn antenna has been proposed in [44] which has a bandwidth of 100 MHz to over 20.00 GHz, reasonably large radiation gain (8 dBi at 2.6 GHz, 16.50 dBi at 18.00 GHz). Furthermore, this antenna does not require a balun at the input, and for monostatic radar application, good isolation can be achieved between the transmitted and received signal. Dielectric foam is used to gradually raise the radiating conductor away from the ground and thus increase antenna radiation [44]. This antenna possesses some drawbacks. The beamwidth of the radiated signal is not controllable and the abrupt termination of the ground plane causes undesirable effects in the near-field that makes it unsuitable for some sensing applications such as medical imaging.

A TEM-horn filled with a dielectric material with permittivity (ε_r) of 4 has been proposed in [45] which has reduced sensitivity to external Electromagnetic Interference (EMI). Instead of triangular conductors, a specially optimized gradual variation of conducting plate has been designed to reduce reflection in the horn. Thus, the impedance through the antenna changes smoothly from 50Ω to $\frac{120\pi}{\sqrt{\varepsilon_r}}\Omega$ and provides a smooth transition of EM waves from antenna to outer space. This antenna shows stable radiation characteristics over a large span of frequency and has a good control of radiation pattern. The difficulty

with this antenna is its large geometrical size which makes it impractical for microwave imaging applications.

Bow-tie antenna families are also widely used in GPR applications. Various modifications have been proposed in the simple bow-tie antennas to improve pulse radiation efficiency and reduce late time ringing. Lasteri *et al.* [46] proposed a UWB bow-tie antenna for GPR where combinations of constant resistive loading and linear capacitive loading have been applied for both improving the pulse radiation and reducing the ringing in the tail. The resistive loading was implemented by using a volumetric microwave absorber at one side of the bow-tie structure and a linear profile of capacitance has been achieved by introducing slots of various sizes along the bow-tie's wings. Although this antenna provides an excellent performance in GPR applications, it is not feasible in UWB MI set up because of its very large geometrical features.

3.4 Microwave Imaging (MI) for Breast Cancer Detection

Researchers are finding new applications for MI in a variety of applications, especially in the field of biological sensing. Moreover, this technique can be utilized for applications like detecting 'water trees' in transmission cable shielding. Among the biological applications, MI has the potential to evaluate the internal properties of breast tissues to detect abnormalities. This is possible due to the high contrast in dielectric properties between the normal and cancerous tissues [2]. To date several methods for microwave

breast imaging have been proposed and successfully implemented. As this thesis mainly focuses on antenna design for microwave breast imaging, a short description of existing detection techniques of breast cancer will be described to provide an insight about the previous and current trends of this research area.

3.4.1 Breast Cancer Detection Methodologies

X-ray mammography is the most prevalent techniques used widely in clinical diagnosis of breast cancer. In addition, Ultrasound, Magnetic Resonance Imaging (MRI), Position Emission Tomography (PET), and electrical impedance scanning are the other techniques being used for detection and diagnosis of breast cancer.

X-ray imaging is a transmission-based method where X-rays from a source pass through the patient and are detected either by a film or an ionization chamber. The X-ray image is based on the differential attenuation of X-rays in different tissue types [47]. X-ray mammography sometimes can not detect all the lesions and it has the miss rate of 10%-15 % [48]. Sensitivity of this method is dependent upon the density of the breast tissues and hormone status of the patients. The quality of image depends on positioning and compression of the breast. Moreover, as the ionizing radiation used by this technique has the danger of damaging tissues, there is a limit on the quantity of the total radiation that a patient can be subjected. Another relatively new technique, digital mammography uses a phosphor screen instead of screen/film combination. This method has reduced radiation dose and images can be stored and retrieved electronically. In addition, image contrast can be adjusted after the X-ray has been taken [47].

In Ultrasound or sonography, high frequency sound waves are reflected from tissues where there is a change in acoustic impedance, and the echoes are used to produce a two dimensional image of the breast. Ultrasound is extremely safe, noninvasive, portable, and relatively inexpensive. It has the ability to distinguish between fluid filled cysts or solid mass in the breast. Moreover, this method is effective for detecting cancer in dense breast tissues [47]. On the otherhand, for impalpable lumps or test operated by inexperienced technologists, Ultrasound can miss the area of interest. Incorrect gain (amount of sound) can also give erroneous test results [48].

MRI is a non-ionizing technique where radio waves and strong magnets are used instead of X-rays. MRI has the full three dimensional imaging capabilities and high spatial resolution (~ 1 mm) [47]. MRI has high sensitivity and so it has high false positive rate. This feature can leads to additional biopsy or work up of the patients. Sometimes MRI can not accurately distinguish between the cancerous and benign conditions. MRI is incompatible for the patients having any permanent ferrous magnetic implants or electronic devices such as pacemaker. Moreover, cost of the MRI scanner is high and it has long examination time. The long term effects of MRI have not properly understood yet and pregnant women are usually advised not to have MRI scan.

In addition to the above mentioned methodologies, various MI techniques mainly classified as passive, hybrid and active methods have been proposed as complements to conventional breast cancer screening.

3.4.1.1 Hybrid MI

Among the hybrid approaches of MI, microwave induced acoustic imaging is the most prevalent which uses microwaves to illuminate the breast tissue. As a result of the illumination by microwaves, selective heating in the malignant tissues occurs. This is due to their higher conductivity and permittivity compared to the normal breast tissues. This heating effect causes expansion of the tissues that generates pressure waves. These pressure waves are detected by ultrasound transducers [49].

3.4.1.2 Active MI

Active MI techniques have been an issue of theoretical and experimental study. Basically two major approaches have been developed: microwave tomography and confocal imaging [49].

3.4.1.2.1 Microwave Tomography

Microwave tomography is one of the most prevailing methods among various active approaches. In this method, the imaging object is immersed in a matching medium depending on its appropriateness for reducing unwanted reflection in the sensor-imaging object interface. Then the imaging object is illuminated by the transmitting antenna system and the scattered field from the breast tissues is captured at different locations surrounding the breast. This measured field is then used to reconstruct shape, location, permittivity, and conductivity profiles to determine exact condition inside the breast. Depending on the object dimensions, separations, discontinuities and inhomogeneities,

the electromagnetic waves undergo multiple scattering within the imaging object. This results in a non-linear problem [49]. Solving inverse scattering problems at microwave frequencies is computationally intensive because of this non-linear nature of the problem. Nonlinear inverse problems can be dealt with by applying iterative optimization methods such as Genetic Algorithms (GA), Particle Swarm Optimization (PSO) and Born iterative approximations. A cost function, which is related to the difference between the predicted scattered field from the object and corresponding measured field, is optimized using an efficient global optimization technique [50].

3.4.1.2.2 Confocal MI

In Confocal Imaging (CI) images are reconstructed by synthetically focusing reflections from the breast tissue and thus this method avoids a complicated image reconstruction algorithm. After illuminating the breast with a low power UWB pulse, the reflected field is measured by the same antenna system located in a fixed position on the top of the breast. To enhance the reflected field from the high contrast region and reduce clutter, a simple time shifting and summing algorithm is applied [51].

3.4.1.2.3 Advantages of Active MI

Active MI has drawn attention of researcher because it offers several potential advantages over the other existing screening methodologies for breast cancer detection. The most important advantage of this method is its potential to offer improved sensitivity and specificity [5]. Though, there has been a lot of progress in mammography; but it still has certain limitations. A study reports that approximately 4%-34% cases of breast cancer are

missed when screened by conventional mammography which can result delay in diagnosis or poor prognosis for the patient [6]. Moreover, conventional mammography fails to distinguish between malignant and benign tissues. In 70% of the cases, cancer detected initially by mammography turned out to be benign [7]. MI could be used as a complementary method in these cases. It is based on the contrast between the electrical properties between the normal and cancerous tissues. Because of the significant contrast, this method has the potential to distinguish between the malignant and the benign tumors and to reduce the false positive rates which is the ratio of false positive test results to total number of patients without disease.

MI offers a very low health risk to the patients as this is a non-ionizing and non invasive method with very low power level [5]. X-ray may cause some detrimental effects to the healthy tissue like risk of radiation induction cancer. It has been stated in [8] that, a woman of before certain age can have more risk of getting cancer caused by mammography than if she had no screening. As an example, a woman screened annually for 40 years from 25-64 or 30-69 years of age with a radiation level of 2 milligray (mGy) per film would have a total risk of radiation induction breast cancer of 0.12% or 0.24% respectively [8].

Another important issue of this method is its versatility. Mammography can not perform well in physically dense tissue. In that case, Ultrasound is usually the alternative option. Ultrasound has also some limitations for breast cancer screening [6]. On the other hand, MI is not based on density of the tissues. Therefore, it does not have this limitation of

detection difficulties in dense tissue and it has a good potential to detect breast cancer among young women.

Conventional mammography is sometimes not comfortable for the patients due to requirement of breast compression [5]. On the other hand, in MI painful breast compression is not required.

3.4.1.2.4 Drawbacks of Microwave Breast Imaging

Although active MI method for breast cancer detection has a very good potential to establish itself as a reliable screening technique, it possess some drawbacks. The shape and the spatial distribution of the dielectric properties of the imaging object are derived from the transmitted (incident) and scattered or reflected (received) field components. Because of objects dimension, separation, discontinuity and inhomogenities, the electromagnetic wave can experience multiple scattering within the object. This introduces non-linearity in the problem and solving inverse scattering problems with non-linear property is complex and difficult in tomography. However, this is not a significant issue if small geometries like breast tumor are being imaged [49]. The spatial resolution of the image constructed with MI is not as good as that of conventional mammography. However, cancerous tissue can still be detected because of the excellent sensitivity of this method [5].

3.5 Antenna Design Requirements for MI

For MI application, in order to recognize closely separated scatterers in the imaging object, a short pulse is required for transmission. If the spatial width of the incident pulse is wider than the object it reflects from, it is difficult to precisely detect the scatterers. Thus, the resolution of image depends greatly on the bandwidth of the applied pulse signal. Therefore, one of the key challenges of UWB antenna design for MI is to achieve a wide impedance BW for distortionless short pulse radiation, while still maintaining acceptable overall efficiency. Impedance matching in a frequency span of at least 7.50 GHz which corresponds to BW greater than 100% of the center frequency is crucial. This ensures that most of the energy is being transmitted and not reflected back from antenna input port as UWB systems operates on very low power level (-41.3 dBm/MHz). It is even more important for the received scattered signal from the imaging object not to be reflected back from receiving antenna because magnitude of the reflected signal has been attenuated significantly.

Aside from attaining sufficient BW, phase linearity is also required for optimal wave reception. This corresponds to near constant group delay within the bandwidth of operation. Group delay is determined by the derivative of the unwrapped phase of an antenna. If the phase response of the antenna is linear throughout the frequency range, group delay will be constant for that frequency range. This phenomenon is an important characteristic used to evaluate a UWB antenna performance because it helps to indicate

how well a UWB pulse will be radiated and to what extent it may be distorted or dispersed.

The radiation pattern and efficiency of UWB antenna are also two significant features which have to be emphasized as well. If the radiation beamwidth is too wide, clutter is introduced because reflections from outside the volume of interest arrive at the antenna and resulting image will have smeared reflections. However, at the same time if the beamwidth of the antenna is too narrow to illuminate the entire volume of interest, more scans are required, but a higher quality image can be obtained with small beamwidth.

To maintain distortionless radiation characteristics over the entire operating frequency with high Polarization Efficiency (PE), cross-polarization components of the antenna have to be small compared to the co-polarization components.

High radiation efficiency over frequency band of operation is imperative for UWB antenna because, as mentioned, power level of the UWB systems is quite low. Excessive losses incurred by antenna can potentially compromise its performance in the imaging system. Conductor, dielectric and other losses have to be minimized in order to maximize the overall radiation efficiency.

Size of the antenna is another considerable feature for imaging purpose that has to be taken into account. A small geometry of the antenna makes it easy to selectively illuminate the object and permits scanning physically close to the subject. On the other

hand, as the antenna size becomes smaller, the radiation efficiency and directional property degrade.

3.6 Some Antenna Designs for MI

As a main sensor in UWB MI set up, selection of proper antenna is crucial. There is intensive ongoing research to optimize the best possible antenna set up for MI. However, the design of high performance antenna system offers significant challenges, as lots of design and performance constraints have to be satisfied.

Fear *et al.* [11] in 2000 used resistively loaded (Wu-King resistive loading profile) dipoles with different lengths in their MI set up as a preliminary system evaluation. These dipoles exhibit well known behavior and they are very easy to construct. However, the BW of resistively loaded dipoles is not sufficient to generate good resolution images. Moreover, resistive loading affects the overall efficiency of the antenna. In addition, control over the radiation pattern can not be achieved through these dipoles. This antenna was chosen due to its compactness.

One of the major problems associated with UWB antennas is its late time pulse ringing effect which is due to reflection of signals at the end of the antenna structure. Typical resistively loaded conical and bow-tie antennas have end reflections 40-50 dB below the exciting pulse [12]. This level of reflection is still not acceptable for biological tissue sensing. A UWB reverberation bow-tie antenna has been proposed in [12] that overcomes this difficulty. The end reflection was found to be -106 dB relative to the exciting pulse.

Li *et al.* [10], in 2003, proposed a small modified UWB ridged pyramidal horn antenna with curved launching plane with the operating frequency of 1.00 GHz-11.00 GHz (Fig. 3-8). The antenna configuration includes a pyramidal horn radiation cavity, a metallic ridge, and a curved metallic launching plane terminated with two parallel chip resistors, 100Ω each. The horn section is connected to the outer conductor of the coax providing current return path and thus eliminates the requirements of a balun and directs radiation to a certain specific direction which makes the antenna directive in nature. The launching plane of this antenna curves towards one of the sidewalls of the horn and is tapered to the feeding point of the antenna. Microwave energy is directed and launched to the surrounding medium by the launching plane and the resistors attached at the terminal of the launching plane helps to suppress reflections from the end.

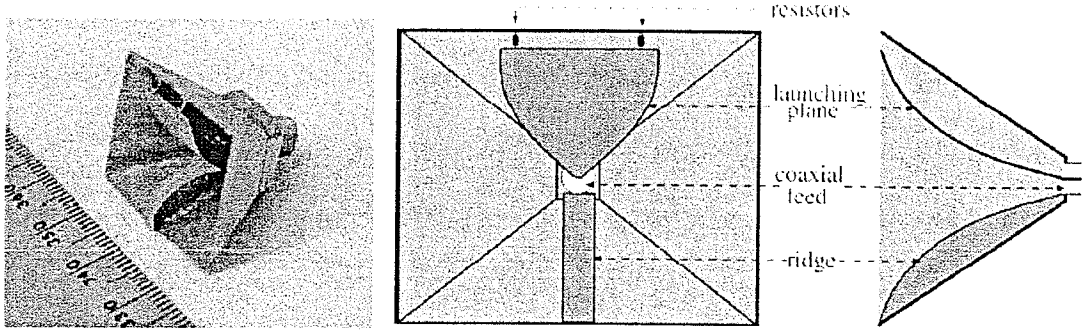

(a) (b)

Fig. 3-8 (a) The pyramidal ridge antenna (b) end and side view of the antenna

(SOURCE: [10] © 2003 IEEE), permission granted on September 4, 2007

The optimized antenna has overall aperture size of 2.50 cm × 2.00 cm and maximum depth of 1.30 cm. Even though this antenna shows good signal fidelity, its radiation

efficiency is not good because of the termination resistors used at the launching plane. Moreover, late time ringing effect is significant for this horn antenna. Fabrication complexity is another issue that makes this antenna inconvenient in some cases.

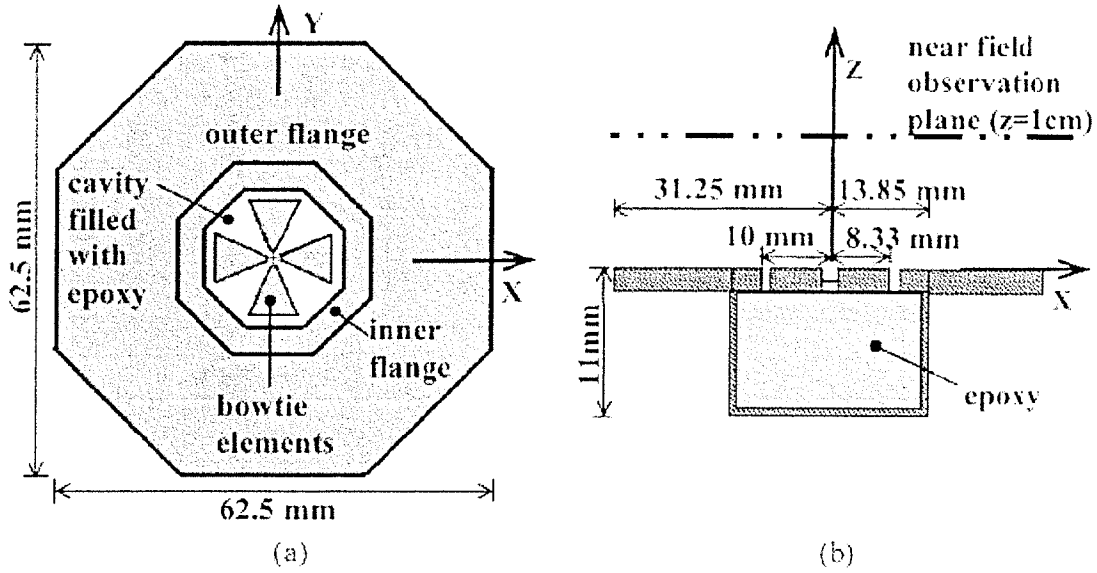

Fig. 3-9 (a) Top view of the antenna system (b) cross section view of the antenna

(SOURCE: [3] © 2005 IEEE), permission granted on September 4, 2007

Yun *et al.* [3] in 2005 introduced a compact antenna system (Fig. 3-9) with two bow-tie elements for their radar based breast cancer detection with operating frequency of 2.00 GHz-4.00 GHz. This antenna system was designed to image tumor with cross-polarized reflections method. The antenna configuration includes two crossed bow-tie elements with flare angle of 45^0 over an octagonal cavity and an attached metal flange. The whole antenna system was immersed in liquid of dielectric property similar to fatty tissue (ε_r=9.00, σ=0.20 S/m) (Fig. 3-9). The octagonal cavity of quarter wavelength at center frequency (3.00 GHz) helps to block electromagnetic waves radiated away from the

breast. The flange facilitates the suppression of unwanted waves e.g. surface waves. As the antenna does not have sufficient BW to radiate narrow UWB EM pulse, it is not possible to generate high resolution images with this antenna. It can only be used for detection.

3.7 Chapter Summary

Introduction to UWB antennas along with some literature reviews focused on UWB antennas for communication, GPR and imaging were the main topic of discussion in this chapter. Moreover, a brief description of various features of MI for breast cancer detection and antenna design requirements for this application were studied.

In this thesis, design details of two UWB planar antennas, one printed and one slot type have been discussed. These have the potential to be used in a MI set up. The initial designs were based on the free space characterizations of antennas. Then, a study of the performance of the designed antennas immersed in three different matching materials was performed to investigate the feasibility of using them for microwave breast imaging. In the next chapter, the first proposed UWB printed monopole antenna will be introduced with its different design features and computed and measured performance will be studied.

Chapter 4 : Diamond Shaped Printed UWB Antenna

4.1 Introduction

Closed forms of analytical formulations can not be established for most of the UWB antenna designs. In fact, UWB antenna design is as much art as it is science. In this chapter design of a novel diamond shaped planar monopole UWB antenna [53], [54] is described which can be used for MI purpose. This antenna has free space measured impedance BW ($S_{11} \leq$-10 dB or VSWR ≤ 2) of 3.80 GHz-11.85 GHz which almost covers the whole UWB BW. Moreover, radiation patterns and group delay of the proposed antenna have been investigated. Antenna radiation characteristics in free space as a simple linear array are also demonstrated. In addition, antenna time domain radiation performance is studied. At the end, the antenna RL when it is immersed in three different matching materials is investigated.

4.2 Development of the Proposed Design

The UWB planar monopole antenna with partial ground plane and various patch shapes has been proposed in [19]-[24] having different sizes and features. Initially, rectangular patch shape with steps [19] with three different patch length with value around half wavelength at lower cut-off frequency of 3.10 GHz has been studied (parameters in Table

4-1). The antenna parameters have been obtained using commercially available simulation software Ansoft HFSS [55] which is a based on Finite Element Method (FEM). FR4 epoxy (ε_r=4.60) with thickness 1.60 mm has been chosen as the substrate material. The antenna feeding structure is a 50Ω microstrip line.

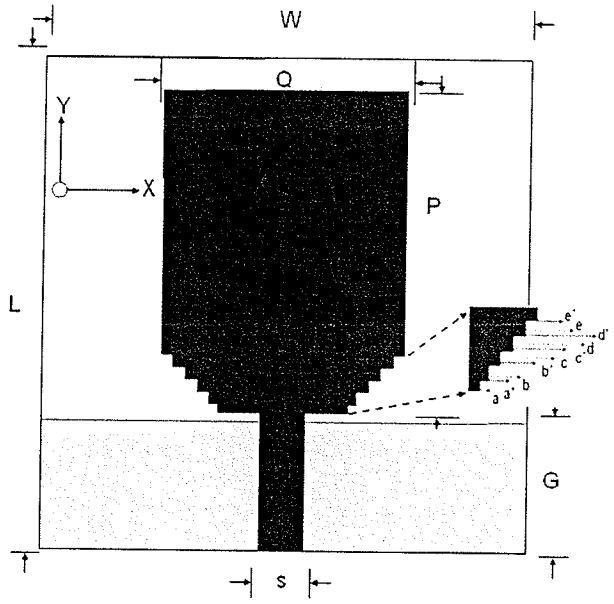

Fig. 4-1 Planar monopole with rectangular patch

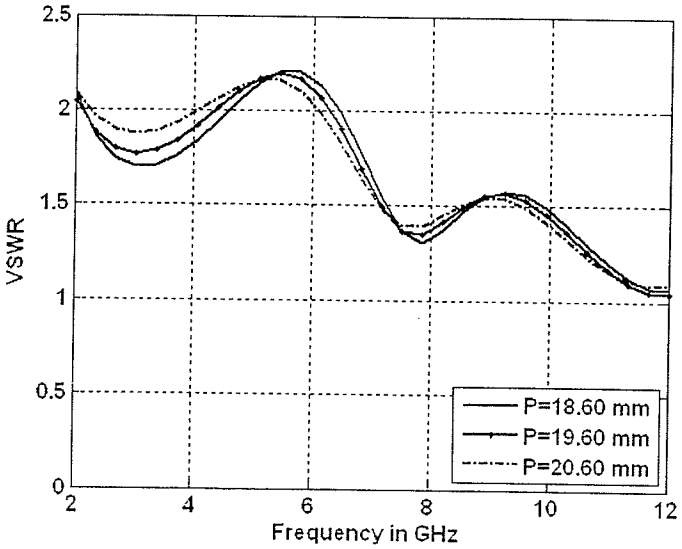

Fig. 4-2 Simulated VSWR for the antenna configuration of Fig. 4-1

Fig. 4-2 shows the simulated VSWR plot for the antenna shown in Fig. 4-1. In this configuration, an impedance mismatch for a span of about 2.00 GHz in the UWB frequency range occurs for each of the monopole length (P). With the increment of the patch length (P), this mismatched band shifts towards lower frequency (Fig. 4-2).

Table 4-1 Parameters of the rectangular shaped planar monopole (parameters shown in Fig. 4-1)

Antenna parameters	Dimensions (mm)
W	30.00
L	30.00
S	2.72
G	7.90
Q	15.00
a	0.50
a'	0.50
b	0.50
b'	0.75
c	0.75
c'	0.75
d	0.75
d'	0.75
e	0.75
e'	0.75

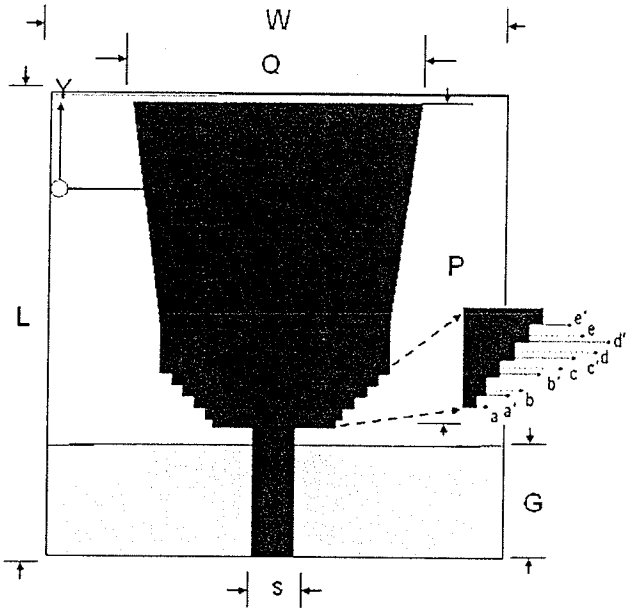

Fig. 4-3 Monopole with patch widened at the top

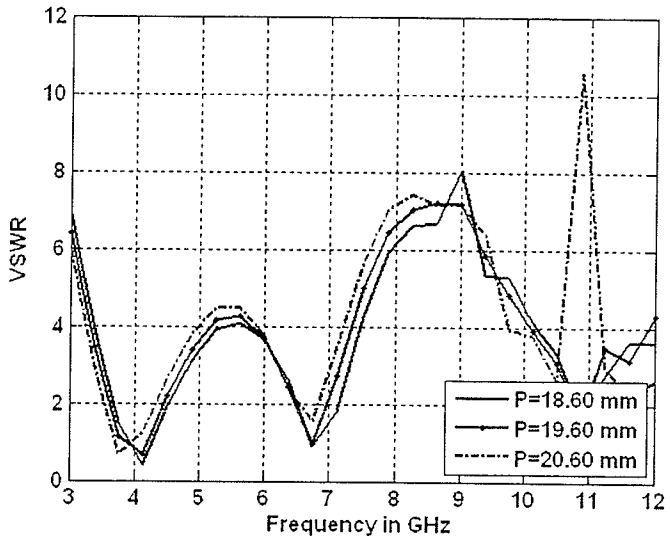

Fig. 4-4 Simulated VSWR for the antenna configuration of Fig. 4-2

For the case of widening of the radiating patch at the top (Fig. 4-3) the matching characteristic of the monopole antenna gets worse. Fig. 4-4 shows the VSWR as a function of frequency for the monopole configuration of Fig. 4-3 with three different

lengths (P). Monopole with widened patch shows very poor matching characteristics (Fig. 4-4) over the UWB frequency range.

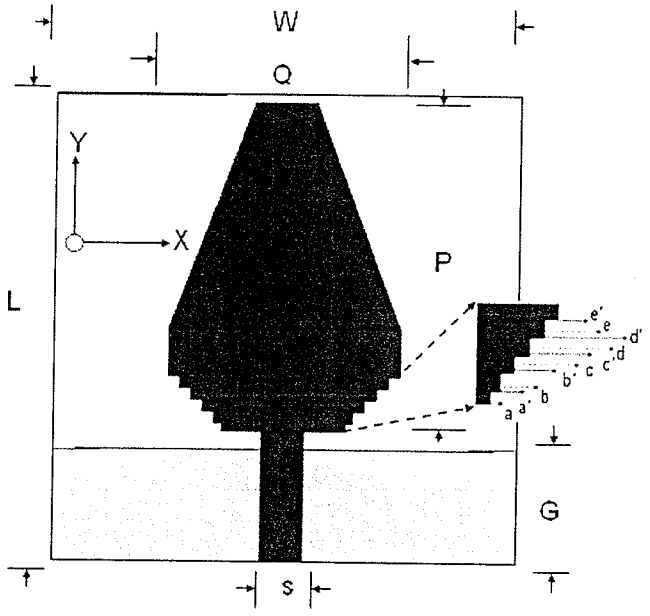

Fig. 4-5 Monopole with patch narrowed at the top

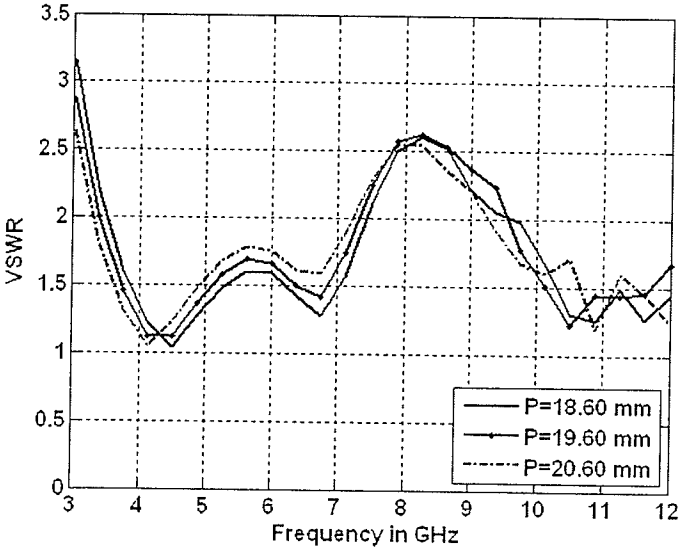

Fig. 4-6 Simulated VSWR for the antenna configuration of Fig. 4-5

Narrowing the monopole patch at the top (Fig. 4-5) has the reverse effect on the impedance matching characteristics than that of widening the patch (Fig. 4-3). The reason is that, by narrowing the patch, more variation in the length of the monopole can be achieved which can support more resonant modes within the frequency of operation, and thus increase the total BW. Fig. 4-6 shows the simulated VSWR plots of the antenna (parameters shown in Table 4-1) with three different heights (P) and and Q of value 19 mm. For the antenna configuration of Fig. 4-5, slight mismatch around 8.00 GHz still persists.

4.3 Geometry and Design of the Diamond Shaped Planar Monopole

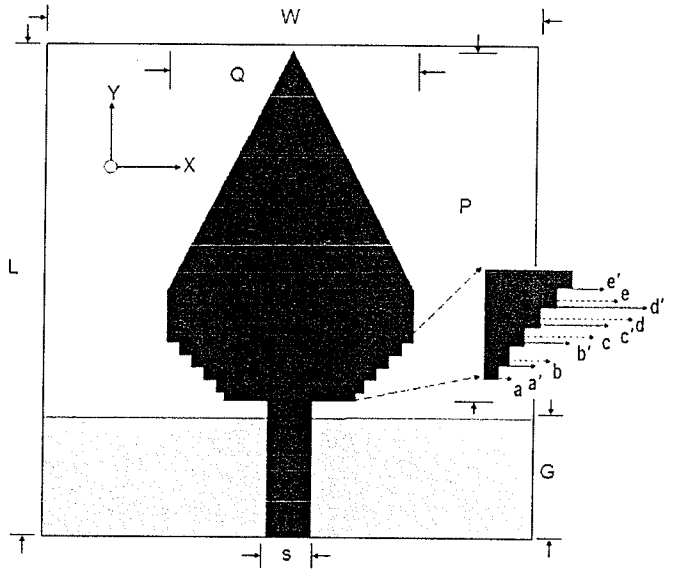

Fig. 4-7 Geometry of the diamond shaped antenna, sizes are given in Table: 4-1

In section 4.2, it was shown that by narrowing the monopole patch, antenna impedance matching characteristics can be improved. With this consideration in mind, monopole configuration with triangular patch has been adopted. Fig. 4-7 shows the geometry of the designed planar monopole antenna. The triangular shaped patch facilitates more variation of resonant lengths along the antenna and helps to achieve better impedance BW. The physical structure of five steps increases the effective electrical length at the lower frequency band (3.00GHz-4.00 GHz) and they help to reduce the overall physical structure of the antenna. Another theory that motivated the introduction of steps is that, their edges and corners provide current nulls, which leads to lower VSWR at nonresonant frequencies. Therefore, this helps achieving a broader impedance BW [43]. Moreover, the triangular radiating patch has more constant radiation characteristics over the wide frequency range when compared to some other patch shapes [27].

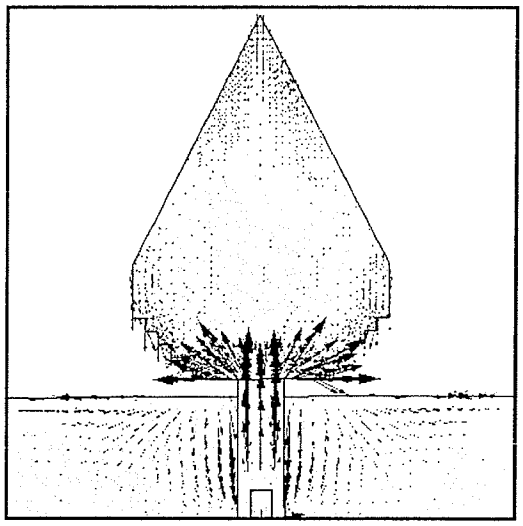

Fig. 4-8 Simulated current distribution along the antenna patch and ground plane at 4.00 GHz

Fig. 4-8 is the simulated current distribution along the patch and ground plane of the antenna. The tuned critical antenna parameters are tabulated in Table 4-2.

Table 4-2 Critical design parameters of the diamond shaped antenna (parameters shown in Fig. 4-1)

Antenna parameters	Dimensions (mm)
W	30.00
L	30.00
S	2.72
G	7.90
P	21.00
Q	15.00
a	0.50
a'	0.50
b	0.50
b'	0.75
c	0.75
c'	0.75
d	0.75
d'	0.75
e	0.75
e'	0.75

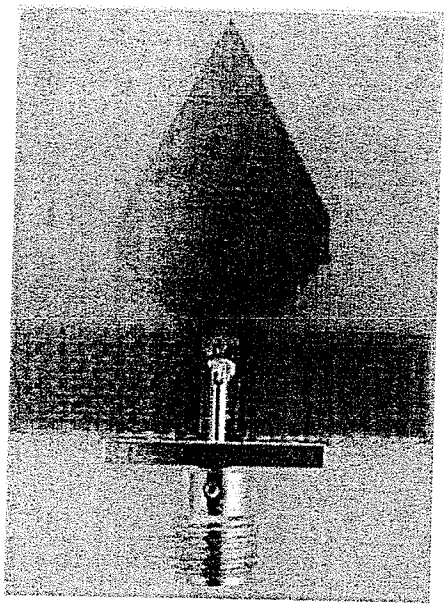

Fig. 4-9 Photograph of the fabricated antenna

4.4 Performance Analysis and Measurement

4.4.1 Antenna in Free Space

The designed antenna was fabricated (Fig. 4-9) in the machine shop at the University of Manitoba and several antenna performance measurements was performed in the antenna lab to verify the validity of the design. The antenna's free space RL, VSWR and group delay measurements were performed using Anritsu ME7808A Vector Network Analyzer (VNA). The antenna radiation pattern measurement was done in the anechoic chamber with CATR facilities (Section. 2.3.2).

4.4.1.1 Return Loss and VSWR

As mentioned earlier, antenna matching is the indication of how much power from the source network arrives at antenna port for radiation and how much is reflecting back. It is one of the prime characterizing features about antenna performance. Input impedance should be matched to the connecting network for efficient radiation and reduced power loss due to reflection.

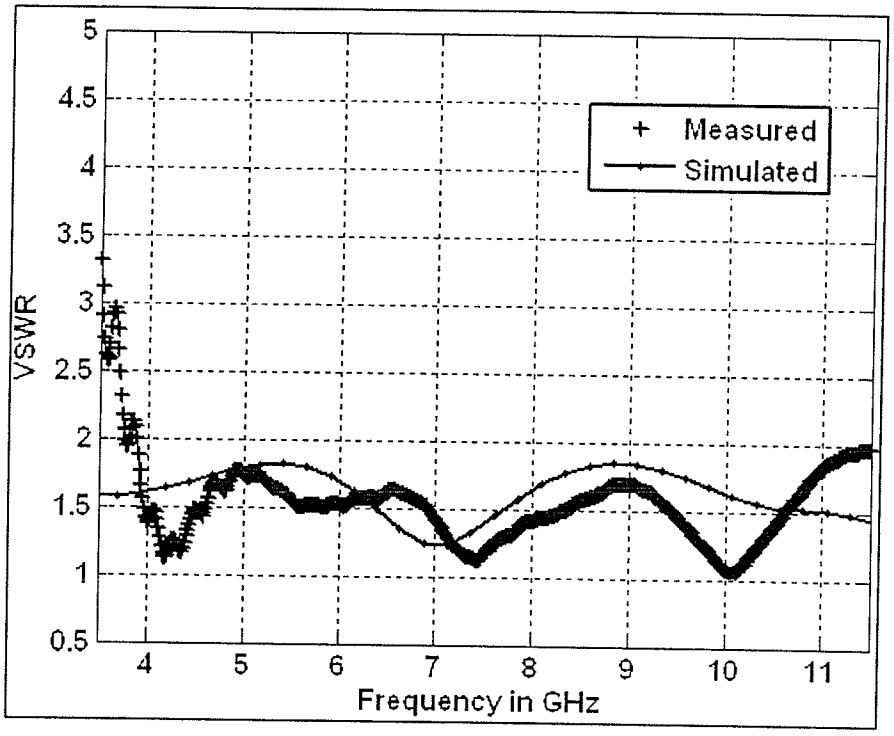

Fig. 4-10 Measured and simulated VSWR

From the plot of the measured VSWR (Fig. 4-10) it can be shown that an impedance BW ($S_{11} \leq$ -10 dB or VSWR ≤ 2) of (3.80 GHz to 11.85 GHz = 8.05 GHz) has been achieved. However, the simulated result displays a larger bandwidth and higher upper cut-off

frequency. A probable explanation for this anomaly of predicted and measured VSWR is the intrinsic properties of FR4 substrate that has been used to design this printed antenna. FR4 is a lossy dielectric whose dielectric constant and dissipation factor are not stable within the range of frequency. This inconsistent behavior of the substrate may be one reason of this anomaly. In addition, as this omnidirectional antenna radiates in all directions, reflections of the radiated waves occur from surrounding devices, cables and the walls of the lab which were not taken into account in the simulation. Moreover, there might be slight discrepancy while fabricating the antenna with small structural features that could also cause this deviation of the result.

4.4.1.2 Measured Group Delay

Group delay and phase linearity are not emphasized in the most narrowband antenna specifications. This is because the band of resonance in a narrowband antenna is governed by the frequency at which the antenna input impedance achieves a linear phase shift of 180^0. This implies the situation of LC resonance and with this condition input impedance has only real component. Phase non-linearity of antenna is basically caused by the reactive components of the input impedance. Narrowband antennas usually show linear phase response and constant group delay at the vicinity of resonant band [43]. As mentioned above, the phase of the radiated field by UWB antenna should be as close to linear as possible with respect to frequency so that it will not distort the shape of the transmitted electrical pulse. In a very broad frequency span, there are modes throughout the frequency band that contain more power than others. Therefore, perfectly linear phase

is not entirely attainable throughout this large frequency bandwidth, and a phase shift is expected.

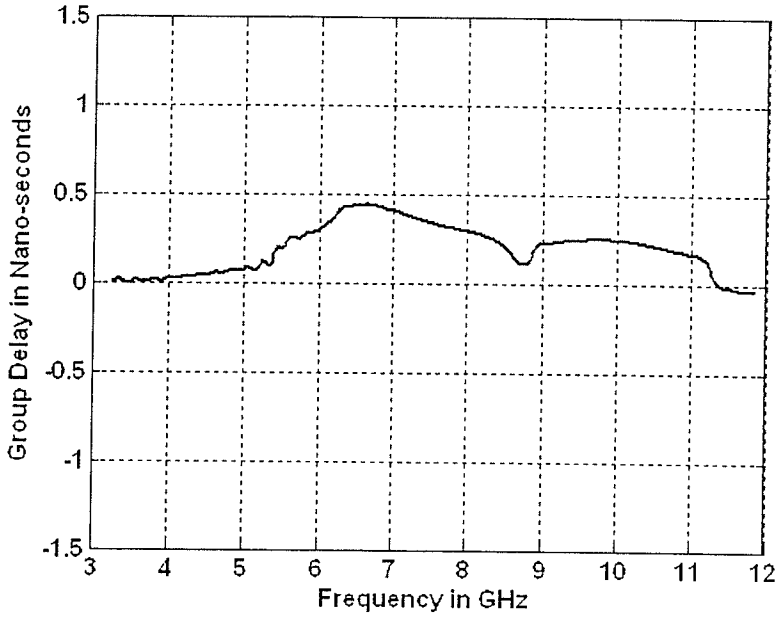

Fig. 4-11 Antenna's measured group delay

The plot of Fig. 4-11 is the group delay variation as a function of frequency, which is obtained by taking the first derivative of the phase of the antenna. It was measured by Anritsu ME 7808 VNA. From Fig. 4-11, it is evident that maximum group delay measured throughout the BW is 0.47 ns. Therefore, it can be expected that, pulse transmitted or received by the antenna will not be seriously distorted, retaining its shape. As VNA provides plots of the difference in group delay with respect to free space, this value can be of negative value at some frequencies. Negative values of group delay in Fig. 4-11 after 11.40 GHz is because of this reason.

4.4.1.3 Radiation Pattern

Antenna radiation pattern demonstrates the spatial distribution of the radiated field components at a certain frequency. By observing the stability of radiation pattern over the bandwidth of operation, antenna's performance stability can be evaluated. Moreover, radiation pattern plots give the insight of the relative magnitude of co-polarization and cross-polarization components in certain observation planes. The following plots (Fig. 4-12 to Fig. 4-14) are the measured and simulated gain patterns at different frequency values (i.e. 4.00 GHz, 6.00 GHz, and 10.00 GHz) in the two principal planes XZ ($\varphi=0^0$) and YZ ($\varphi=90^0$), when the antenna lies on the XY ($\theta=90^0$) plane (Fig. 4-7). Fig. 4-12 (a) is the XZ plane ($\varphi=0^0$) gain patterns at 4.00 GHz where co-polarization components show omnidirectional radiation characteristics for both the simulated and measured cases. The small ripples in the measured gain patterns are due to the interaction between the antenna and the support for the measurement set up. Fig. 4-12 (b) is the YZ plane ($\varphi=90^0$) patterns, which represent the antenna's bidirectional radiation property with peak radiation directed along at $\theta=0^0$ and $\theta=180^0$. As the antenna is very small in size, radiation from the long connecting cable in the measurement set up was significant and it added to the cross-polarized field of the antenna in that plane ($\varphi=90^0$). This could be the reason for higher cross-polarization levels than the simulated values in the YZ plane.

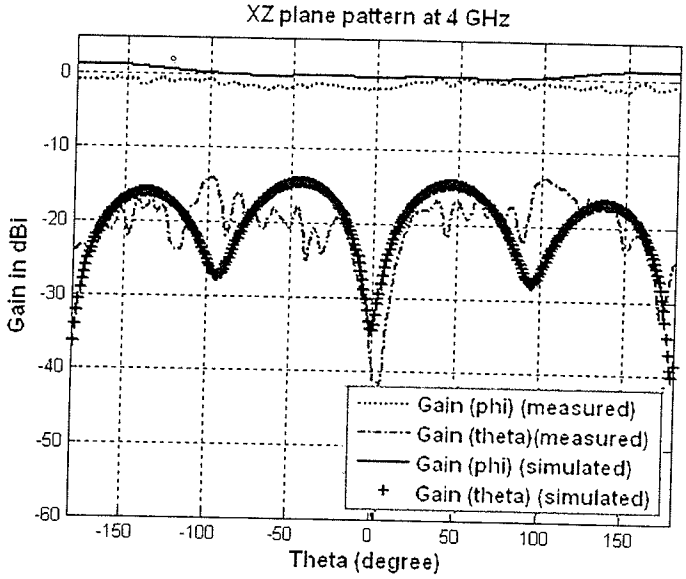

(a)

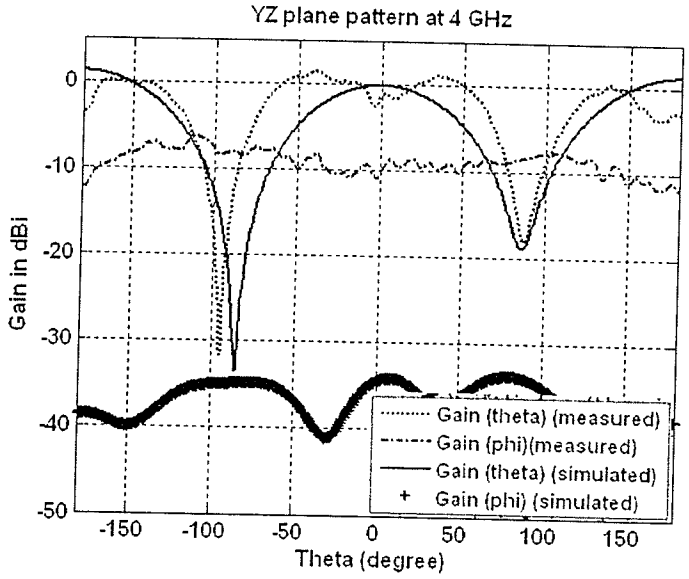

(b)

Fig. 4-12 Measured and simulated gain patterns at 4.00 GHz (a) XZ ($\varphi = 0^0$) plane (b) YZ ($\varphi = 90^0$) plane

Fig. 4-13 (a), (b) are the gain patterns at 6.00 GHz at XZ ($\varphi=0^0$) and YZ ($\varphi=90^0$) planes. At 6.00 GHz, gain in XZ plane ($\varphi=0^0$) has omnidirectional property like at 4.00 GHz. In

YZ ($\varphi=90^0$) plane, the antenna has bidirectional property with maximum measured gain of 2.82 dBi at 6.00 GHz.

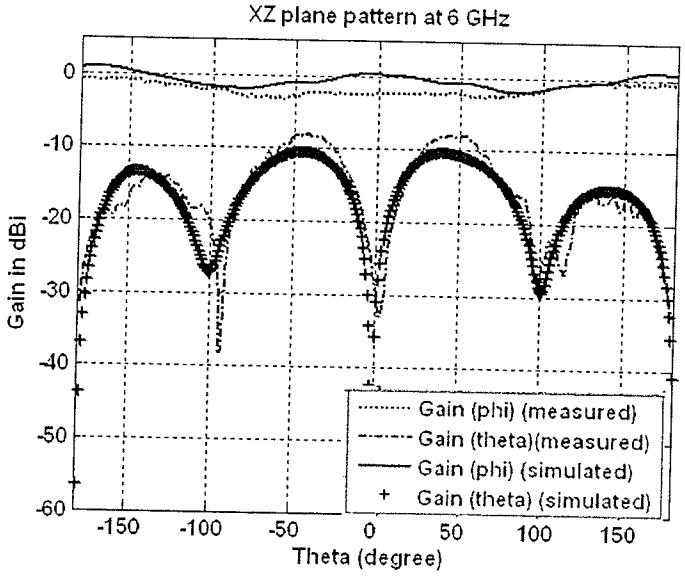

(a)

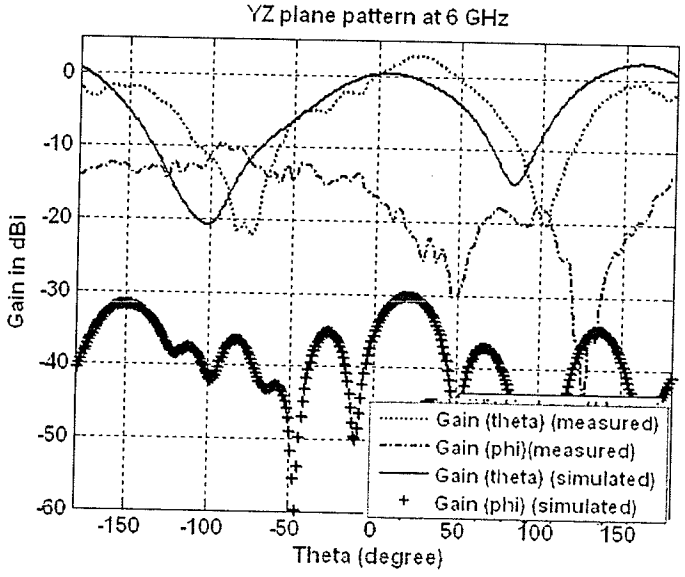

(b)

Fig. 4-13 Measured and simulated gain patterns at 6.00 GHz (a) XZ ($\varphi= 0^0$) plane (b) YZ ($\varphi=90^0$) plane

Patterns at 10 GHz are shown in Fig. 4-14 (a) and (b). At 10.00 GHz, the cross-polarization levels increase significantly in both planes. Normalized polar plots of gain at 4.00 GHz, 6.00 GHz and 10.00 GHz are included in Fig. 4-15

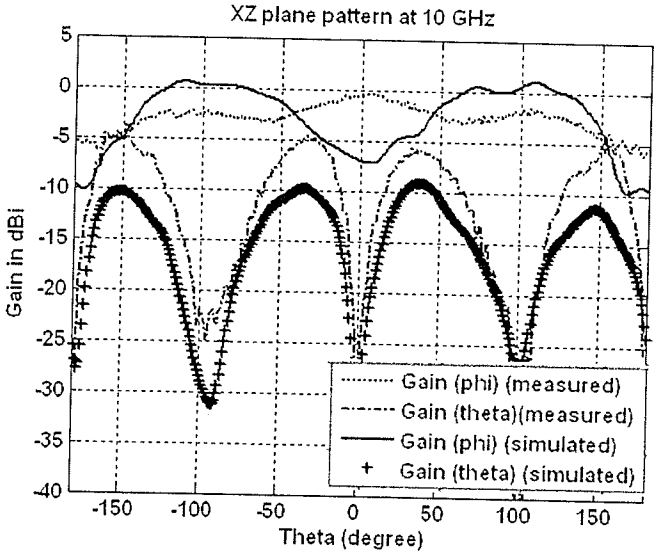

(a)

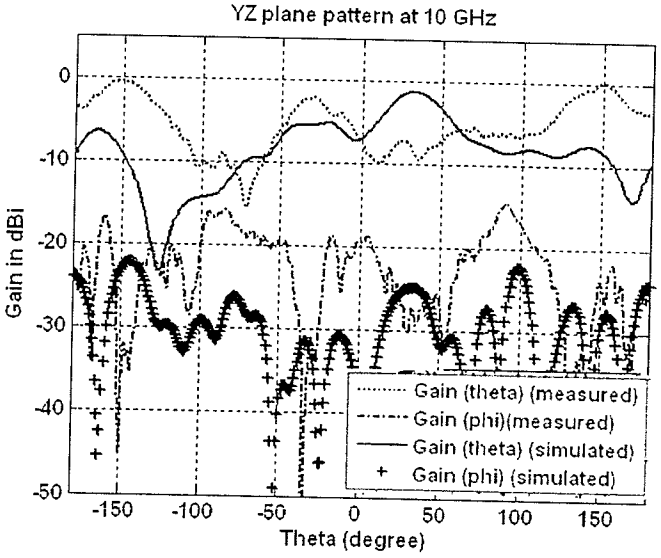

(b)

Fig. 4-14 Measured and simulated gain patterns at 10.00 GHz (a) XZ ($\varphi = 0^0$) and (b) YZ ($\varphi = 90^0$) plane

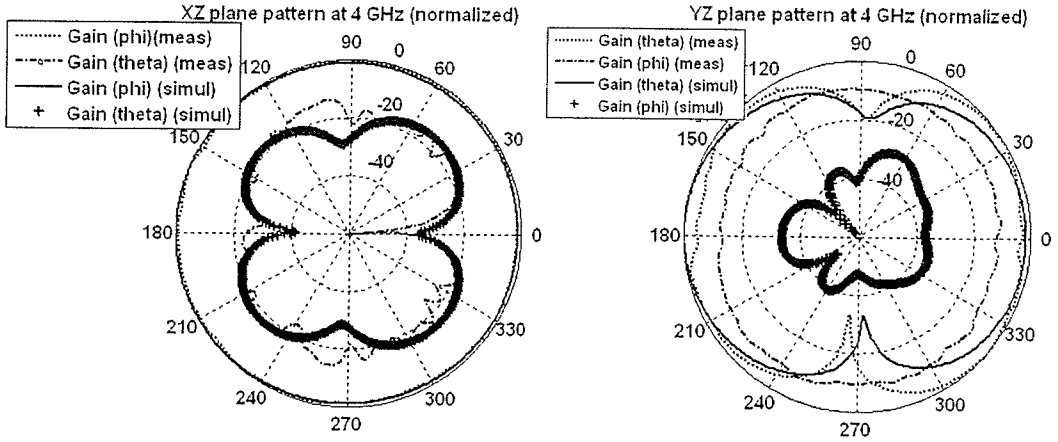

(a)

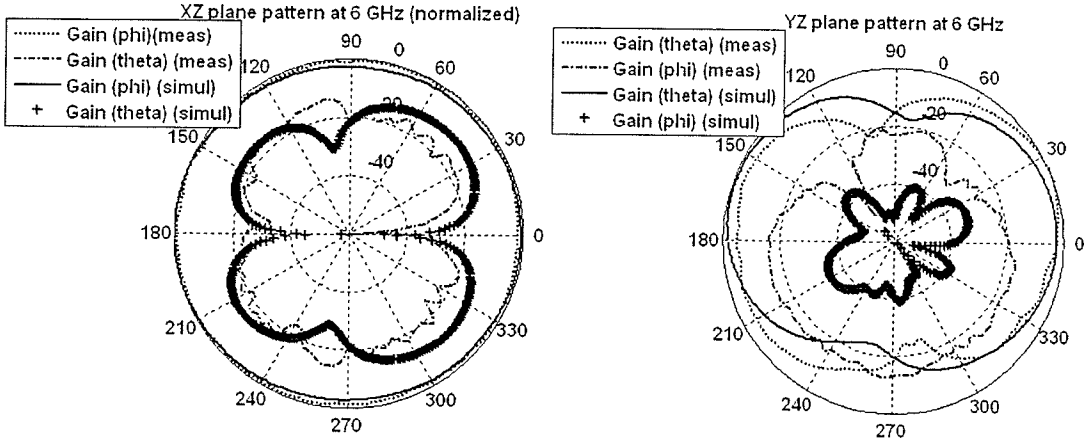

(b)

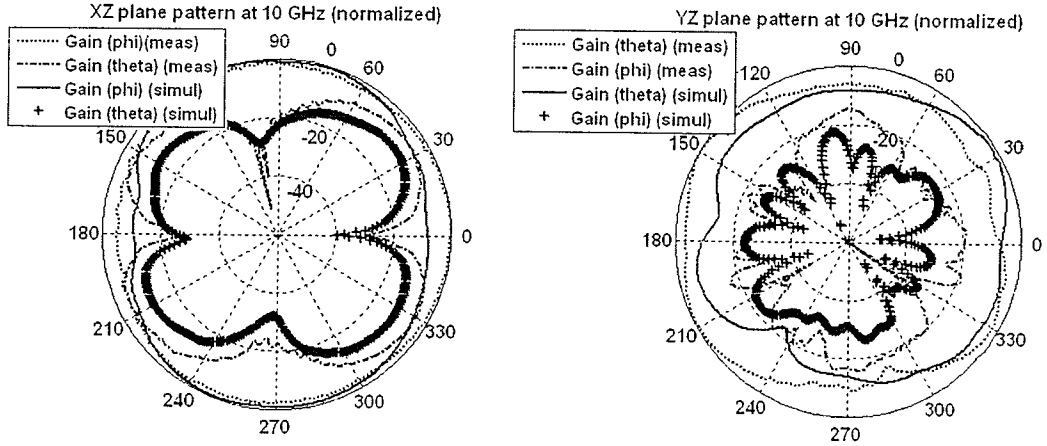

(c)

Fig. 4-15 Far-field radiation pattern at XZ and YZ plane (a) 4.00 GHz (b) 6.00 GHz (c) 10.00 GHz

Fig. 4-16 and Fig. 4-17 are the measured and simulated maximum co-polarization and cross-polarization gain variation as a function of frequency in the two principal planes YZ ($\varphi=0^0$) and XZ ($\varphi=90^0$).

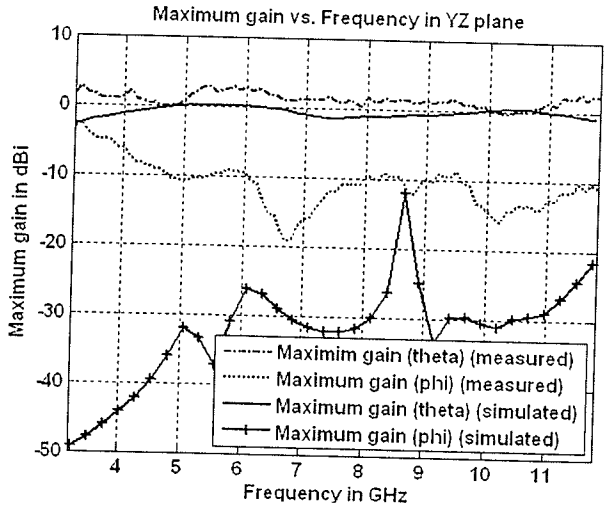

Fig. 4-16 Maximum gain vs. Frequency in YZ ($\varphi=90^0$) plane

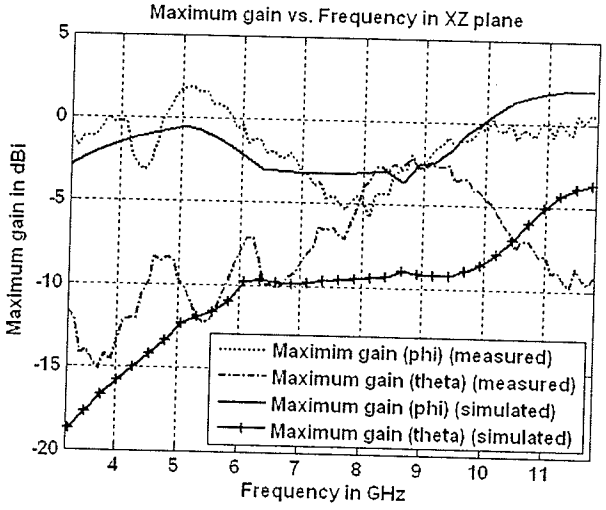

Fig. 4-17 Maximum gain vs. Frequency in XZ ($\varphi=0^0$) plane

In the YZ ($\varphi=90^0$) plane, the maximum variation of the measured co-pol gain is 3 dBi. The measured cross-pol gain has higher values than the simulated values. This is because

of the radiation of the long connecting cable whose radiated field added directly to the cross-polarization level of the antenna in this plane. The co-pol gain in the XZ plane ($\varphi=0^0$) shows larger variation in the operating frequency BW maximum value of 8 dBi.

4.4.1.4 Radiation Pattern of Linear Array

In this section free space radiation characteristics of a two elements linear broadside array of the antenna has been calculated. In order to achieve maximum of the array factor of a uniform linear array towards the broadside direction, each of the elements should have the same amplitude and phase excitation. Though, the separation between the elements can be of any value, if the distance between each element is multiple of wavelength (λ) grating lobes in other directions also occur. For the case of, $\lambda <$ spacing$< 2\lambda$, scanning of the main beam in different angles are achieved. Fig. 4-18 shows the configuration of the linear array with two elements oriented towards Z axis and separated by 25.00 mm ($\lambda/2$ at 6.00 GHz in free space). Uniform magnitude and phase excitation have been applied to each element.

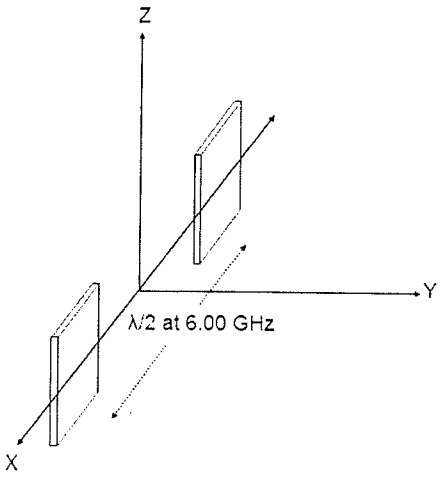

Fig. 4-18 Configuration of the 2-elements broadside array

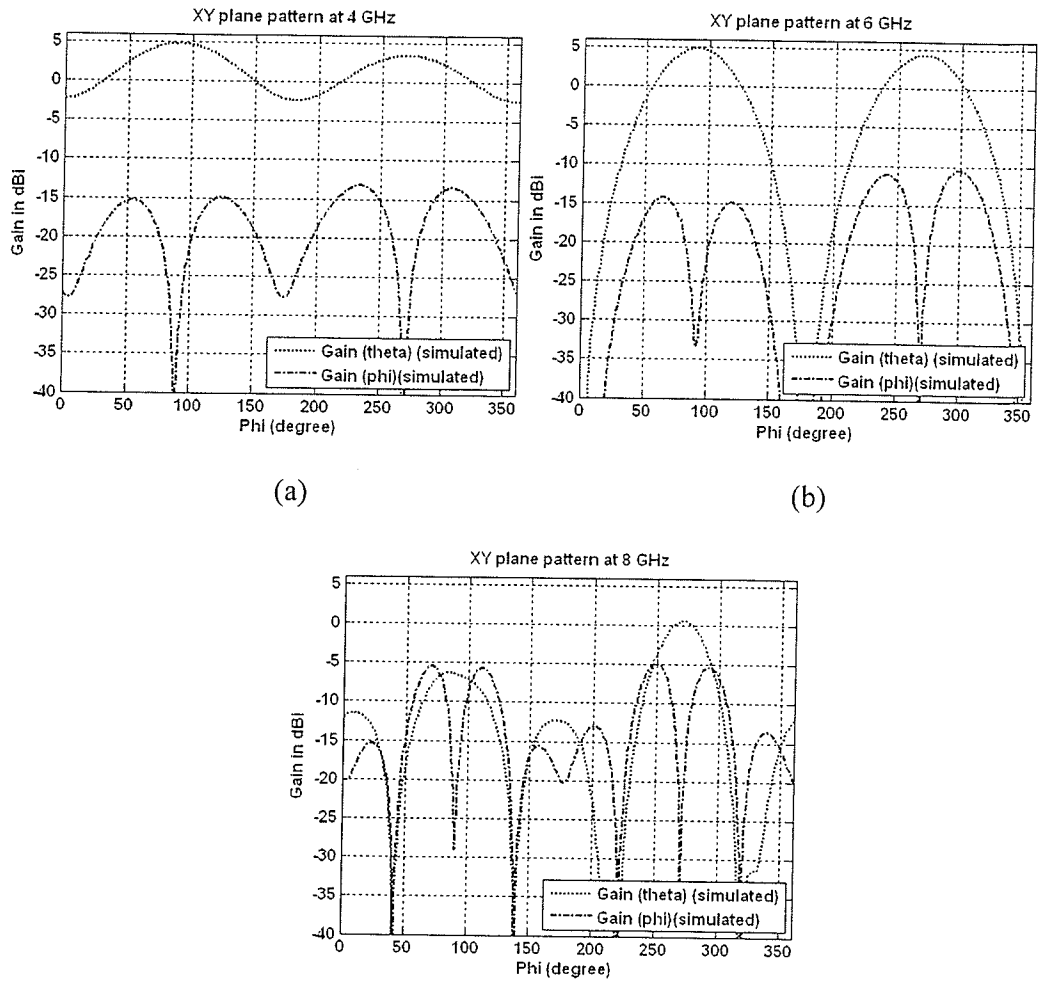

Fig. 4-19 Radiation pattern of the 2-elements broadside array at (a) 4.00 GHz, (b) 6.00 GHz and (c) 8.00 GHz in XY ($\theta=90^0$) plane

Fig. 4-19 (a) is the XY plane ($\theta=90^0$) pattern at 4.00 GHz (0.67λ spacing), where maximum radiations are in broadside (along $\varphi=90^0$ and $\varphi=180^0$) with Half Power BeamWidth (HPBW) of 90^0. At 6.00 GHz with 0.50λ spacing between the elements, the maximum gain is 5 dBi along the phi=90^0 direction with no grating lobes. At 8.00 GHz

the spacing between the elements is equivalent to 1.33λ and the main beam is scanned towards phi=270^0.

4.4.1.5 Time Domain Performance Analysis

As mentioned earlier, the UWB antenna's performance is basically determined by its ability to transmit or receive short EM pulses without incurring a lot of deviation or distortion of the original source pulse. Time domain antenna response can be divided into two parts: the main pulse and the tail (Fig. 4-20).

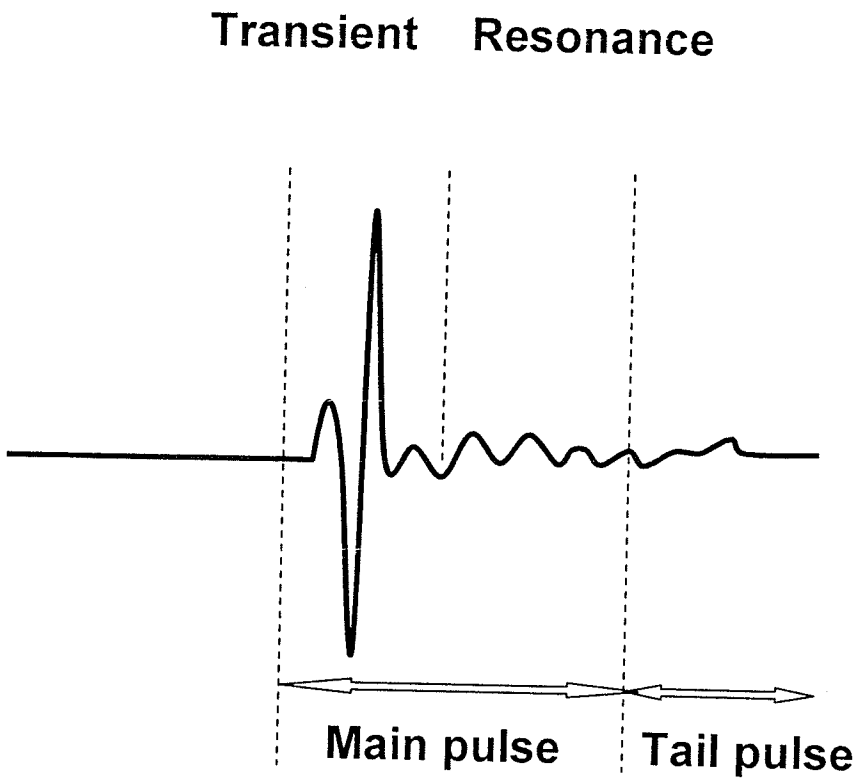

Fig. 4-20 Illustration of a typical time domain response from an antenna

In the main pulse, there are two distinguishable regions: transient region and resonance region. The transient region is the response due to the excitation pulse and the resonance

region is the effect of reflections in the internal antenna structure (e.g. end of antenna structure, antenna shielding, etc.). In the design of UWB antenna, the design goal is to eliminate the resonance region and minimize the tail as much as possible. The most effective method of reducing the tail is to resistively load the antenna to reduce reflection from the end terminal of the antenna [52]. However, this method compromises the overall efficiency of the antenna.

4.4.1.5.1 Time Domain Antenna Response

To investigate the designed antenna's feasibility for UWB pulse radiation, time domain simulation has been performed using commercially available simulation software Remcom's XFDTD [56], which is based on the Finite Difference Time Domain (FDTD) technique. In the simulation model, antenna was excited with a first derivative of Gaussian pulse of 0.25 ns time duration and radiated pulse at different points in the far-field both in the azimuth and zenith planes were calculated to study the antenna's ringing effect.

4.4.1.5.2 Antenna Excitation

Gaussian pulse has DC to high frequency components in its spectrum. DC component of the excitation pulse is one of the factors that contribute to the pulse ringing. The derivative of Gaussian pulse does not contain low frequency signal components including DC. Therefore, it is more suitable for pulse radiation. A Gaussian derivative pulse of duration 0.25 ns (Fig. 4-21) was used to excite the antenna.

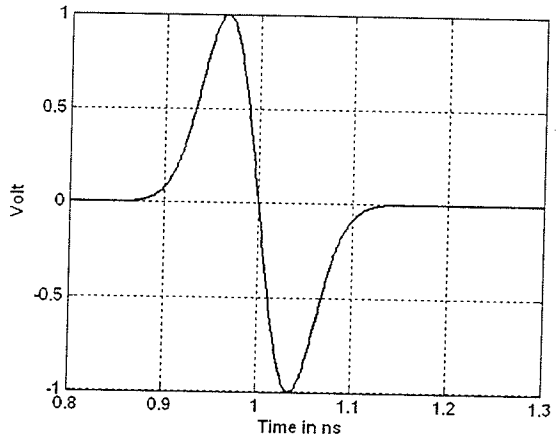

Fig. 4-21 Gaussian derivative pulse for the antenna excitation

Fig. 4-22 shows pulse response at the input port of the antenna as a function of time. The response is in the form of damped sinusoid of duration 1.15 ns that has peak amplitude of 0.65 volt with doublet type form. The fast decay of the pulse at the antenna port towards zero ensures the convergence of the time domain simulation.

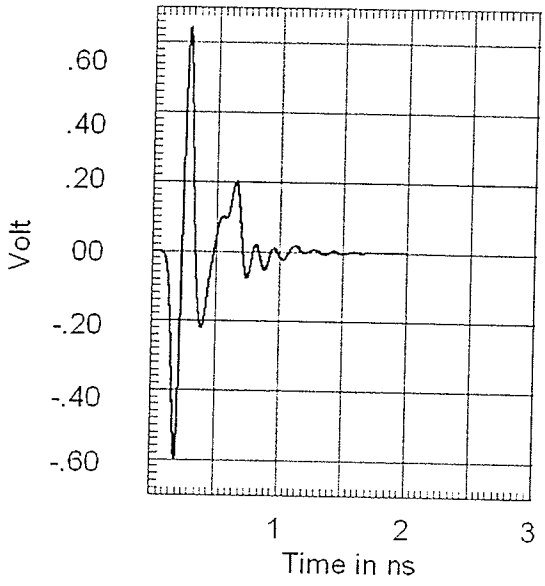

Fig. 4-22 Input signal at the antenna port

4.4.1.5.3 Far-field Pulse Radiation

Fig. 4-23 (a)-(c) show co-polarization components of the far-field at three angles ($\theta=0^0$, $\varphi=0^0$), ($\theta=45^0$, $\varphi=0^0$) and ($\theta=90^0$, $\varphi=0^0$) in XZ or zenith plane as a function of time, while the antenna structure lies on the XY plane ($\theta=90^0$). These observations correspond to three points surrounding the width of the antenna structure.

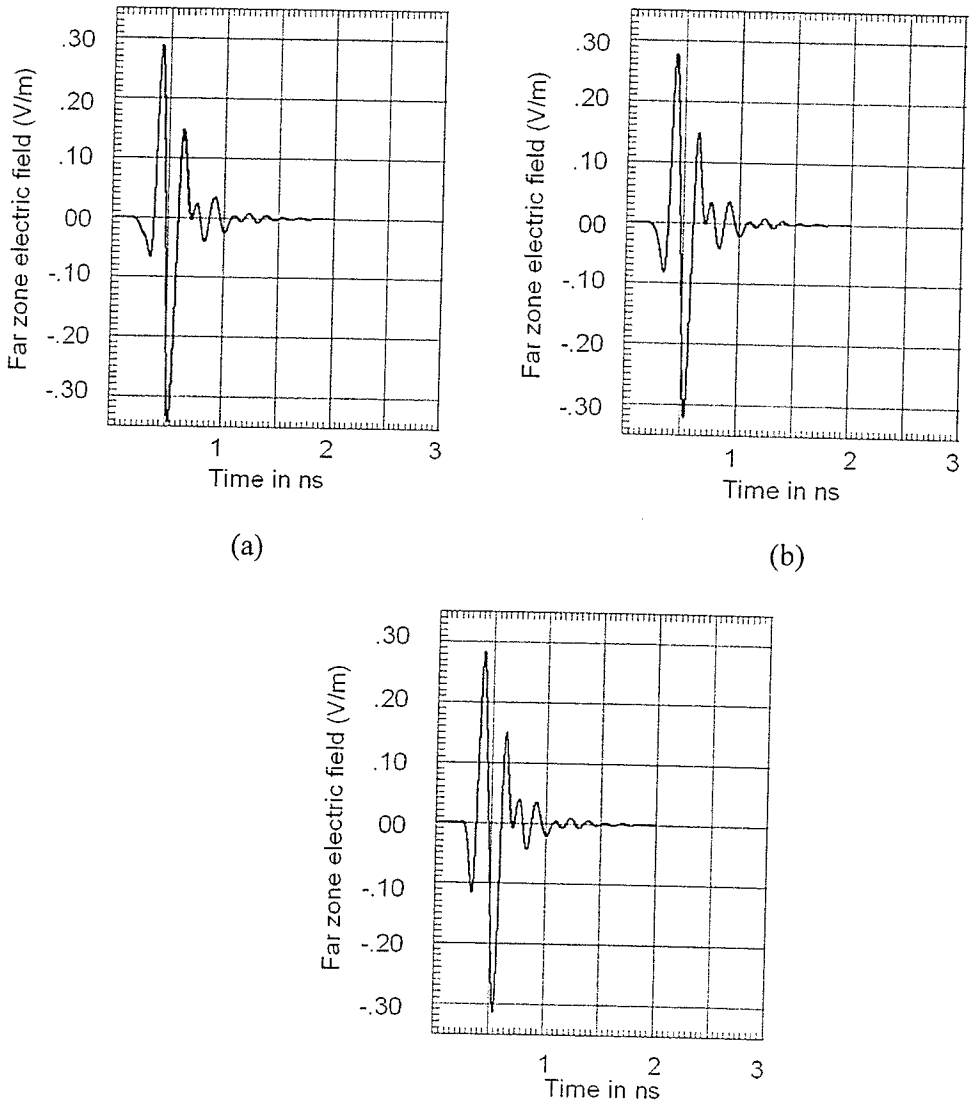

Fig. 4-23 Pulse radiation (a) ($\theta=0^0$, $\varphi=0^0$) (b) ($\theta=45^0$, $\varphi=0^0$) (c) ($\theta=90^0$, $\varphi=0^0$)

Fig. 4-23 (a) which shows the antenna response for ($\theta=0^0$, $\varphi=0^0$), illustrates a relatively moderate ringing effect of value near 0.60 ns. For all the three points in XZ plane, magnitude of the electric field is below 0.32 V/m.

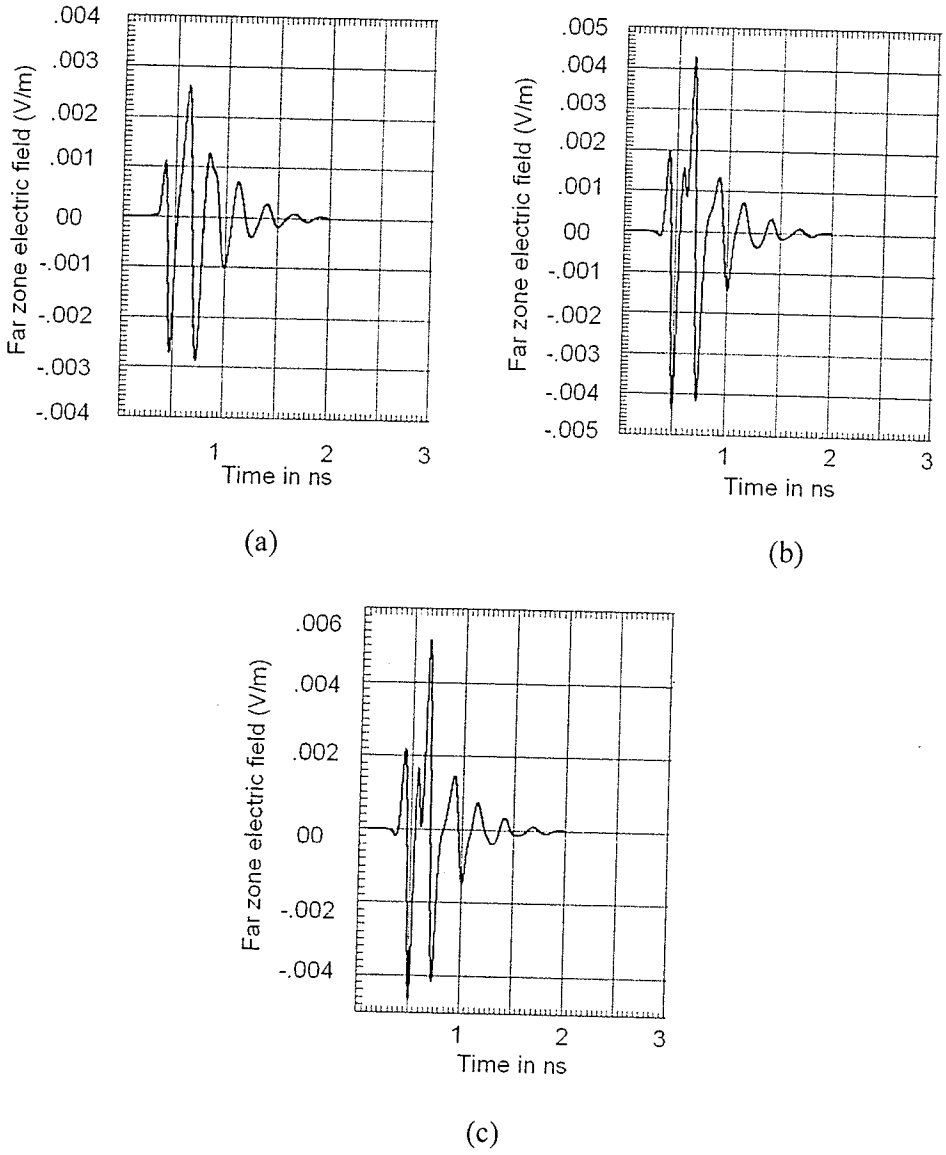

Fig. 4-24 Pulse radiation (a) ($\theta=0^0$, $\varphi=90^0$) (b) ($\theta=45^0$, $\varphi=90^0$) (c) ($\theta=90^0$, $\varphi=90^0$)

Fig. 4-24 (a)-(c) show the co-polarization components at three angles ($\theta=0^0$, $\varphi=90^0$), ($\theta=45^0$, $\varphi=90^0$) and ($\theta=90^0$, $\varphi=90^0$) in YZ plane, while the antenna structure lies on the XY ($\theta=90^0$) plane. These observation points correspond to three points in a plane over the middle of the antenna structure surrounding the antenna length. Comparing Fig. 4-24 with Fig. 4-23, ringing effects are more significant in YZ ($\varphi=90^0$) plane. This implies that the radiated pulse in the YZ ($\varphi=90^0$) plane gets more distorted than that of in the XZ ($\varphi=0^0$) plane. Moreover, radiated electric field strength at the XZ ($\varphi=0^0$) plane is higher than that of the YZ ($\varphi=90^0$) plane.

4.4.2 Antenna Immersed in Matching Materials

In breast imaging, selection of coupling material between antenna and the imaging medium is imperative. Generally, a significant reflection occurs at the antenna and breast interface, thus reducing signal power. Introducing a coupling medium at the interface can improve matching and reduce a significant amount of reflection. Therefore, this is a key issue to improve image quality [57]. Different research groups have used different materials where permittivity of the material matches to skin, fatty tissue or oil. Intensive research is still going on to find out the best fit coupling material.

Several considerations have to be taken into account. A lossy material with low conductivity whose permittivity is compatible with the breast tissue is desirable to provide acceptable imaging capabilities. Moreover, the material has to be safe, clinically acceptable and low cost. In addition, impact on environment after disposing the material has to be considered.

For many years, saline has been used as a convenient coupling material because of the low contrast with the predominantly high water content of the body, suitability to come in contact with the human body and low cost. Moreover, its permittivity can be changed by varying the concentration of salt in the solution [58]. Search for alternative liquids which offer lower intrinsic contrast with breast on average has been going on.

Some organic compounds like ethyl alcohol have also the potential to be a coupling liquid as a low permittivity medium. They are easily disposable and inexpensive, but when diluting with water to achieve low permittivity, the level of fumes becomes unacceptable for clinical use [58].

Glycerine can also be combined with various proportions with water or saline to achieve desired permittivity and conductivity, optimized for breast imaging [58]. Glycerine is non toxic, inexpensive and doesn't have much detrimental effect on environment. The drawbacks of using glycerine solution are its widely varying permittivity over the microwave frequency range and its high conductivity.

Li *et al.* [5] have used low permittivity and conductivity material like soybean oil (ε_r= 2.60, σ=0.05 S/m at 6 GHz) in their MI experimental setup. Sill *et al.* [54] used similar oil with ε_r=3 with promising results in their Tissue Sensing Adaptive Radar (TSAR) method for breast imaging. Shannon *et al.* [4] applied margarine with ε_r=7.50-6.50 and σ=0.10-0.80 S/m for the frequency range of 1.00 GHz to 13.00 GHz. Margarine's dielectric property is similar to the dielectric property of fatty tissue. Shanon was able to

image the dielectric properties of stimulant phantom and tumor material. Wu *et al.* [59] reported that relative permittivity of Vaseline at room temperature is a constant value of around 2.50 for frequencies from 2.00 GHz up to 20.00 GHz. As this value is close to the value of soybean oil permittivity and it shows a constant behavior over a large frequency range, Vaseline is a promising candidate for coupling medium. Moreover, Vaseline is readily available, a safe material and clinically acceptable.

In this thesis, antenna performance while immersed in three different low permittivity materials; margarine, soybean oil and Vaseline, has been studied. In the simulation model the whole antenna structure was immersed in a rectangular box full of the corresponding liquid and antenna's impedance bandwidth was calculated. The dimension of the rectangular box used in the model was 130.00 mm × 63.00 mm × 102.00 mm. Therefore, the side walls of the box are within far-field region of the antenna and thus, near-field coupling from the box material is avoided. The thickness and permittivity of the box material were ignored for simplicity. Fig. 4-25shows the simulation model.

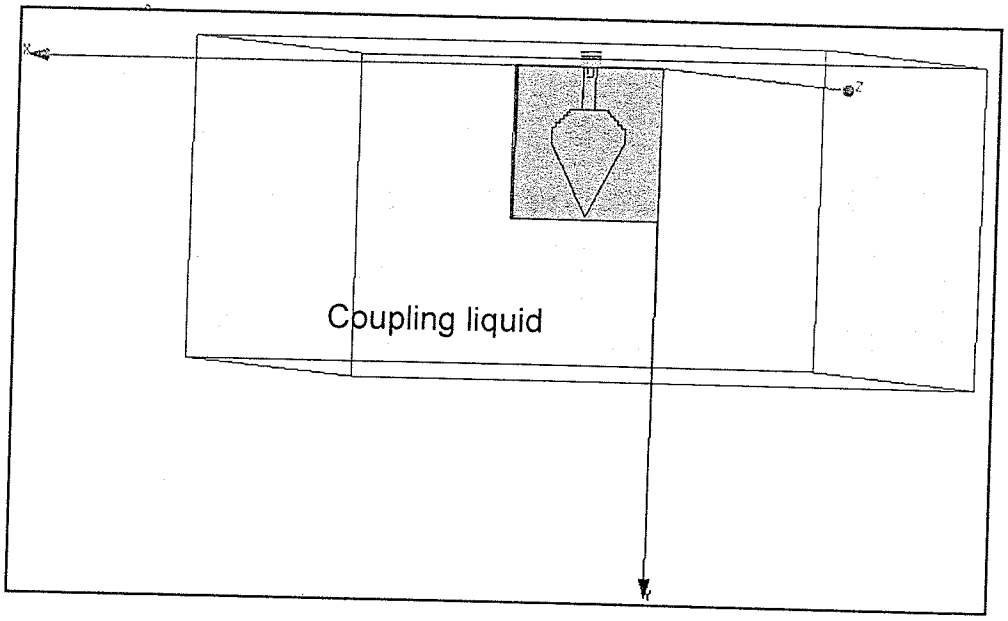

Fig. 4-25 Simulation model for antenna immersed in matching liquid

4.4.2.1 Margarine

Shannon *et al.* [4] used a homogeneous mixture of Becel and Parkey margarine in a ratio of 2.50:1 as matching material in their experimental set up. The permittivity of the mixture was measured with a specially designed probe and was found to be within the range of 6.50 to 7.50 in the frequency band of 1.00 GHz to 13.00 GHz. The conductivity variation at 4^0C was within the range of 0.10 S/m to 0.80 S/m, with a linear variation with frequency [4]. These properties are in close proximity to the properties of fatty tissue and this mixture is reasonably a proper coupling material. The antenna's impedance matching characteristics was simulated while immersed in the rectangular box full of that material and return loss measurement was performed using Anritsu ME7808A VNA. A relative permittivity (ε_r) of 6.50 to 7.50 was used in the simulation using a 'Piecewise Linear

Material Input' option of Ansoft HFSS [55] to incorporate the frequency dependency. A constant conductivity of value 0.80 S/m was used. Fig. 4-26 shows a significant improvement of impedance BW (S_{11} ≤-10 dB) over that of free space. Introduction of margarine significantly reduces the lower cut-off frequency of the impedance BW to1.82 GHz. It can be concluded that in terms of impedance matching the antenna shows a good performance in the margarine mixture.

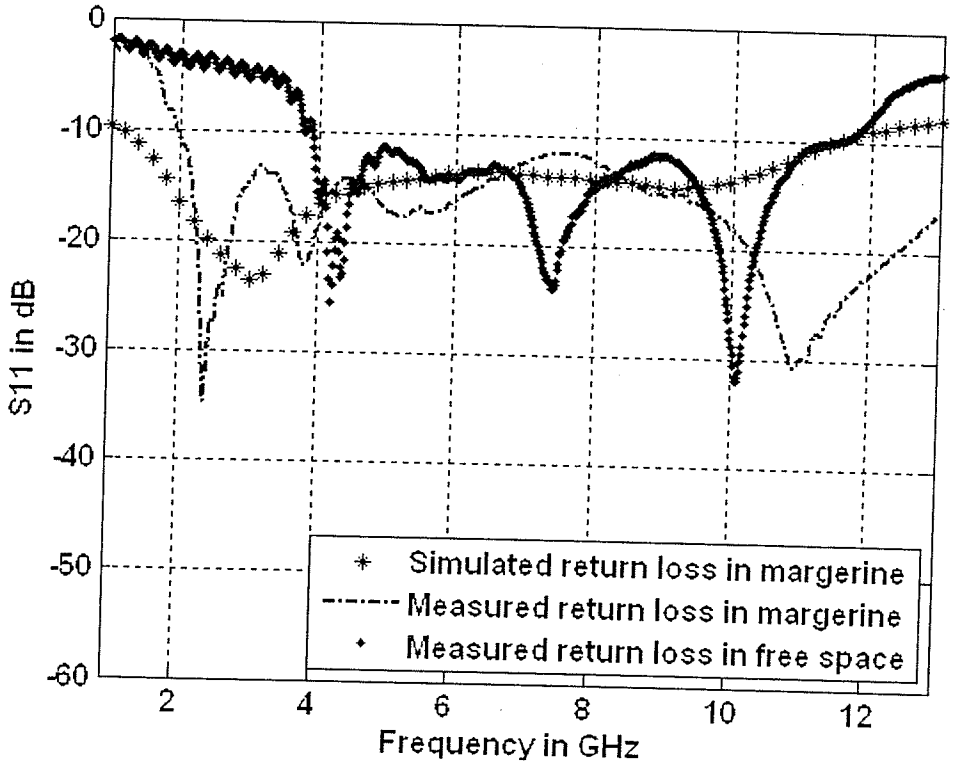

Fig. 4-26 Return loss in margarine and free space

The difference between the calculated and measured return loss is probably due to the permittivity difference from the value used in the simulation, which results from inhomogenity of mixture of the two types of margarine used. No measurement has been performed to determine the actual permittivity and conductivity of the mixture used in the

measurement. Moreover, air bubble trapped inside the mixture might alter the actual permittivity of the mixture. Also note that nominal values of permittivity and conductivity measured in [4] was at 4^0C, but the RL measurement in this work was performed at room temperature. This fact might also have some impacts on the differences between measurement and simulation results.

4.4.2.2 Soybean Oil

Soybean oil is inexpensive, readily available and non toxic. Moreover, its dielectric properties (ε_r=2.6, σ=0.05 S/m at 6 GHz) resembles very low water content fatty tissue [5]. The antenna is simulated while immersed in the rectangular box filled with soybean oil as shown in Fig. 4-25. Fig. 4-27 shows the RL curve of the antenna immersed in soybean. The simulation and measurement results show a good impedance matching with lower cut-off frequency of 2.50 GHz. Since, in MI, the penetration depth is low and dispersion is very significant at higher frequencies [9], antenna behavior above 13.00 GHz was not studied. The slight variation between the measured and calculated results could probably be due to the difference between real and simulated values of permittivity and conductivity. Moreover, a constant value of permittivity (ε_r=2.60) and conductivity (σ =0.05 S/m) were used in the simulation neglecting the dispersion effect that might be present in the reality.

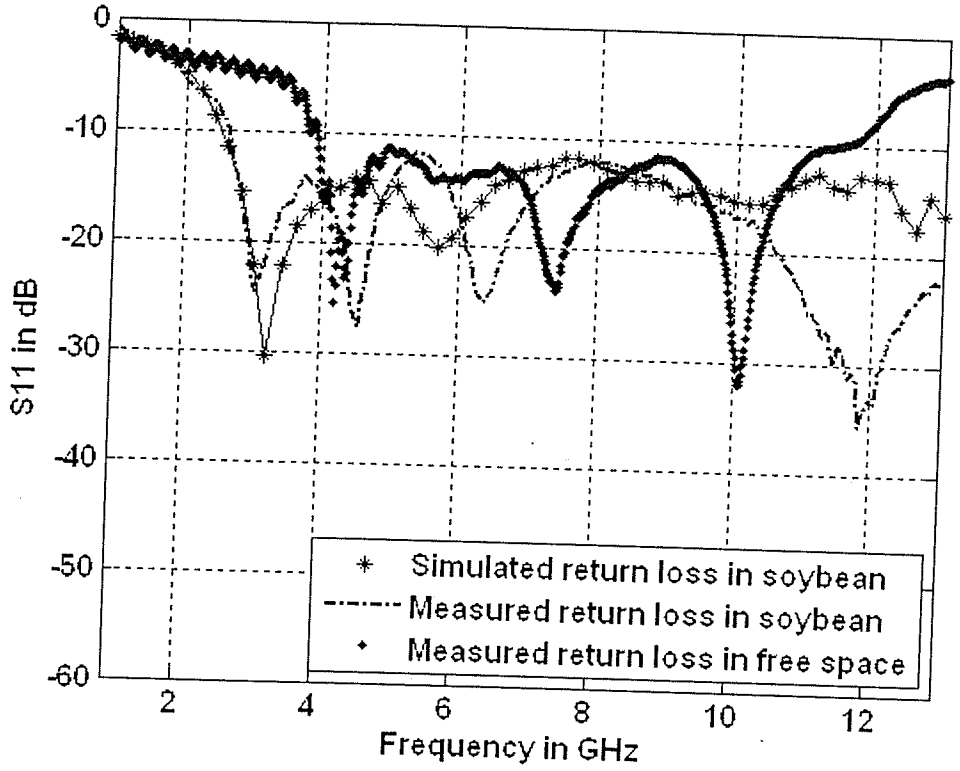

Fig. 4-27 Return loss in soybean oil and free space

4.4.2.3 Vaseline

It has been reported in [59] that Vaseline possesses a very consistent dielectric property (ε_r=2.50, σ=0.011 S/m) over a wide range of frequencies and its dielectric property is similar to very low water content fatty tissue. Since Vaseline is a good matching material, antenna impedance BW immersed in Vaseline was simulated and measured. A very good impedance BW starting from 2.60 GHz was achieved. The measured result shows better matching characteristics compared to free space except slight mismatch around 6.00 GHz. Fig. 4-28 shows the RL curves of the antenna immersed in Vaseline and in free space. The variation between the measured and simulated results is probably due to the

difference of permittivity and conductivity values of Vaseline used in the simulation model with actual case and dispersion effect that was not accounted in the simulation.

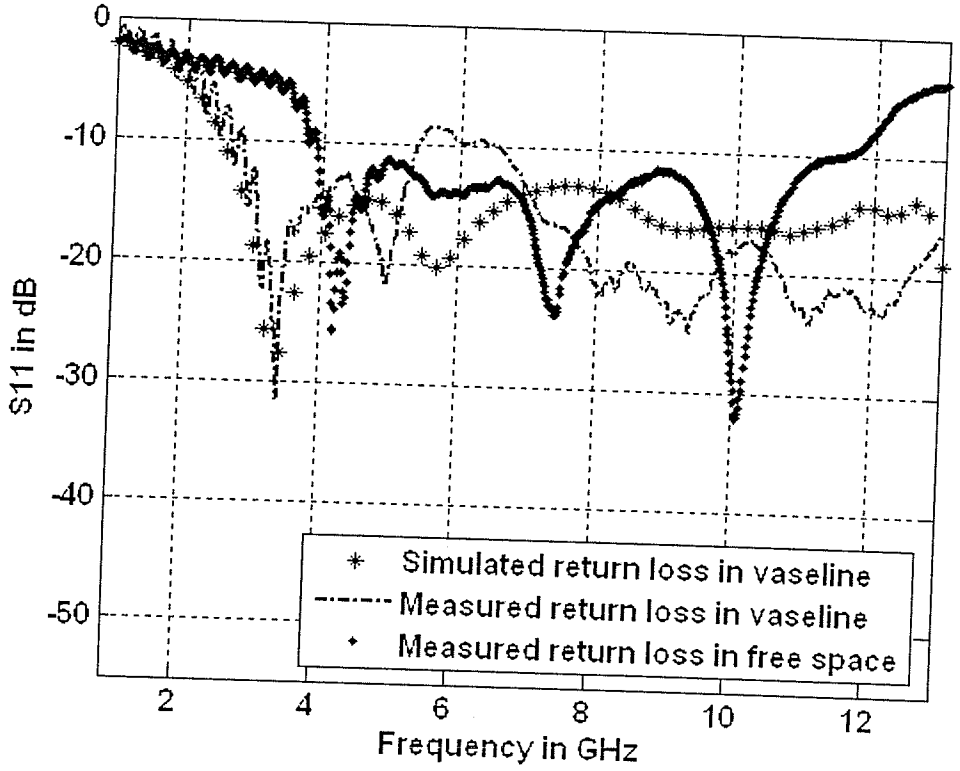

Fig. 4-28 Return loss in Vaseline and free space

4.5 Chapter Summary

A new diamond shaped printed UWB monopole antenna design was proposed in this chapter which can attain free space and inliquid impedance BW more than 100%. Design details and some computed and measured parameters of this antenna are also presented. Obtained results show a great performance that makes this antenna suitable for MI application.

In the next chapter a new design and performance analysis of a UWB wide slot antenna will be presented.

Chapter 5 : CPW Fed UWB Slot Antenna

5.1 Introduction

In this chapter, design and development of a Co-Planar Waveguide (CPW) fed UWB taper arc slot antenna [61], [62] is introduced and some antenna parameters measurement and simulation results such as RL, VSWR, radiation pattern and group delay are described. The obtained results illustrate a free space impedance BW of 9.69 GHz (from 2.89 GHz to 12.58 GHz) and fairly stable radiation pattern over large BW. Moreover, some time domain simulation results and antenna matching characteristics while immersed in coupling materials have been illustrated. A very good agreement between the predicted values and measurements has been achieved. The design considerations for achieving broadband operation of this printed antenna have also been described in details.

5.2 Geometry and Design

A variety of feed-slot combinations for the UWB slot antennas has been described in [26]-[38]. The slot antenna proposed in this chapter was designed on a dielectric substrate of thickness 1.60 mm and relative permittivity ε_r=2.50, and is depicted in Fig. 5-1. A feed of similar shape and with a size of one third to half of a slot usually provides optimum coupling and good matching [24]; therefore a taper arc radiating slot and a tuning stub of the same shape with approximately one third of the slot has been placed inside the slot.

The maximum height of the feed stub was obtained to a value of 42.50 mm. The radius of curvature of the feed stub (half of **d1**) has been tuned to a value of 7.50 mm which is equal to the half wavelength at the upper cut-off frequency of 12.50 GHz. The radius of the slot (half of **D1**) has the value of 24.85 mm that corresponds to the half wavelength value around 3.50 GHz.

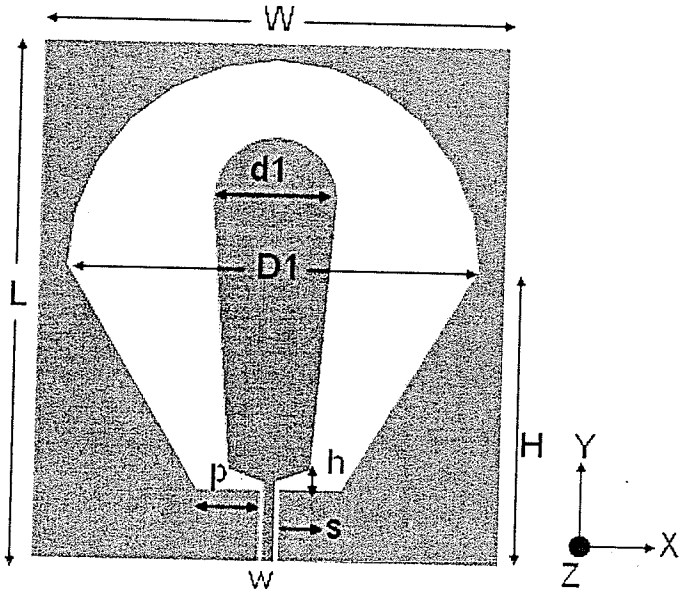

Fig. 5-1 Geometry of the slot antenna, dimensions given in Table 5-1

The tapering enables the slot to sustain multiple resonant modes and thus ensures wideband operation [38]. Tapering also helps to reduce antenna's physical area by creation of larger slot length in a smaller area. Coupling between the feed-slot combination and impedance matching at the higher frequency range depends on the gap width '**h**' [26]-[27]. The base of the tuning stub has been linearly tapered to provide a good impedance match. The variation impedance matching characteristics of the antenna with the varying values of '**h**' have been shown in Fig. 5-2. For value of **h**=3 mm, the

best impedance match in the frequency range were obtained. Simulated surface current distribution along the antenna structure at 4.00 GHz has been shown in Fig. 5-3. The critical tuned dimensions of the antenna obtained from Ansoft HFSS [55] have been tabulated in Table 5-1.

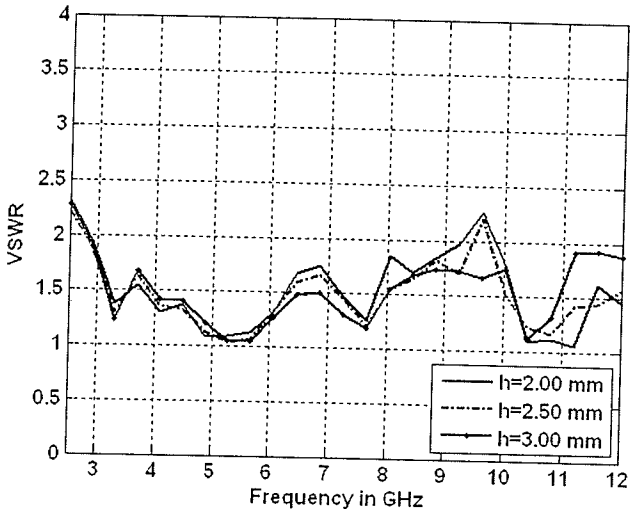

Fig. 5-2 Variation of impedance BW with feed-slot gap-'h'

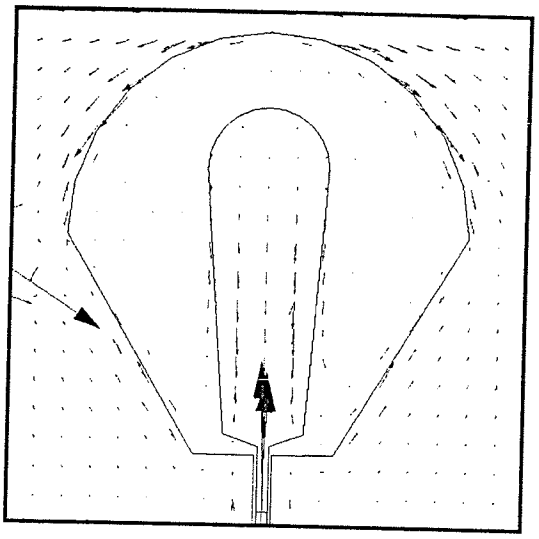

Fig. 5-3 Simulated current distribution along the antenna surface at 4.00 GHz

Table 5-1 Critical design parameters of the wide slot antenna

(Parameters shown in Fig. 5-1)

Parameters	Dimensions (mm)
L	63.00
W	64.00
H	35.85
D1	49.70
d1	15.00
p	7.50
h	3.00
w	1.50
s	0.43

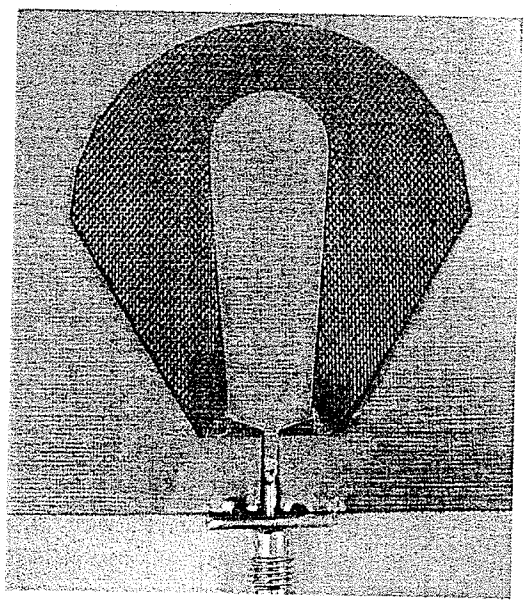

Fig. 5-4 Photograph of the fabricated slot antenna

5.3 Performance Analysis and Measurement

5.3.1 Free Space

The designed slot antenna has been fabricated (Fig. 5-4) in the machine shop at the University of Manitoba and several antenna performance measurements have been performed in the antenna lab to verify the expected and measured results for the validation of the design. Antenna's free space RL, VSWR and group delay measurement have been performed using Anritsu ME7808A VNA at the antenna lab of University of Manitoba. The antenna far-field radiation pattern measurement has been performed in the

anechoic chamber with CATR facilities (Section 2.3.2) at the antenna lab in University of Manitoba.

5.3.1.1 Return Loss and VSWR

Antenna input impedance should be matched to the connecting network for efficient radiation from the antenna, while reducing power loss due to reflection at the port.

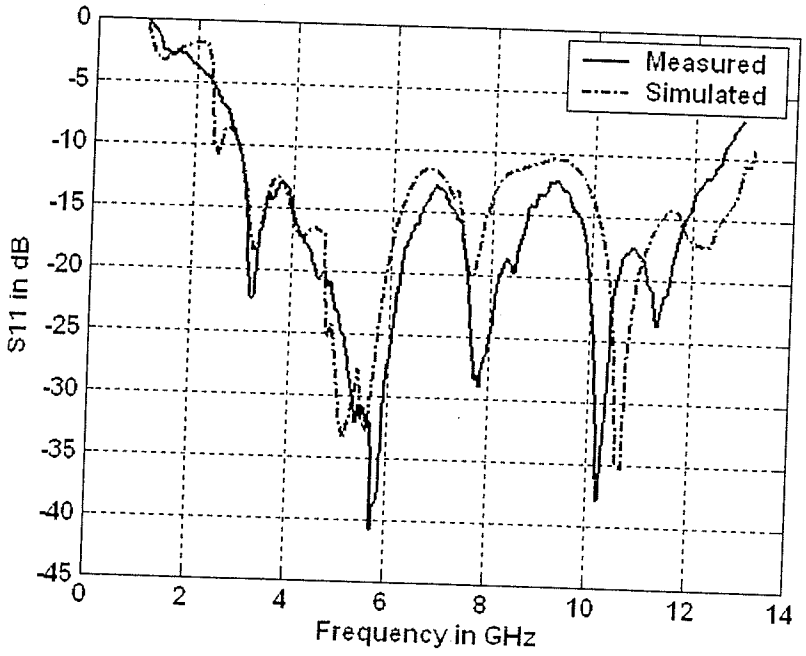

Fig. 5-5 Measured and simulated return loss

From the plot of the measured return loss (Fig. 5-5), it is evident that impedance BW (S_{11} ≤-10 dB or VSWR≤2) of (2.89 GHz to 12.58 GHz=9.69 GHz) has been achieved which covers the whole UWB frequency range. Moreover, the calculated and measured values show an excellent agreement with each other. However, slight deviation of the upper cut-

off frequency of the antenna can be attributed to mainly fabrication inaccuracy and computational exigencies of simulation software.

The measured and simulated VSWR curve (Fig. 5-6) of the antenna also supports the good impedance matching behavior of the antenna over the whole UWB frequency band that corresponds to 125% impedance BW.

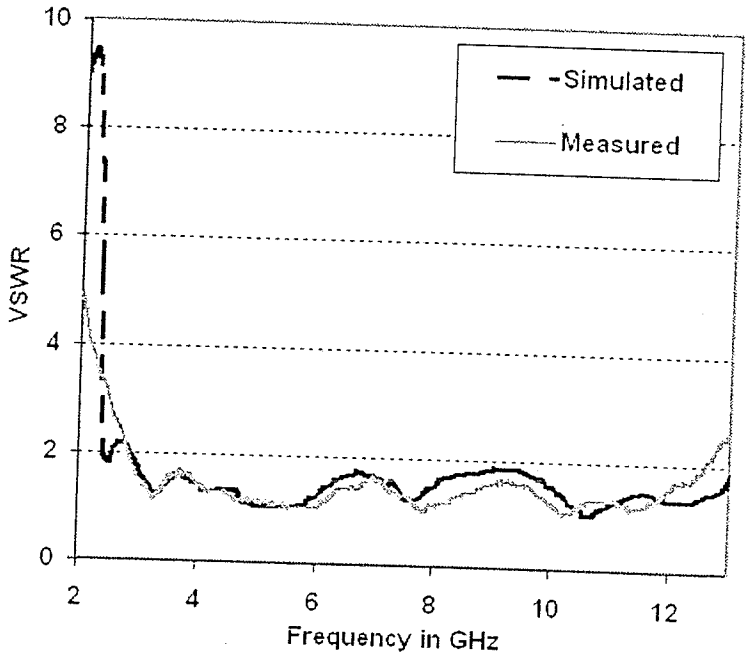

Fig. 5-6 Measured and simulated VSWR

5.3.1.2 Measured Group Delay

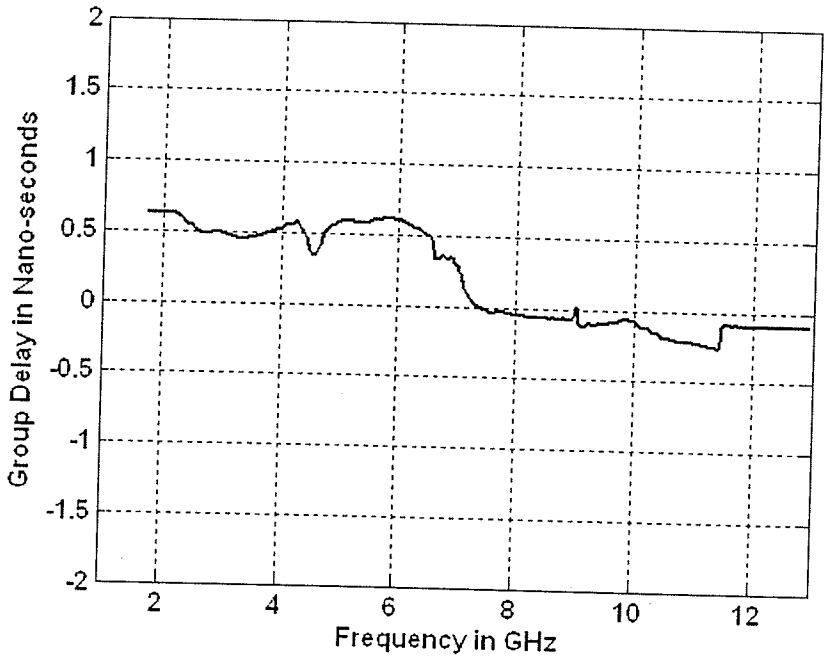

Fig. 5-7 Measured group delay

The plot of Fig. 5-7 is the group delay variation as a function of frequency. The group delay of the antenna was measured by Anritsu ME 7808 VNA at the antenna lab, University of Manitoba. This plot shows that maximum group delay variation over the BW of operation of the antenna is less than 0.60 ns, with an average of 0.30 ns approximately. Therefore, it can be expected that, the antenna transfer function will not have significant detrimental effect on the UWB pulse radiated by the antenna and pulse shape will be retained. As VNA plots the difference in group delay with respect to free space, this group delay variation can be of negative value at some frequency band. Fig. 5-7 illustrates negative values of group delay after 8.00 GHz for this reason.

5.3.1.3 Radiation Pattern

The following plots (Fig. 5-8 to Fig. 5-10) are the measured and simulated far-field components of the radiation pattern of the antenna at different frequency values (i.e. 4.00 GHz, 6.00 GHz, and 8.00 GHz) in the XZ ($\varphi=0^0$) and YZ ($\varphi=90^0$) planes when antenna lies on the XY ($\theta=90^0$) plane. Fig. 5-8 (a) is the XZ ($\varphi=0^0$) plane gain pattern at 4.00 GHz. with maximum gain along the direction, $\theta=0^0$ of value 2.12 dBi. But, the cross-polarization level in XZ ($\varphi=0^0$) plane is high. The measured YZ plane ($\varphi=90^0$) pattern (Fig. 5-8 (b)) shows higher cross-polarization values than the simulated case. This is due to the close proximity of the connecting probe to the slot edge and radiation from the cable of the measurement set up. Fig. 5-9 (a) and (b) are the gain patterns at 6.00 GHz. Patterns become more directive after 8.00 GHz (Fig. 5-10). At 8.00 GHz maximum measured gain in XZ ($\varphi=0^0$) plane along $\theta=0^0$ is 6.26 dBi. This aberration occurs because of the unequal phase distribution of the signal at the slot at higher frequencies. Actually, this phenomenon is one of the common drawbacks of UWB slot antennas. Moreover, cross-polarization components achieve higher values as frequency of operation increases.

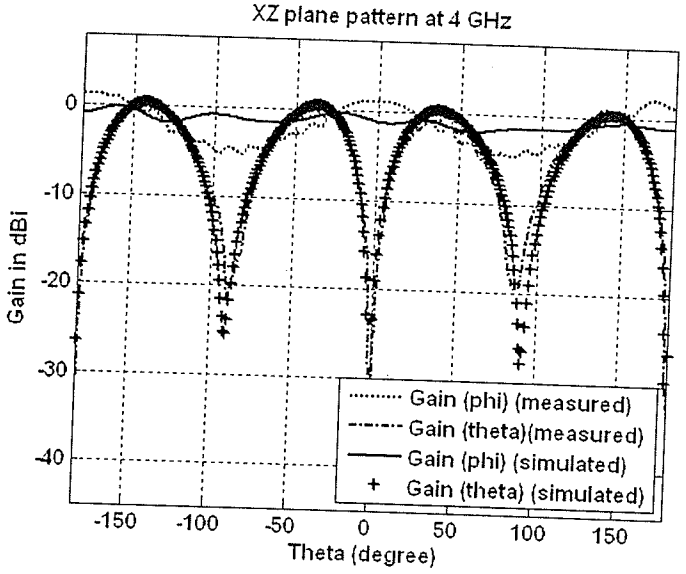

(a)

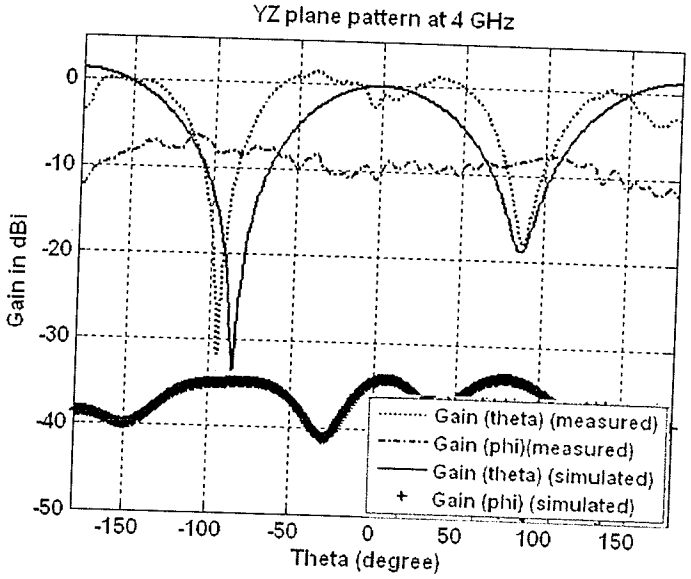

(b)

Fig. 5-8 Measured and simulated gain patterns at 4.00 GHz (a) XZ ($\varphi = 0^0$) plane, (b) YZ ($\varphi = 90^0$) plane

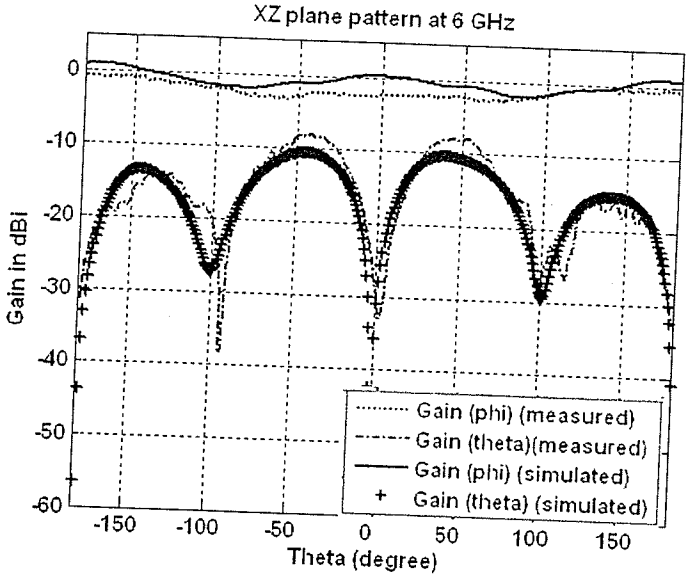

(a)

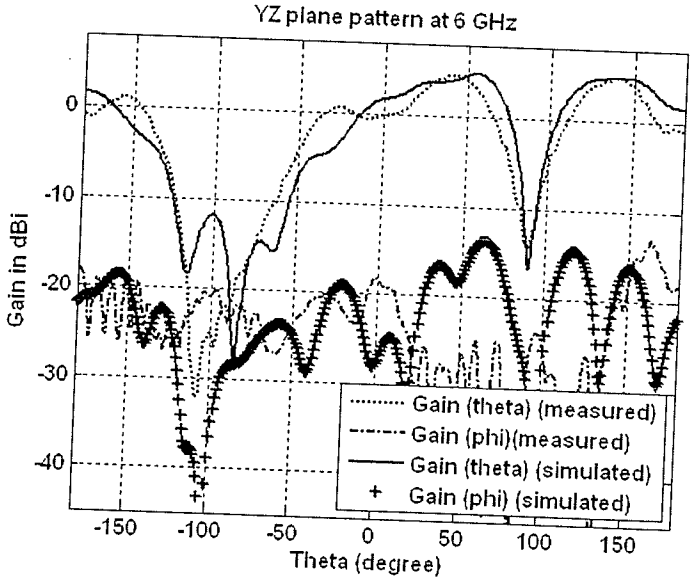

(b)

Fig. 5-9 Measured and simulated gain patterns at 6.00 GHz (a) XZ ($\varphi = 0^0$) plane, (b) YZ ($\varphi = 90^0$) planes

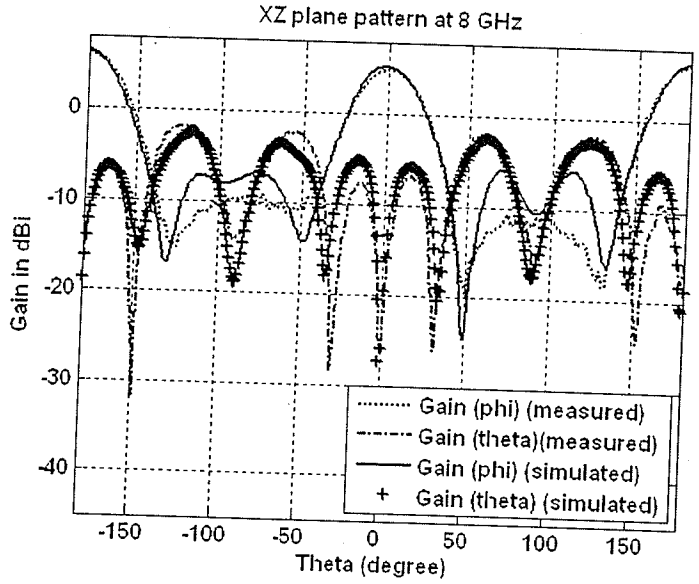

(a)

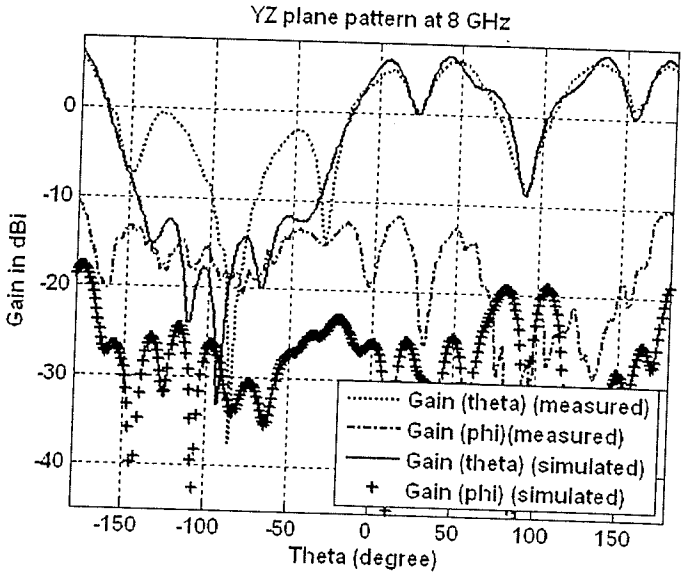

(b)

Fig. 5-10 Measured and simulated gain patterns at 8.00 GHz (a) XZ ($\varphi = 0^0$) plane, (b) YZ ($\varphi = 90^0$) plane

Fig. 5-11 (a)-(c) are the normalized polar plots of the XZ ($\varphi=0^0$) and YZ ($\varphi=90^0$) plane gain patterns of the antenna at 4.00 GHz, 6.00 GHz and 8.00 GHz.

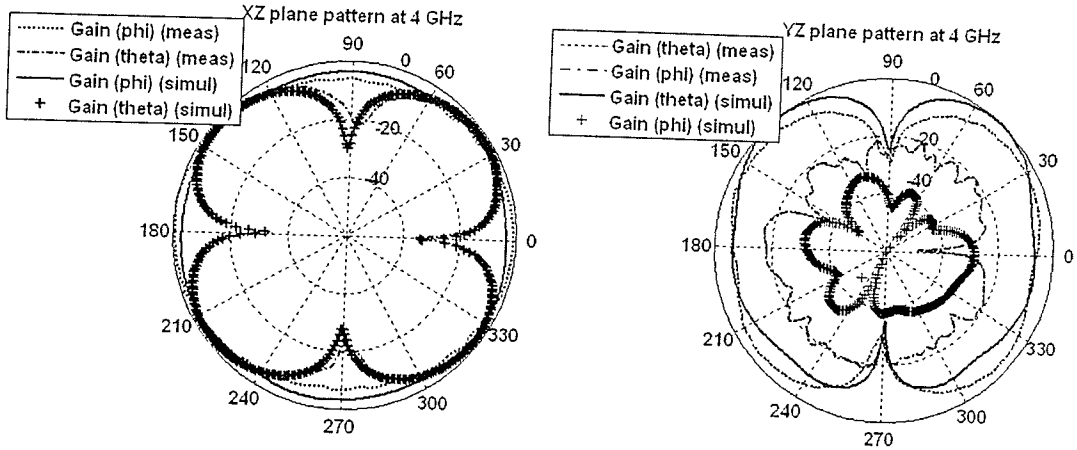

(a)

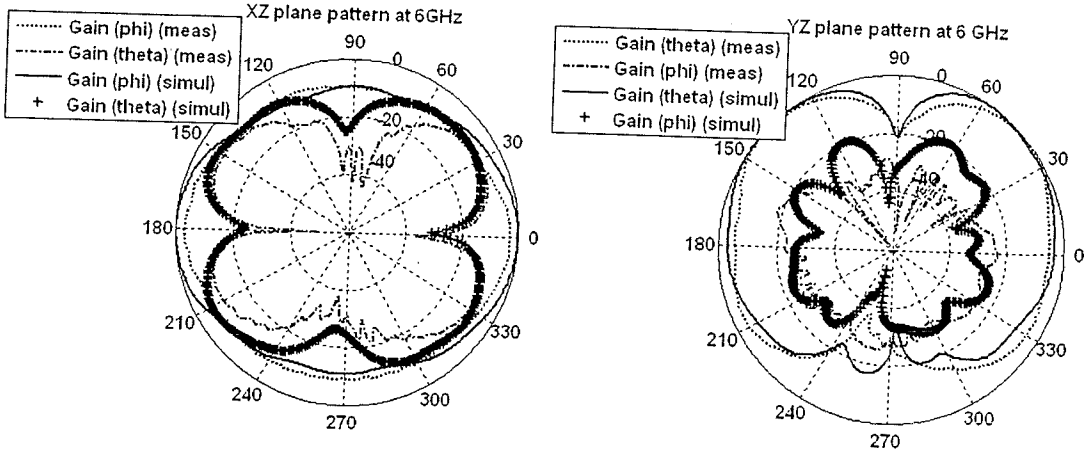

(b)

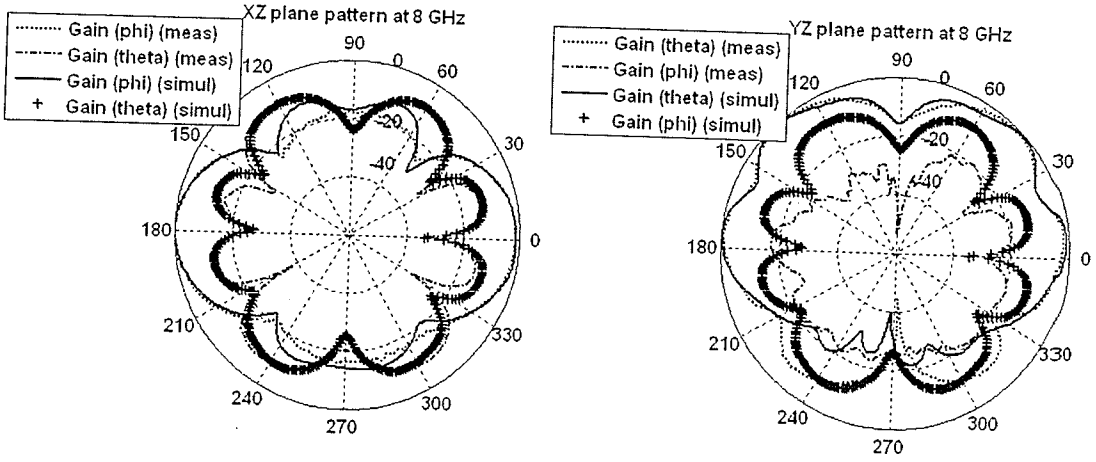

(c)

Fig. 5-11 Far-field radiation patterns at XZ and YZ plane (a) 4.00 GHz (b) 6.00 GHz (c) 8.00 GHz

Fig. 5-12 and Fig. 5-13 are the plots of YZ ($\varphi=90^0$) and XZ ($\varphi=0^0$) plane maximum gain of the radiated field components with frequency.

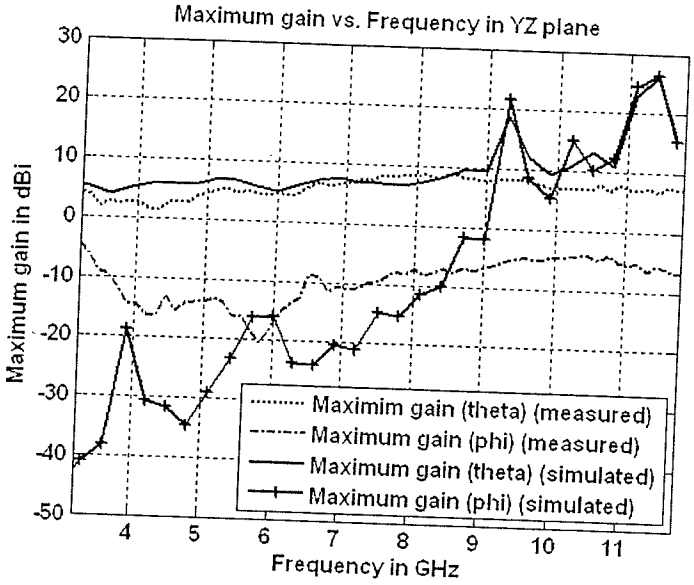

Fig. 5-12 Maximum gain vs. Frequency in YZ ($\varphi=90^0$) plane

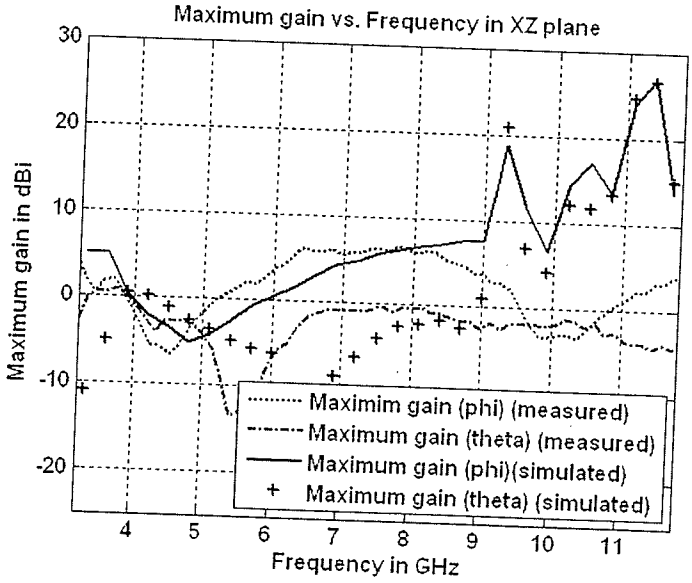

Fig. 5-13 Maximum gain vs. Frequency in XZ ($\varphi=0^0$) plane

The maximum variation of the co-polarization gain in YZ ($\varphi=90^0$) plane is around 6 dBi in the frequency span of 3.00 GHz to 12.00 GHz. However, the simulated values of co-polarization gain after 9.00 GHz shows large variations and have higher values. This is probably due to the computational exigencies at the higher frequncies. The simulated and measured XZ ($\varphi=0^0$) plane maximum gain components agree well with each others except deviations after 10.00 GHz.

5.3.1.4 Radiation Pattern of Linear Array

Fig. 5-14 shows the configuration of the linear array of two elements along X-axis and oriented towards Z-axis separated by 25.00 mm ($\lambda/2$ at 6.00 GHz). Uniform magnitude and phase excitation have been applied to each element for broadside pattern.

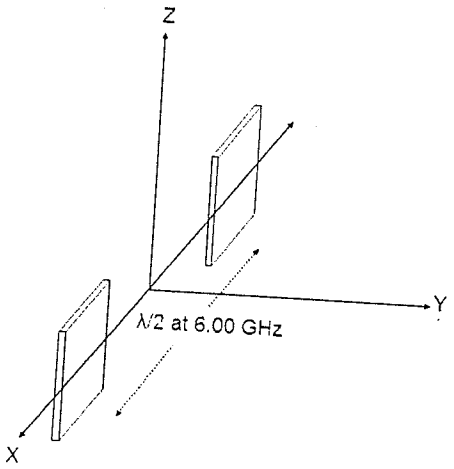

Fig. 5-14 Configuration of the 2-elements broadside array

Fig. 5-15 (a) is the simulated XY plane ($\theta=90^0$) radiation pattern at 4.00 GHz, where maximum radiations are in broadside (along $\varphi=90^0$ and $\varphi=180^0$) with HPBW of 50^0. At

6.00 GHz the maximum radiation is 3.19 dBi and there is no sidelobes in the XY ($\theta=90^0$) plane. At 8.00 GHz, the spacing between the elements is 1.33λ and the maximum gain of 8.92 dBi with HPBW of 30^0 is directed along 90^0 and 270^0.

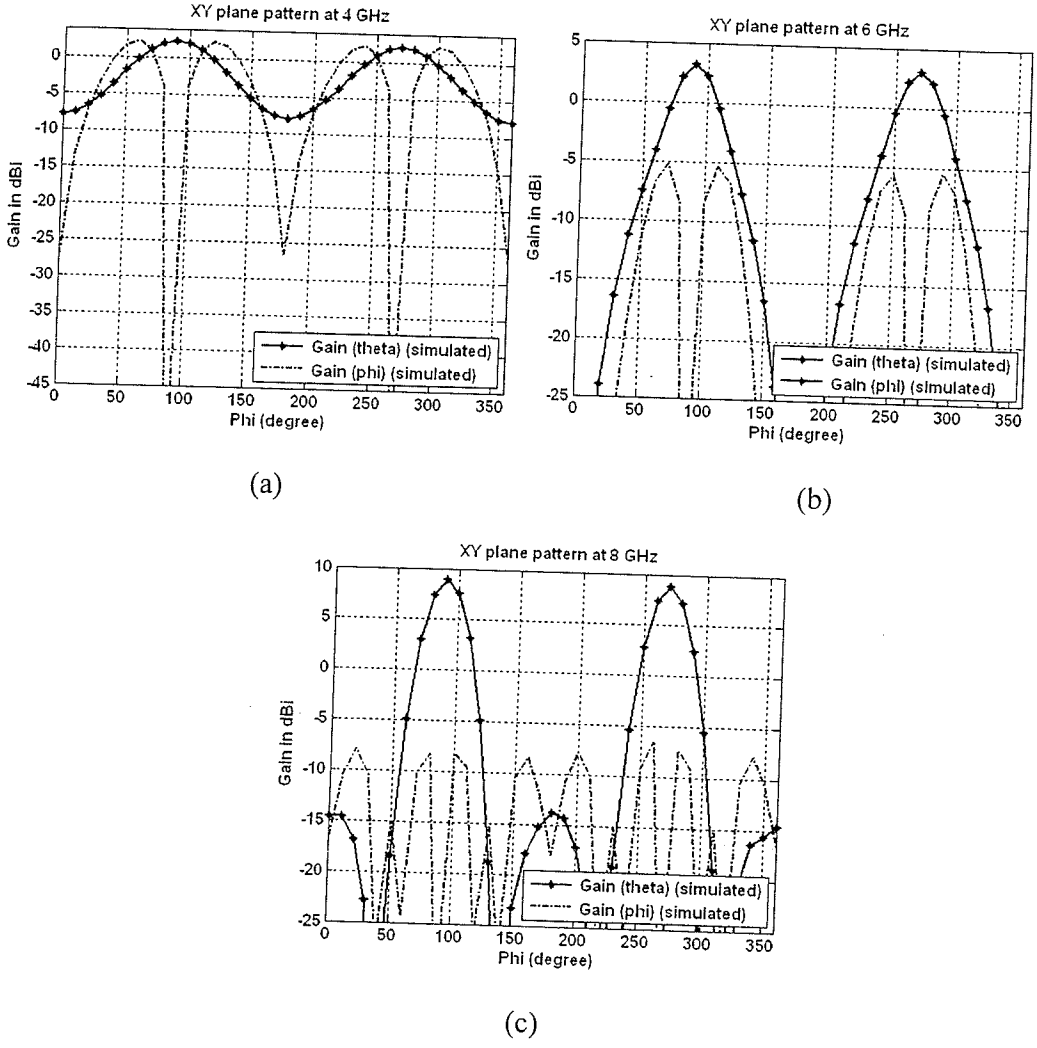

Fig. 5-15 Radiation pattern of the 2-elements broadside array at (a) 4.00 GHz, (b) 6.00 GHz and (c) 8.00 GHz in XY ($\theta=90^0$) plane

5.3.1.5 Time Domain Performance Analysis

As mentioned before, the UWB Antenna's performance is basically determined by its ability to transmit or receive short EM pulses without incurring much deviation or distortion of the original source pulse. To investigate the designed antenna's feasibility for UWB pulse radiation, some time domain simulation was performed using Remcom's XFDTD [56]. In the simulation model, antenna was excited with a first derivative of Gaussian pulse of very narrow time duration and radiated pulse at different points in the far-field both in azimuth and zenith planes were found to examine the ringing of the radiated pulse from the antenna.

5.3.1.5.1 Antenna Excitation

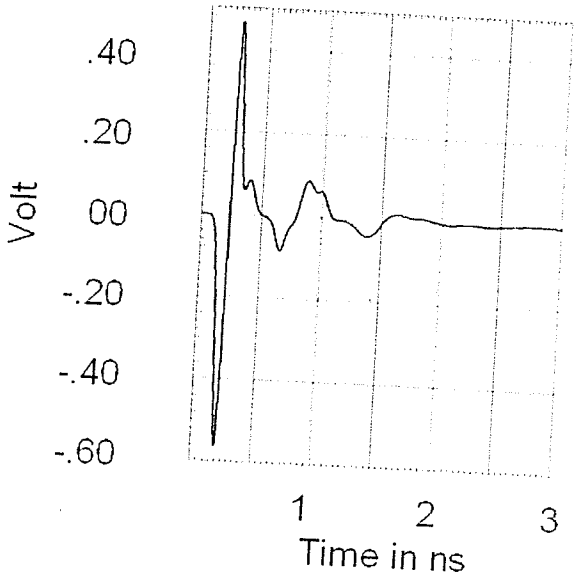

Fig. 5-16 Input signal at the antenna port

A Gaussian derivative pulse of duration 0.25 ns (Fig. 4-21) has been used as an excitation pulse by the source to excite the antenna. Fig. 5-16 shows pulse at the input port of the antenna as a function of time which is in the form of a damped sinusoid with maximum value of 0.58 V.

5.3.1.5.2 Far-field Pulse Radiation

Fig. 5-17 (a)-(c) show co-polarization components of the far-field for three angles ($\theta=0^0$, $\varphi=0^0$), ($\theta=45^0$, $\varphi=0^0$) and ($\theta=90^0$, $\varphi=0^0$) in the XZ or zenith plane as a function of time, while the antenna structure lies on the XY ($\theta=90^0$) plane. These observations correspond to three points surrounding the width of the antenna structure.

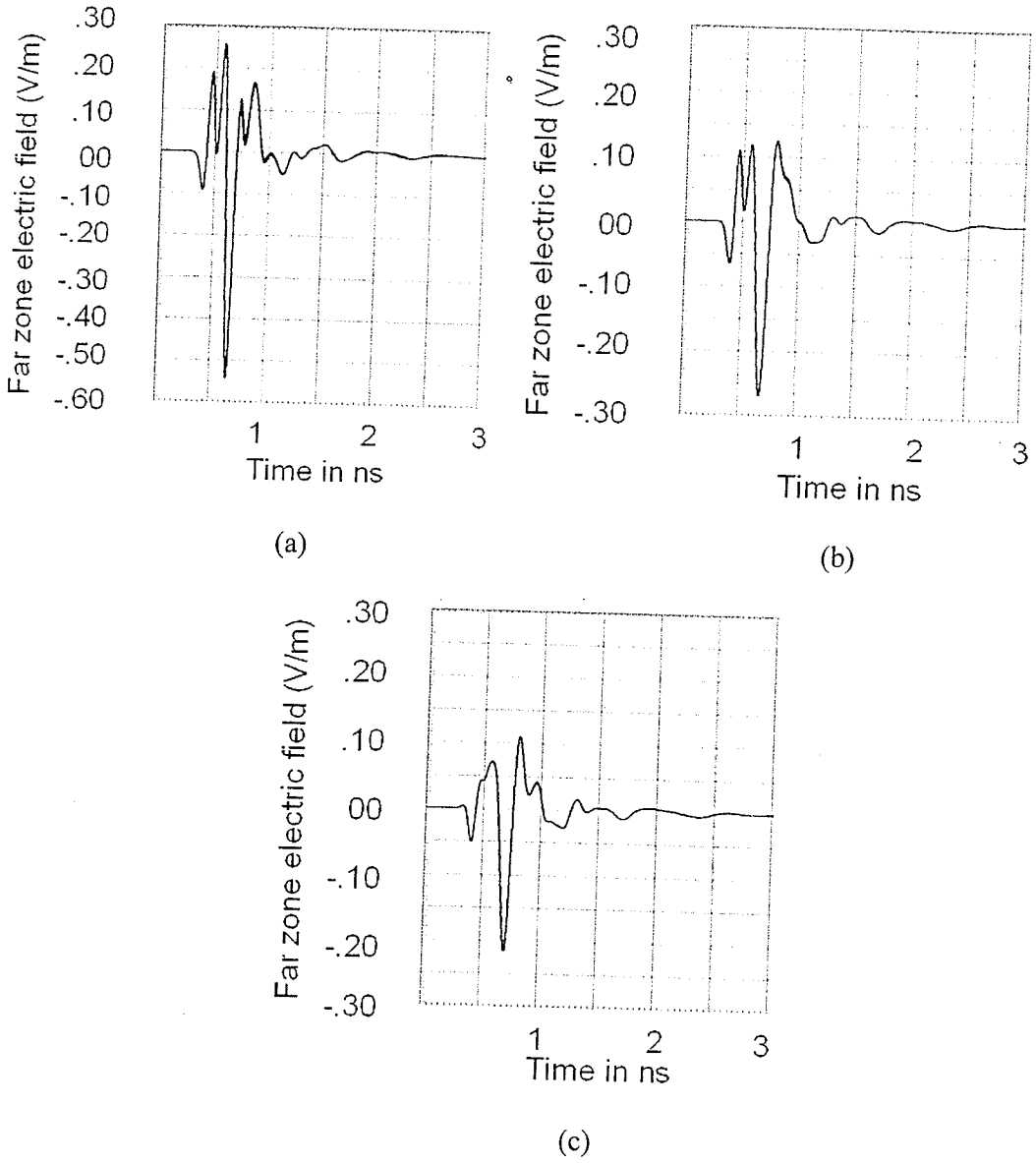

Fig. 5-17 Pulse radiation (a) ($\theta=0^0$, $\varphi=0^0$) (b) ($\theta=45^0$, $\varphi=0^0$) (c) ($\theta=90^0$, $\varphi=0^0$)

Fig. 5-17 (a) is the time domain pulse plot just vertically above the antenna ($\theta=0^0$, $\varphi=0^0$) which illustrates ringing effect incurred by the antenna of value near 1.00 ns with maximum field strength of -0.54 V/m. In the other two points in XZ plane (Fig. 5-17 (b), (c)), the pulse ringing is same but field strength is less than that of ($\theta=0^0$, $\varphi=0^0$).

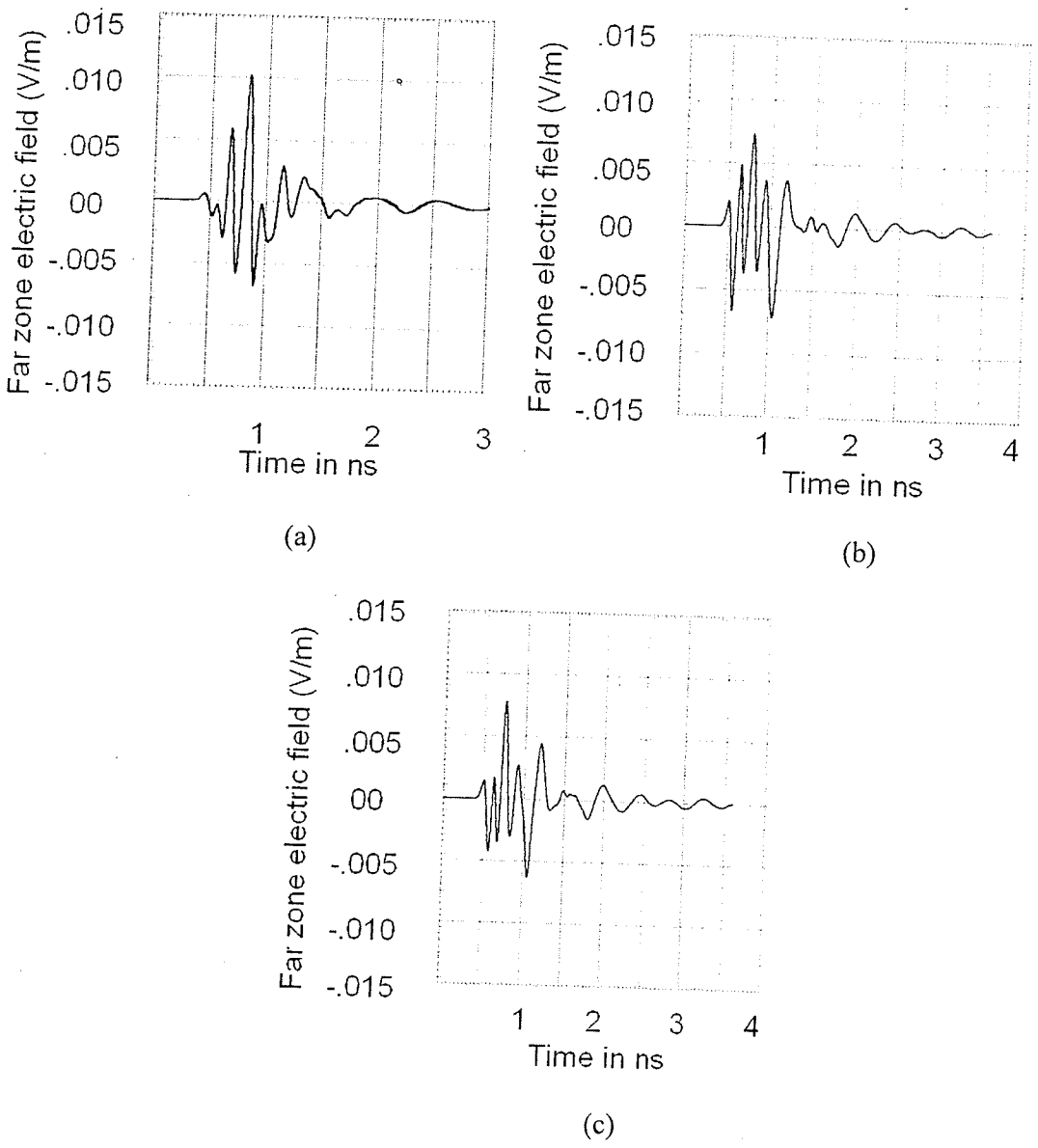

Fig. 5-18 Pulse radiation (a) ($\theta=0^0$, $\varphi=90^0$) (b) ($\theta=45^0$, $\varphi=90^0$) (c) ($\theta=90^0$, $\varphi=90^0$)

Fig. 5-18 (a)-(c) show co-polarization components of the far-field at three angles ($\theta=0^0$, $\varphi=90^0$), ($\theta=45^0$, $\varphi=90^0$) and ($\theta=90^0$, $\varphi=90^0$) in the YZ ($\varphi=90^0$) plane as a function of time, while the antenna structure is placed on the XY ($\theta=90^0$) plane. These observations correspond to three points in a plane over the middle of the antenna structure along the antenna length. In comparison between the far-field pulses in the XZ ($\varphi=0^0$) plane (Fig.

5-17) to YZ plane (Fig. 5-18), the ringing effect of the pulse is more significant in YZ ($\varphi=90^0$) plane. Moreover, maximum field strength is lower (54 times) in the YZ ($\varphi=90^0$) plane.

5.3.2 Antenna Immersed in Matching Materials

In this section, antenna impedance BW while immersed in three different low permittivity materials such as margarine, soybean oil and Vaseline has been studied, similar to the printed monopole antenna (Chapter 4)

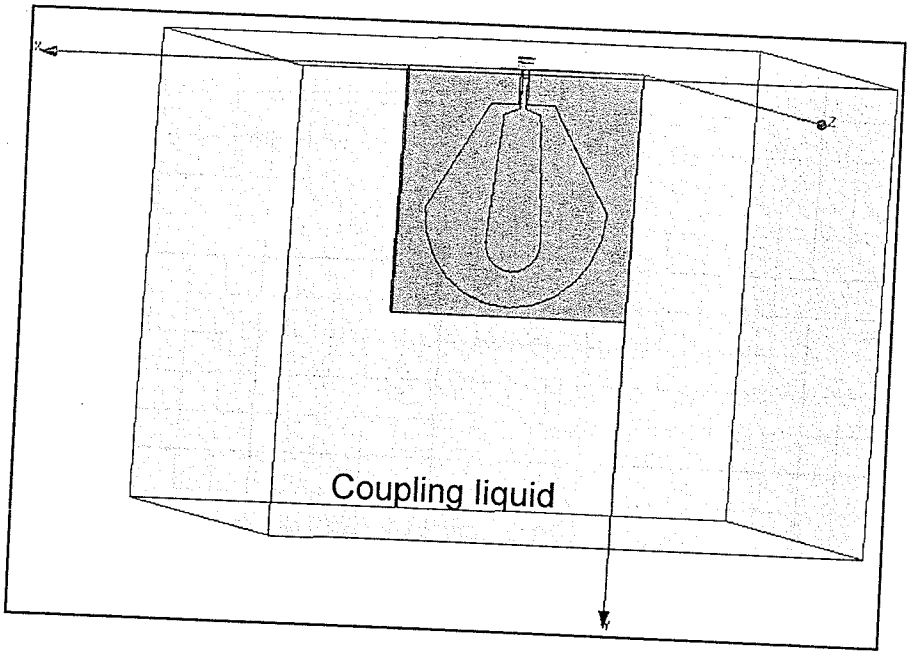

Fig. 5-19 Simulation model of the antenna immersed in the matching liquid

5.3.2.1 Margarine

The RL of the slot antenna has been simulated (Fig. 5-19) and measured when the whole antenna structure was immersed in the margarine mixtures having permittivity within the

range of 6.50 to 7.50 in the frequency range of 1.00 GHz to 13.00 GHz. The conductivity variation of that homogeneous mixture is within the range of 0.10 S/m to 0.80 S/m with a linear variation with frequency. These dielectric properties are in close proximity to the properties of fatty tissue and this is a reasonably suitable material as a coupling material.

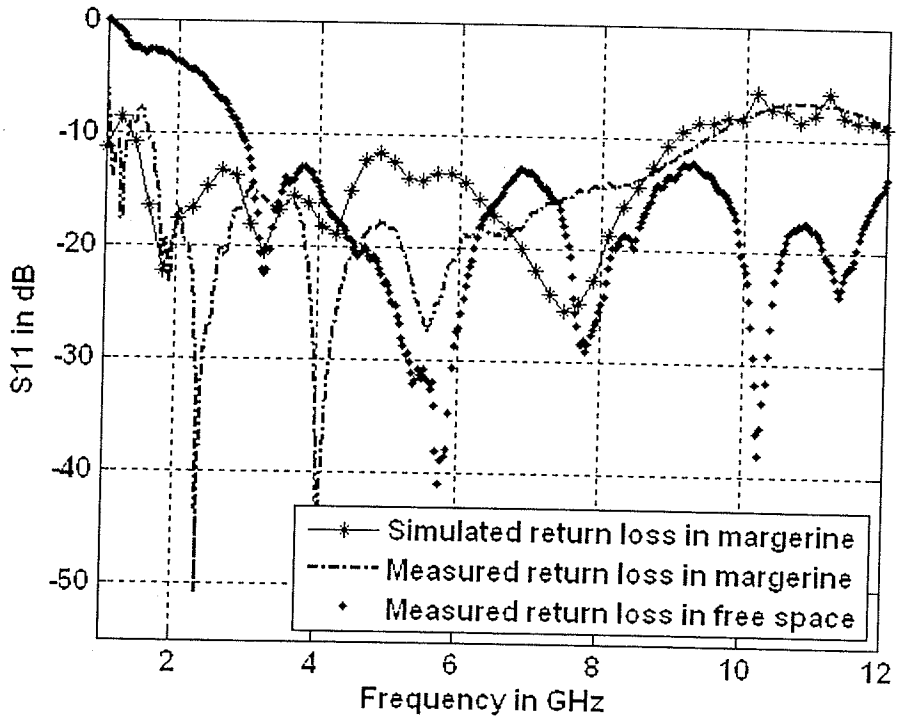

Fig. 5-20 Return loss in margarine and free space

Fig. 5-20 shows the impedance BW ($S_{11} \leq -10$ dB) of 7.90 GHz (1.60 GHz-9.50 GHz) has been achieved which depicts greater than 100% impedance BW. It is observable that total BW of the antenna reduces in margarine compared to that in free space, but the lower cut-off frequency of the antenna reduces significantly from 2.89 GHz in free space to 1.60 GHz in margarine mixture. Overall, this antenna still shows a reasonably good performance in the margarine mixture.

5.3.2.2 Soybean Oil

Soybean oil's dielectric properties (ε_r=2.60, σ=0.05 S/m at 6.00 GHz) are similar to very low water content fatty tissue [5]. The matching characteristic of the designed slot antenna is calculated while immersed in the rectangular box filled with soybean oil as shown in Fig. 5-19.

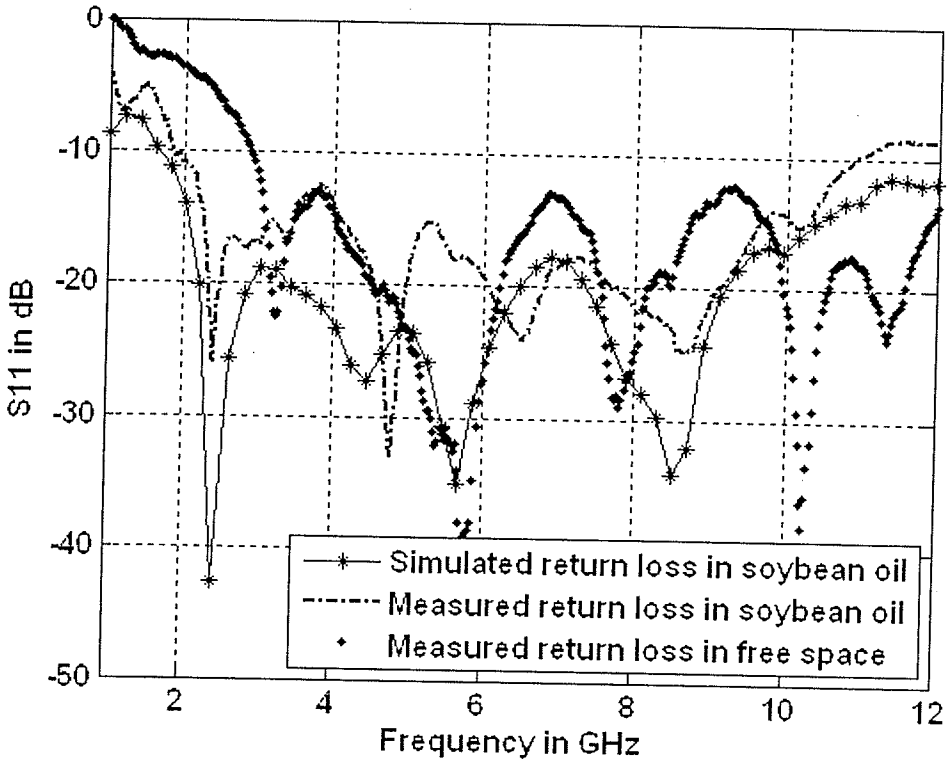

Fig. 5-21 Return loss in soybean oil and free space

Fig. 5-21 shows the RL curve of the antenna immersed in soybean. The simulation result shows a good impedance matching ($S_{11} \leq$-10 dB) of frequency span of 9.10 GHz from 1.80 GHz to 10.90 GHz. Similar to the previous case of margarine, lower cut-off frequency has been lowered in soybean oil to 1.80 GHz. The small variation between the

measured and the simulated values is probably due to the difference of the permittivity and conductivity values used in the calculation than the real set up values and dispersive nature of the soybean that was neglected in the simulation.

5.3.2.3 Vaseline

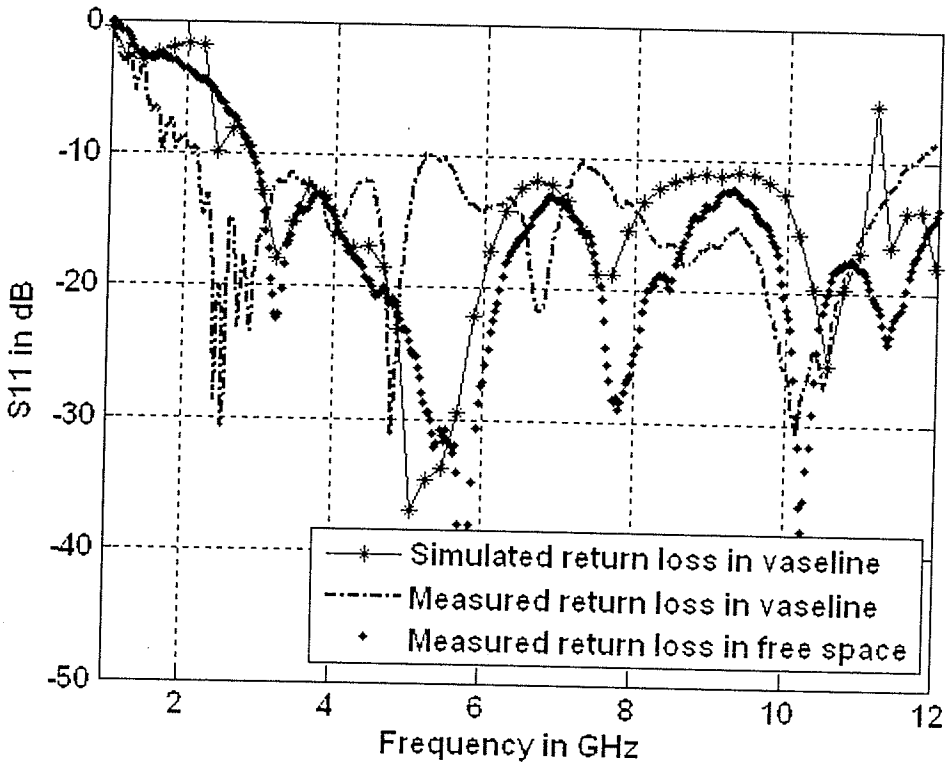

Fig. 5-22 Return loss in Vaseline and free space

Antenna impedance BW immersed in Vaseline was also simulated and measured. Very good impedance BW of 9.50 GHz starting from 2.15 GHz to 11.65 GHz was achieved. Fig. 5-22 shows the RL curve of the antenna immersed in Vaseline and in the free space.

5.4 Chapter Summary

A novel UWB printed taper-arc slot antenna design was proposed in this chapter which can attain free space and in-liquid impedance BW more than 100%. Design details and some computed and measured parameters of this antenna are also presented elaborately. Both calculated and measured results show a great promise of the antenna to be used in MI experimental set up.

Chapter 6 : Conclusions and Guidance for Future Research

6.1 Conclusions

In this thesis a comprehensive representation of two new UWB antennas including design, simulation and testing is presented. Some essential fundamental considerations in antenna design, analysis and measurement have been outlined initially. In addition, a resourceful study of different UWB antenna topologies has been presented to provide a background to the development of UWB antenna research arena. For both of the designed antennas several parameters like impedance BW, group delay, radiation pattern, gain and pulse ringing effect are investigated to evaluate the strengths and shortcomings of the designs.

Between the two designed antennas, the diamond shaped printed antenna attained measured free space impedance BW from 3.80 GHz to 11.85 GHz. Though this corresponds to BW greater than 100%, still it is necessary to bring the lower cut-off frequency down to utilize the lower band of frequency. This antenna shows improved impedance match while immersed in three matching materials: margarine, soybean oil and Vaseline. One of the limitations associated with that antenna is the lower value of directivity or gain. This is because of the antenna's near omnidirectional radiation

pattern, small size and lossy characteristics of the FR4 substrate. Although, the radiation pattern of the antenna shows reasonably stable characteristics over a large frequency BW, the cross-polarization components of the radiated field start to increase relative to the co-polarization components as frequency increases.

The slot antenna designed, achieved larger free space impedance BW of 2.89 GHz to 12.58 GHz compared to the diamond shaped printed monopole. The directivity value is also greater than that of the diamond antenna. The main shortcoming of the slot antenna is higher value of cross polarized components. The group delay variation is more in the slot antenna, so the diamond shaped printed antenna demonstrates slightly better time domain performance. In different coupling materials, both of the antennas demonstrate different matching characteristics. For example, in margarine the diamond shaped antenna's return loss is better than the slot antenna. On the contrary, in Vaseline, the slot antenna demonstrates better matching characteristics than the diamond shaped antenna.

6.1.1 Thesis Contributions

The discussion and the achieved results for the two designed antennas in this dissertation should provide an insightful perspective on elementary requirements on antenna systems, different topologies of UWB antennas, and their design and testing. Moreover, UWB antennas' impedance match response in certain matching materials was investigated. It was shown that printed planar antennas can be a good supplement of other complex and volumetric antennas used in MI applications.

6.2 Guidance for Future Works

From the acquired results for both antennas, it is evident that antenna design and structure require some refinement to have a better performance under the defined specifications.

In this thesis, antenna time domain performance is only simulated. Time domain measurements still have to be carried out to validate the prediction.

Similarly, after experimental set up is implemented, the antenna's performance as a part of the whole system should be examined.

An investigation for the radiation characteristics of the array of both antennas can be made.

Further studies can be made to reduce the cross-polarization level of the both antennas. An attempt can be made to increase the vertical components of the current to improve polarization purity by introducing more slots along the patch which can guide current in the antenna along the desired direction. Attempts can be taken to improve the efficiency of printed monopole antenna by reducing losses associated with it.

Bibliography

[1] C. A Balanis, Antenna Theory- Analysis and Design, Third edition, John Wiley and Sons, Inc, Hoboken, New Jersy, USA, 2005.

[2] M. Converse, E. J. Bond, B. D. Van Veen, and S. C. Hagness, "A computational study of ultra-wideband versus narrowband microwave hyperthermia for breast cancer treatment," IEEE Transactions on Microwave Theory and Techniques, vol. 54, no. 5, pp. 2169 -2180, May 2006.

[3] X. Yun, E. C. Fear, and R. H. Johnston, "Compact antenna for radar-based breast cancer detection" IEEE Transactions on Antennas and Propagation, vol. 53, no. 8, pp. 2374-2380, 2005.

[4] C. J. Shannon, "A Dielectric Filled Slot-line Bow-tie Antenna for Breast Cancer Detection," M.Sc. thesis, The University of Calgary, 2004.

[5] X. Li, S. K. Davis, S. C. Hagness, D. W. van der Weide, and B. D. VanVeen, "Microwave imaging via space—time beamforming: experimental investigation of tumor detection in multilayer breast phantoms," IEEE Transaction on Microwave Theory Techniques, vol. 52, no. 8, pp. 1856–1865, 2004.

[6] P. T. Huynah, A. M. Jarolimek, and S. Daye, "The false-negative mammogram" Radio Graphics, vol. 18, no. 5, pp. 1137- 1154, April 1998.

[7] J. G. Elmore, M. B. Barton, V. M. Moceri, S. Polk, P. J. Arena, and S. W. Fletcher, "Ten-year risk of false positive screening mammograms and clinical breast

examinations," The New England Journal of Medicine, vol. 338, no. 16, pp. 1089–1096, April 1998.

[8] J. Law, "Cancers detected and induced in mammographic screening: new screening schedules and younger women with family history," The British Journal of Radioalgy, vol. 70, pp. 62-69, January1997.

[9] A. Sabouni, S. Noghanian, and S. Pistorius, " Frequency dispersion effects on FDTD model for breast tumor imaging" IEEE Antennas and Propagation Symposium, pp. 1410-1413, Albuquerque, NM, USA, July 2006.

[10] J. Bond, X. Li and S. C. Hagness, "Numerical and experimental investigation of an ultra wideband ridged pyramidal horn antenna with curved launching plane for pulse radiation," IEEE Antennas and Wireless Propagation Letters, vol. 2, pp. 259–262, 2003.

[11] E. C. Fear and M. A. Stuchly, "Microwave breast tumor detection: antenna design and characterization," IEEE Antennas and Propagation Symposium, vol. 2, pp. 1076-1079, Boston, USA, July 2000.

[12] S. C. Hagness, A. Taflove, and J. E. Bridges, "Wideband ultralow reverberation antenna for biological sensing," Electronics Letters, vol. 33, no. 19, pp. 1594–1595, 1997.

[13] M.-K. Jung, "Microstrip monopole antennas for ultra wideband applications", M. Eng. project report, University of Manitoba, Winnipeg, Canada, 2006.

[14] H. Arai, Measurement of Mobile Antenna Systems, Artech House Publishers, 2001.

[15] "Group Delay"

http://www.microwaves101.com/encyclopedia/groupdelay.cfm#flatness

visited on June 21, 2007.

[16] H. Schantz, The Art and Science of Ultra WideBand Antennas, Artech House Publications, Boston, London, 2005.

[17] M. A. Peyrot-Solis , G. M. Galvan-Tejada, and H. Jardon-Aguilar, "State of the art in ultra-wide band antennas", Proceedings of 2nd International Conference on Electrical and Electronics Engineering (ICEEE) and XI Conference on Electrical Engineering (CIE 2005), Mexico City, Mexico, pp. 101-105, September, 2005.

[18] Y. Kim and D-H. Kwon, "CPW feed planar ultra wide band antenna having a frequency band notch function," Electronics Letters, vol. 40, no 7, pp. 403-405, 2004.

[19] K-H. Kim, Y-J. Cho, S-H. Hwang and S.-O Park, "Band notched UWB planar monopole antenna with two parasitic patches," Electronics Letters, vol. 41, no. 14, pp. 783-785, 2005.

[20] S. H. Choi, J. K. Park, S. K. Kim and J. Y. Park, "A new ultra wideband antenna for UWB applications," Microwave and Optical Technology Letters, vol. 40, no. 5, pp. 399-401, 2004.

[21] J. Liang, C. C. Chiau, X. Chen and C. G. Parini, "Printed circular disc monopole antenna for ultra-wideband applications," Electronics Letters, vol. 40, no. 20, pp. 1246-1247, 2004.

[22] K. Kiminami, A. Hirata and T. Shiozawa, "Double sided printed bow-tie antenna for UWB communications," IEEE Antennas and Wireless Propagation Letters, vol. 3, no. 1, pp. 152-153, 2004.

[23] N. Low, J. H. Cheong, and C. L. Law, "Low cost PCB antenna for UWB applications," IEEE Antennas and Wireless Propagation Letters, vol. 4, pp. 237-239, 2005.

[24] M. Yanagi, S. Kurashima, T. Arita, and T. Kobayashi, "A planar UWB monopole antenna formed on a printed circuit board," http://www.fujitsu.com/downloads/MICRO/fcai/input/uwb_monopole_antenna.pdf, visited October 11, 2006.

[25] T. Yang, William A. Davis, and Warren L. Stutzman, "Small, planar, ultra-wideband antennas with top-loading" IEEE Antennas and Propagation. Symposium, vol. 2A, pp. 479-482, Washington DC, USA, July 2005.

[26] S-W. Qu, C. Ruan, "Bandwidth enhancement of wide-slot antenna fed by cpw and microstrip line," IEEE Antennas and Propagation Letters, vol. 5, no.1, pp. 15-17, 2006.

[27] Y. F. Liu, K. L. Lau, Q. Xue, C. H. Chan, "Experimental studies of printed wide slot antenna for wideband applications," IEEE Antennas and Propagation Letters, vol. 3, no.1, pp. 273-275, 2004.

[28] T. A. Denidni and M. A. Habib, "Broadband printed CPW feed circular slot antenna," Electronics Letters, vol. 42, no 3, pp. 135-136, 2006.

[29] H.-D. Chen, "Broadband CPW-fed square slot antennas with a widened tuning stub," IEEE Transaction on Antennas and Propagation., vol. 51, no. 8, pp. 1982–1986, 2003.

[30] M. K. Kim, K. Kim, Y. H. Suh, and I. Park, "A T-shaped microstrip-line-fed wide-slot antenna," IEEE Antennas and Propagation Symposium, vol. 3, pp. 1500–1503, Boston, USA, July 2000.

[31] Y. W. Jang, "Broadband cross-shaped microstrip-fed slot antenna," Electronics Letters, vol. 36, no. 25, pp. 2056–2057, 2000.

[32] A. M. Abbosh, M. E. Bialkowski, J. Mazierska and M.V. Jacob, "A planar UWB antenna with signal rejection capability in the 4-6 GHz band," IEEE Microwave and Wireless Components Letters, vol. 16, no. 5, pp. 278-280, 2006.

[33] J.-Y. Sze and K. L. Wong, "Bandwidth enhancement of a microstrip line-fed printed wide-slot antenna," IEEE Transaction on Antennas Propagation., vol. 49, no. 7, pp. 1020–1024, 2001.

[34] P. H. Rao, "Feed effects on the dimensions of wide-band slot antennas," Microwave Optical Technology Letters, vol. 40, no.1, pp. 77–79, 2004.

[35] P. H. Rao, V. F. Fusco and R. Cahill, "Linearly polarized radial stub fed high performance wide-band slot antenna," Electronics Letters, vol. 37, no. 6, pp. 335–337, 2001.

[36] Y. W. Jang, "Experimental study of large bandwidth three-offset microstripline-fed slot antenna," IEEE Microwave Wireless Components Letters, vol. 11, no.10, pp. 425–426, 2001.

[37] J.-Y. Chiou, J.-Y. Sze, and K.-L. Wong, "A broad-band CPW-fed strip loaded square slot antenna," IEEE Transaction on Antennas Propagation, vol. 51, no. 4, pp. 719-721, 2003.

[38] H. M. Jafari, M.J. Deen, S. Hranilovic and N.K. Nikolova, "Slot antenna for UWB applications," IEEE Antennas and Propagation Symposium, pp.1107-1110, Albuquerque, NM, USA, July 2006.

[39] K.-L. Wong, Y-W. Chi and C.-H. Wu, "Wideband tri plate monopole antenna", Electronics Letters, vol, 40, no. 24, pp. 1517-1519, 2004.

[40] M. Cabedo-Fabres, E. Antonino-Daviu, A. Valero-Nogueira and M. Ferrando-Bataller, "Analysis of wide band planar monopole antennas using characteristic modes" IEEE Antennas and Propagation Symposium, vol. 3, pp. 733-736, Columbus, Ohio, USA, June 2003.

[41] K.-L. Wong, C-H Wu, and S.–W. Su, "Ultra wide band square planar metal-plate monopole antenna with a trident-shaped feeding strip," IEEE Transactions on Antennas and Propagation, vol. 53, no. 4, pp. 1262-1269, 2005.

[42] G. Agrawall, N. P. Kumar, and K. P Roy, "Wide-band planar monopole antennas", IEEE Transactions on Antennas and Propagation, vol. 46, no. 2, pp. 294–295, 1998.

[43] J. Powell, "Antenna Design for Ultra Wide Band Radio," M.Sc. thesis, Massachusetts Institute of Technology (MIT), 2004.

[44] C. Nguyen, J.-S. Lee and J.-S. Park, "Ultra-wideband microstrip quasi-horn antenna," Electronics Letters, vol. 37, no.12, pp. 731-732, 2001.

[45] A. G. Yarovoy, A. D. Schukin, I. V. Kaploun, and L. P. Ligthart, "The dielectric wedge antenna" IEEE Transactions on Antennas and Propagation, vol. 50, no. 10, pp. 1460-1472, 2002.

[46] A. A. Lestari, A. G. Yarovoy, and L. P. Ligthart, "RC-loaded bow-tie antenna for improved pulse radiation," IEEE Transactions on Antennas and Propagation, vol. 52, no. 10, pp. 2555-2563, 2004.

[47] A. Webb, Introduction to Biomedical Imaging, IEEE Press Series in Biomedical Engineering, John Wiley and Sons, Inc, 2003.

[48] O. Peart, Mammography and Breast Imaging- Just the Facts, McGraw Hill Professional, 2005.

[49] E. C. Fear, S. C. Hagness, P. M. Meaney, M. Okoniewski, and M. A. Stuchly, "Enhancing breast tumor detection with near-field Imaging", IEEE Microwave Magazine, vol.3, no. 1, pp. 48-56, 2002.

[50] S. Noghanian, A. Sabouni and S Pistorius, "A numerical approach to microwave imaging based on genetic algorithm optimization," Proceedings of SPIE, vol. 6177, March 2006.

[51] G. Bindu, A. Lonappan, V. Thomas, C. K. Aanandan, and K. T. Mathew, "Active microwave imaging for breast cancer detection", Progress in Electromagnetics Research, PIER 58, pp. 149-169, 2006.

[52] R. V. de Jongh, A. G. Yarovoy, L. P. Ligthart, V. Kaploun, A. D. Schukin, "Design and analysis of new GPR antenna concepts", Proceedings of Seventh International Conference on Ground Penetrating Radar, vol. 1, pp.81-86, Kansas, USA, May 1998.

[53] I. Hossain, S. Noghanian and S. Pistorius, "Design and performance investigation of a diamond shaped compact ultra wide band antenna," IEEE Antennas and Wireless Propagation Letters, under review.

[54] I. Hossain, S. Noghanian and S. Pistorius, "A diamond shaped small planar ultra wide band antenna for microwave imaging purpose" IEEE Antennas and Propagation Symposium, pp. 5713-5716, Honolulu, Hawaii, USA, June 2007.

[55] User's manual, Ansoft HFSS 10, www.ansoft.com.

[56] User's manual XFDTD 6.4, www.remcom.com.

[57] J. M. Sill and E. C. Fear, "Tissue sensing adaptive radar for breast cancer detection: study of immersion liquids," Electronics Letters, vol. 41, no. 3, 2005.

[58] P. M. Meany, S. A. Pendergrass, M.W. Fanning, D. Li and K. D. Paulsen, "Importance of using a reduced contrast coupling medium in 2D microwave breast imaging," Journal of Electromagnetic Waves Application, vol.17, pp. 333-355, 2003.

[59] W. Wu and C. E. Smith, "Dielectric measurements using the HP 85070A probe," Proceedings of IEEE Southeastcon, vol. 1, pp. 83-86, Birmingham, USA, April 1992.

[60] E. C. Fear and M. A. Stuchly, "Confocal microwave imaging for breast tumor detection: comparison of immersion liquids," IEEE Antennas and Propagation Symposium, vol. 1, pp. 250-253, Boston, Massachusetts, USA, July 2001.

[61] I. Hossain, S. Noghanian and S. Pistorius, "Co-planar waveguide fed taper arc slot antenna for ultra wide band applications," IEEE Antennas and Wireless Propagation Letters, under review.

[62] I. Hossain, S. Noghanian and S. Pistorius, "A CPW fed ultra wide band taper arc slot antenna" EMTS 2007 International URSI Commission B- Electromagnetic Theory Symposium, Ottawa, ON, Canada, July 2007.